**Title**
Effects of Efference on Hair Cell Bundle Mechanics



**Author**
Lin, Chia-Hsi Jessica

**Publication Date**
2022

Peer reviewed|Thesis/dissertation

UNIVERSITY OF CALIFORNIA

Los Angeles

# Effects of Efference on Hair Cell Bundle Mechanics

A dissertation submitted in partial satisfaction

of the requirements for the degree

Doctor of Philosophy in Physics

by

Chia-Hsi Jessica Lin

2022

ABSTRACT OF THE DISSERTATION

Effects of Efference on Hair Cell Bundle Mechanics

by

Chia-Hsi Jessica Lin
Doctor of Philosophy in Physics
University of California, Los Angeles, 2022
Professor Dolores Bozovic, Chair

Hair cells in both the auditory and vestibular systems receive efferent innervation. A number of prior studies have indicated that efferent regulation serves to diminish the overall sensitivity of the auditory system. The efferent pathway is believed to affect the sensitivity and frequency selectivity of the hair cell by modulating its membrane potential. However, its effect on the mechanical response of the hair cell has not been established. We explored how stimulation of the efferent neurons affects the mechanical responsiveness of an individual hair bundle. We tested this effect on *in vitro* preparations of hair cells in the sacculi of American bullfrogs (*Rana catesbeiana*) of both genders. Efferent stimulation routinely resulted in an immediate increase of the frequency of hair bundle spontaneous oscillations for the duration of the stimulus. Enlarging the stimulus amplitude and pulse length, or conversely, decreasing the inter-pulse interval led to oscillation suppression. Additionally, we tested the effects of efference on the hair bundle response to mechanical stimulation. The Arnold Tongues of hair cells undergoing efferent actuation demonstrated an overall desensitization with respect to those of unstimulated cells.

In addition to fine-tuning the response, the efferent pathway strengthens the auditory system for optimal performance by protecting the inner ear from noise-induced damage. Although it has been well-documented that efference helps defend against hair cell and synaptic extinction, the mechanisms of its otoprotective role have still not been established. Specifically,

the effect of efference on an individual hair cell's recovery from mechanical overstimulation has not been demonstrated. Prior research on hair bundle mechanics has shown that a high-amplitude mechanical deflection detunes a bundle from its innately oscillatory regime – rendering it quiescent for intervals dependent on the applied signal. We explored the impact of efferent stimulation on this recovery using the same *in vitro* American bullfrog saccular hair cell preparations. Efferent actuation concomitant with the hair bundle's relaxation from a high-amplitude deflection vastly changed the recovery profile and often entirely eliminated the transition to quiescence. Furthermore, we did not find efferent modulation to influence the magnitude of the mechanically-induced offset in a statistically significant manner. Our findings indicate that the efferent system acts as a control mechanism that determines the dynamic regime in which the hair cell is poised.

The dissertation of Chia-Hsi Jessica Lin is approved.

Mayank R. Mehta

Peter M. Narins

Giovanni Zocchi

Dolores Bozovic, Committee Chair

University of California, Los Angeles

2022

*To my family ...*

*without whom I would not be*

*where I am today.*

# Table of Contents

# List of Figures

# Acknowledgments

I am forever indebted to my mentor and PhD advisor, Dolores Bozovic, for supporting me and guiding me throughout my time at UCLA. Dolores allowed me to pursue my own course of action and gave me room to learn from experience, yet always stepped in with advice when needed. I could not have asked for a more kind and understanding mentor than Dolores, and it is only through her nurturing that I was able to blossom into the scientist that I am today.

I am deeply grateful to Elizabeth Mills for mentoring me during my first years in the Bozovic lab. She selflessly gave so much of her time to showing me the ropes and was always happy to help when asked.

I extend my profound gratitude to my committee members: Peter Narins, Mayank Mehta, and Giovanni Zocchi, for their kind words and encouragement through the years.

I genuinely appreciate having had the opportunity to work with and get to know my friends and colleagues in the Bozovic lab: Bas Meenderink, Yuki Quiñones, Tracy Zhang, Justin Faber, Janaki Sheth, Joey Marcinik, Nick Senofsky, Martín Toderi, Dima Vaida, and Inbal Mizrahi. Everyone contributed to the pleasant atmosphere of the lab; I will always treasure all the delightful and thought-provoking conversations.

I want to express my gratitude to all the previous and current Physics Department staff who could always be counted on to provide knowledge and assistance.

Lastly, I would like to thank Krystal Alfonso for being a true friend from the moment we both began our doctoral journeys at UCLA. I cherish our friendship immensely.

# Curriculum Vitae

| | |
|---|---|
| 2010 – 2014 | B.S. in Physics, University of California, Santa Barbara. |
| 2014 – 2016 | M.S. in Physics, University of California, Los Angeles (UCLA). |
| 2014 – 2018 | Teaching Assistant, Physics and Astronomy, UCLA. |
| 2015 – Present | Graduate Student Researcher, Physics and Astronomy, UCLA. |
| 2022 – Present | Physics 5L Lab Coordinator, Physics and Astronomy, UCLA. |

# Publications

Lin, Chia-Hsi Jessica, and Dolores Bozovic. "Effects of Efferent Activity on Hair Bundle Mechanics." *Journal of Neuroscience* 40.12 (2020): 2390-2402.

Lin, Chia-Hsi Jessica, and Dolores Bozovic. "Impact of Efferent Activity on Hair Cell Response to Mechanical Overstimulation." (Feb. 2022). Manuscript submitted for publication in the *Journal of Neuroscience*.

# CHAPTER 1

# Dynamics of Hearing

## 1.1 Introduction

The auditory system furnishes us with rich information about the external environment. It contributes crucially to the ability of numerous species to navigate in space, enables communication with conspecifics, and provides important cues for the avoidance of danger and localization of food sources, amongst a plethora of applications. In order to perform these functions, the system must be able to detect extremely weak signals – sometimes as low as 0 dB [90, 43] – and frequently parse these signals from an environment crowded with both multiple competing streams of information and potentially much louder background noise.

## 1.2 Hair Cell Mechanics

An intricate process takes place when we hear a sound. When a sound wave, or pressure wave, enters the outer ear, it strikes the eardrum and causes the eardrum to vibrate. These vibrations are transmitted to the inner ear via the three ossicles of the middle ear. The acoustic energy is transferred through the oval window and flows along the basilar membrane through the cochlea [28].

### 1.2.1 Hair Bundle

The hair cell is a fundamental element of the inner ear and derives its name from the organelle, termed the hair bundle, that resides on its apical surface above the cell soma. The hair bundle is comprised of actin-filled stereovilli (stereocilia) arranged in a semi-crystalline pattern, with rows of increasing height terminating in a kinocilium. The mechanically-gated ion channels of each row of stereovilli are connected to an adjacent row of stereovilli via tip links. When a hair bundle is deflected by sound, the hair cell's mechanoelectrical transduction process allows for the conversion of sound waves into electrical signals. Thus, the hair bundle's transduction mechanism provides a crucial step in detecting an auditory signal [28].

### 1.2.2 Mechanoelectrical Transduction

A hair cell's mechanoelectrical transduction is the fundamental process by which sound waves are converted into electrical signals. Displacement of the hair bundle by an incoming sound modulates the open probability of a stereovilli's transduction channels, with a positive displacement (towards the kinocilium) increasing the open probability, and vice versa. The tension induced in the tip links causes the opening of transduction channels and enables the influx of ionic currents. $K^+$ and $Ca^{2+}$ ions flow into the hair cell through the stereocilia. This generates a depolarization of the membrane potential, or the potential difference between the cell soma and the surrounding fluid. Depolarization of the cell induces the opening of voltage-gated $Ca^{2+}$ channels in the soma, which leads to an influx of $Ca^{2+}$. The $Ca^{2+}$ ions cause the vesicles located near the base of the soma to fuse with the membrane and release their neurotransmitters. The neurotransmitters bind to receptors on the post-synaptic afferent terminal, which produces a signal that is sent to the brain. The $Ca^{2+}$ ions also activate $Ca^{2+}$-sensitive $K^+$ channels. This brings about an efflux of $K^+$ from the cell soma and a repolarization of the hair cell back to its resting membrane potential [42].

### 1.2.3 Active Motility and Spontaneous Oscillations

Hair cells are capable of detecting sounds that displace the hair bundle by only 5 Å [43]. It has been observed in several species, such as frog [70], turtle [8], and gecko (Fig. 1.1), that these hair bundles spontaneously oscillate in the absence of a stimulus. These spontaneous oscillations give us evidence of an active process in the hair cell, and examining these spontaneous oscillations provides us with a method for exploring the nonlinear dynamics of hair cells [14, 78, 104].

## 1.3 The Efferent System

The efferent system has been regularly attributed to aiding the auditory system in its communicational and navigational tasks [45, 39, 38, 75, 74, 84, 34]. Recent research has uncovered even more utilities of the efferent pathway. A set of studies has demonstrated that intact efferent innervation from the lateral olivocochlear (LOC) and medial olivocochlear (MOC) nuclei is crucial to maintaining the appropriate balance between both ears [19, 58]. Since the comparison of interaural signals is essential to accurate sound localization [97, 113], a delicate calibration between the signals received from the two ears must be maintained. Moreover, the efferent architecture has been shown to have a significant function in the "cocktail party effect", which refers to the ability to parse one particular auditory stream from a complex acoustic environment [30, 52, 48, 1, 99, 58]. However, it appears that the main functional duties of the auditory efferent neurons are control over the auditory system's sensitivity of detection [2, 38, 74, 75, 19, 84, 99, 34, 57, 107] and protecting the auditory system from noise-induced damage [36, 87, 62, 102, 12, 20, 79].

### 1.3.1 Sensitivity of Detection

As hearing loss constitutes a critical and potentially growing public health problem, understanding the role of the efferent system in controlling hearing sensitivity merits further study. Although a broad literature has established the importance of the efferent pathway in auditory function [36, 74, 75, 30, 1], much less is known about the mechanisms by which it exerts

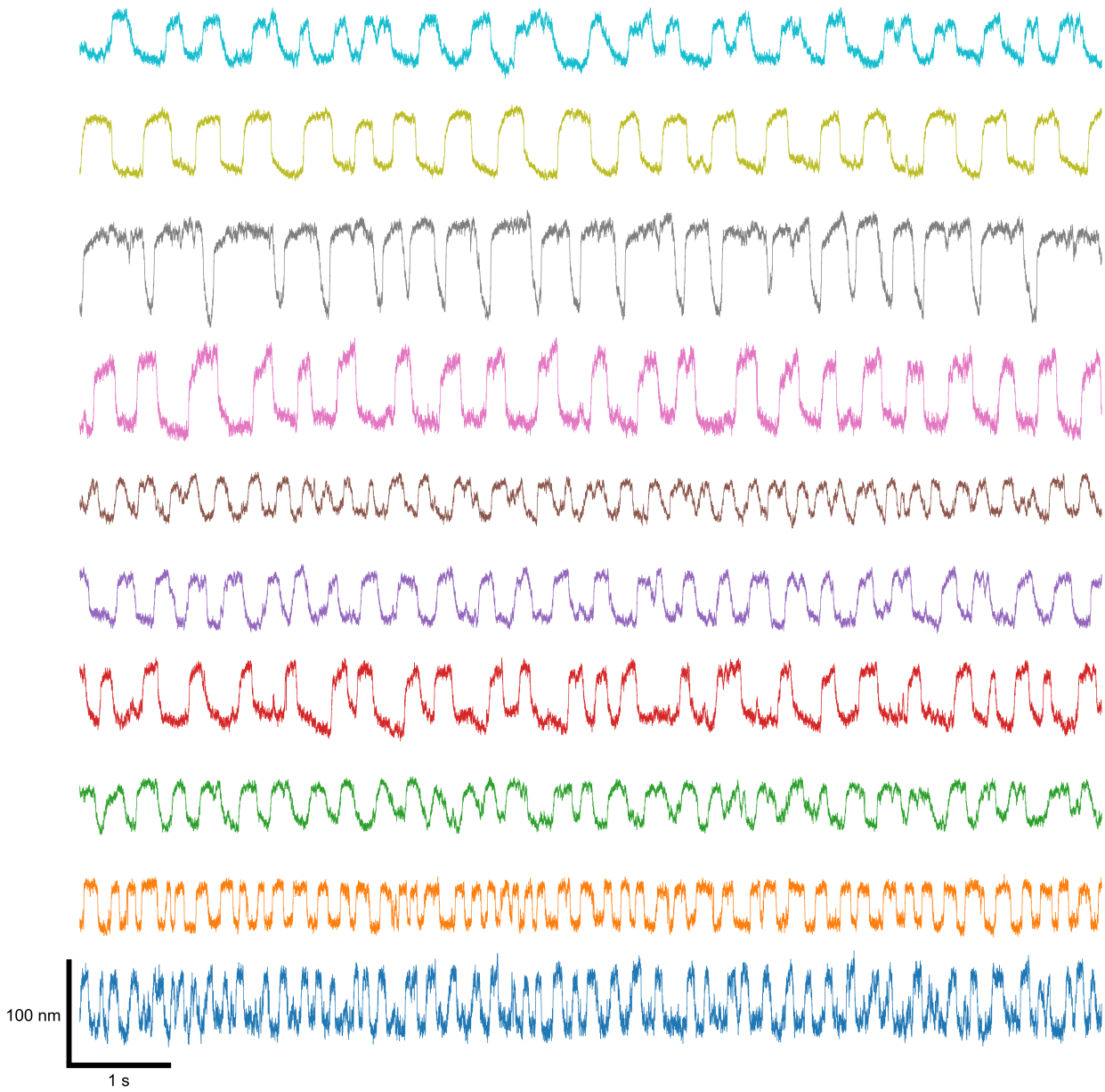


Figure 1.1: We detected active hair bundle motility in hair cells of the Tokay gecko sacculus. Spontaneous oscillations are displayed for ten hair bundles procured from two sacculi, shown in different colors, and offset for clarity.

its effect. It has been shown that efferent stimulation suppresses basilar membrane displacement evoked by characteristic frequency tones [77, 94, 18]. Efferent actuation must therefore play a modulatory role in the mechanical response. However, there has been thus far no direct demonstration of the impact of efferent activity on the mechanical responsiveness of the hair bundle. As damage to this delicate system leads to hearing loss, a protective mechanism that modulates the hair bundle's sensitivity of response would be highly beneficial.

### 1.3.2 Otoprotection

The delicate machinery of the inner ear is required to sustain very intense signals, sometimes as high as 120 dB [43], without suffering immediate and irreparable damage. Intense sounds have been observed to cause temporary threshold shifts in humans and other mammals, as well as to have an effect on cochlear microphonics. This indicates an underlying protective mechanism [17, 73, 81, 54, 20]. At the level of the hair cell, a high-amplitude mechanical deflection was shown to detune the bundle from an oscillatory regime and render it temporarily quiescent [46]. However, the trajectory of a hair cell's recovery to its original oscillatory state is not yet known.

The efferent system has been linked to the auditory system's inherent otoprotective capacity, and a number of studies have shown that severing efferent neurons leads to greater levels of ototoxicity. Specifically, exposure to moderate or loud sounds was shown to generate higher levels of noise-induced damage (hair cell and synaptic deterioration) in subjects with severed efferent innervation [112, 63, 51, 102, 64]. As noise-induced hearing loss presents a significant public health problem, it is important to fully understand the role of the efferent architecture in protecting the auditory epithelia from acoustic trauma. However, thus far, there has been no direct examination of the influence of efferent activity on a hair bundle's intrinsic recovery from mechanical overstimulation.

## 1.4 Dissertation Outline

In this work, we focus on the effect of efference on individual hair cells. In Chapter 2, we present a new and less-invasive method of stimulating the auditory efferent neurons. In Chapter 3 and Chapter 4, we explore the hypothesis that actuating efferent neurons directly affects the mechanical response of a hair bundle. Specifically, we surmise that efferents modulate the bundle's intrinsic active oscillations and lead to a reduction of its sensitivity to mechanical stimulus. To test this hypothesis, we performed experiments on semi-intact preparations that maintained the hair bundles' active motility. Mechanical measurements were combined with efferent stimulation, allowing us to directly probe the efferent impact on a hair cell's mechanical response. Finally, in Chapter 5 and Chapter 6, we investigate the hypothesis that activating the efferent system directly affects a hair cell's recovery from large mechanical deflections. This hypothesis was again tested with experiments conducted on individual hair bundles located within semi-intact preparations that preserve the hair bundles' active motility. We begin by examining the oscillatory characteristics of a hair bundle regaining its innate dynamics after a severe mechanical deflection. Various paradigms of efferent actuation were then paired with mechanical overstimulation to probe the impact of efference on a hair cell's recovery dynamics.

## 1.5 Significance

The efferent system is an important aide for the performance of the auditory system. It has been seen to contribute to sound detection and localization, ototoxicity prevention, and speech comprehension. Although measurements have demonstrated that efference suppresses basilar membrane movement, there is still much unknown about how efferent activity affects hearing mechanics. Moreover, the efferent system has been directly implicated in mitigating noise-induced deterioration in the inner ear. Specifically, acoustic trauma generated more advanced levels of hair cell extinction and synaptic damage in subjects with impaired efferent innervation. However, it is still not known how efferent stimulation effectuates its protective role at the level of an individual hair cell. In this work, we explore the mechanical basis

for the efferent system's capabilities at the level of the hair bundle. We present optical recordings, Arnold Tongues, and sensitivity curves that show a hair bundle is desensitized by efferent stimulation. We also demonstrate that efferent activation drastically changes the dynamics of hair bundle recovery following mechanical overstimulation. These findings indicate that the efferent system provides a biological feedback mechanism that controls both the dynamic state and the mechanical sensitivity of a hair cell.

# CHAPTER 2

# Efferent Stimulation of Hair Cells in the American Bullfrog Sacculus

## 2.1 Introduction

We introduce a novel method for electrically stimulating the efferent neurons of the American bullfrog saccular hair cells. Our efference setup is based on the protocol described by Castellano-Muñoz et al. [15]. This new protocol is both less invasive and more biologically-relevant than the one more commonly performed [32]. We first explore the collective response of individual hair bundles to efferent actuation using our efference setup. Utilizing a host of receptor-targeted and channel-targeted chemical blockers, we then confirm that our efference method does indeed electrically stimulate the efferent synapses.

## 2.2 Materials and Methods

### 2.2.1 Biological Preparation

Research was conducted following animal-handling and euthanasia protocols approved by the University of California, Los Angeles Chancellor's Animals Research Committee, in accordance with federal and state regulations. Experiments were performed on *in vitro* preparations of sacculi extracted from adult North American bullfrogs (*Rana catesbeiana*) of both genders. The animals were anesthetized (sodium pentobarbital: 150 mg/kg), double pithed, and then decapitated. Sacculi were excised from the inner ears of the animals. Saccular maculae were mounted in a two-compartment chamber, which simulated the fluid

partitioning of the *in vivo* environment. The basolateral membrane was bathed in artificial perilymph (in mM: 110 $Na^+$, 2 $K^+$, 1.5 $Ca^{2+}$, 113 $Cl^-$, 3 D-(+)-glucose, 1 $Na^+$ pyruvate, 1 creatine, 5 HEPES), and the apical surface was immersed in artificial endolymph (in mM: 2 $Na^+$, 118 $K^+$, 0.25 $Ca^{2+}$, 118 $Cl^-$, 3 D-(+)-glucose, 5 HEPES). Both solutions were titrated to match the pH and osmolarity of the physiological conditions in the otic labyrinth and freshly oxygenated immediately prior to use. The overlying otolithic membrane was enzymatically dissociated from the epithelium with 50 $\mu$g/mL collagenase IA-S (Sigma Aldrich) for 8 – 9 minutes and gently removed. Spontaneous oscillations were observed in hair bundles after the membrane was decoupled and could be sustained for several hours following dissection. For control experiments, 2 $\mu$M strychnine (Sigma Aldrich), 1 $\mu$M tubocurarine chloride (Tocris Bioscience), or 50 $\mu$M apamin (Sigma Aldrich) was added to the artificial perilymph [101, 35, 111]. The solution in the basal compartment was replaced via a fluid exchange, and measurements were repeated after a five minute incubation period [93, 83, 77].

### 2.2.2 Imaging and Tracking Hair Bundle Motion

Data acquisition was performed inside an acoustically-isolated chamber (Industrial Acoustics Company) with the microscope setup mounted on a vibration-isolation table (Technical Manufacturing Corporation). Preparations were imaged in an upright optical microscope (Olympus BX51WI) with a water immersion objective (Olympus XLUMPlanFL N, 20×, 1.00 NA). Images were further magnified (for ∼400× total magnification with camera pixel resolution of 52.1 nm/px) and projected onto a high-speed CMOS camera (Photron FASTCAM SA1.1) recording at 1000 frames per second. Hair bundles were imaged at the focal plane intersecting the tallest row of stereocilia, and a hair bundle's position was derived for displacements toward and away from its kinocilium. From these recordings, the motion of a hair bundle was tracked with software written in MATLAB (The MathWorks). The position of the hair bundle in each frame was determined by calculating the center of gravity of its intensity profile along a row of pixels. To enhance the signal-to-noise ratio, this calculation was performed with at least 10 rows of adjacent pixels to extract the mean position in each frame. The time-dependent position trace of a hair bundle's movement was obtained by

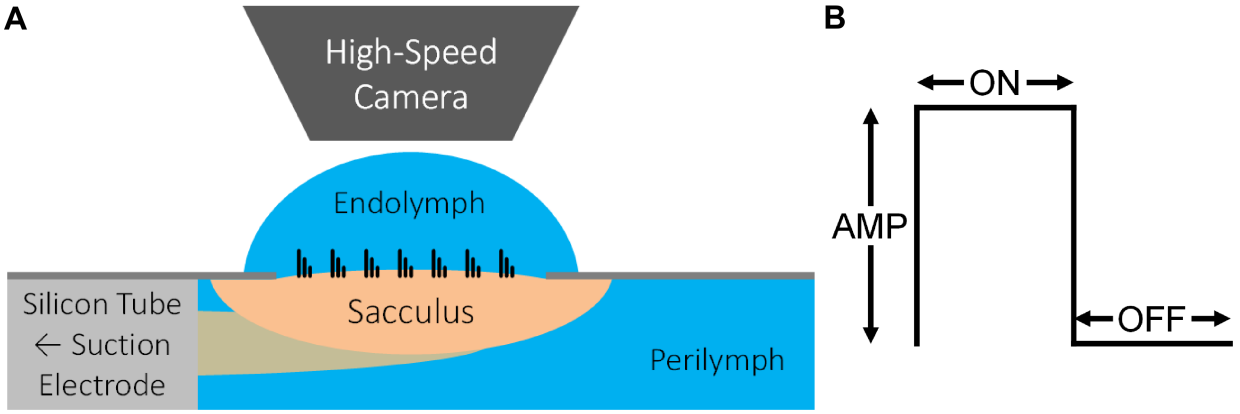


Figure 2.1: **A**) The efferent neurons of the bullfrog sacculus were stimulated by inserting the eighth cranial nerve into a silicon tube, which was connected to a suction electrode. A current stimulus was provided to the suction electrode via a linear stimulus isolator. A two-compartment setup was employed to mimic the ionic concentrations of the natural fluid environment of the sacculus. **B**) Each pulse of a pulse train stimulus was characterized by its amplitude, pulse duration ('on' time) and inter-pulse interval ('off' time).

plotting the mean position for each frame of the recording. For each preparation, multiple hair bundles could be tracked in a field of view. Recordings of bundles within the same epithelium were therefore obtained simultaneously for all stimuli applied.

### 2.2.3 Efferent Stimulation

The saccular nerve was pulled into a 0.5 mm diameter silicon tube [15], which was electrically connected to the positive electrode of a bipolar suction electrode (A-M Systems). The reference electrode was placed into the basolateral compartment (Fig. 2.1A). The preparations were measured to have resistances in the 1 – 2 MΩ range. A linear stimulus isolator (World Precision Instruments A395) provided 10 – 250 $\mu$A of current to the suction electrode, and stimulus protocols were sent to the isolator via LabView (National Instruments). Throughout this manuscript, a pulse train will be described by its 'on' (pulse duration) and 'off' (inter-pulse interval) times (Fig. 2.1B). A typical recording consisted of 2 – 7 s without efferent stimulus, followed by 5 – 7 s of efferent activity, and terminating with a return to the control (no efferent stimulus) condition for 7 – 14 s.

## 2.3 Data Analysis

### 2.3.1 Determination of Oscillation Frequency, Amplitude and Open Probability

In this manuscript, positive displacement in the traces corresponds to motion towards the kinocilium and leading to channel opening, consistent with the standard convention in the literature. Before analysis, the effects of slow drift in the epithelium were subtracted from hair bundle position traces. Traces of hair bundles that underwent only efferent stimulation were split into three sections corresponding to recordings obtained before, during, and after the application of the efferent stimulus and analyzed separately. Each section was established as being oscillatory only if its Hartigans' dip statistic was greater than 0.01 and the associated $p$-value was less than 0.001, an indication of multi-modality in the position distribution [37, 95, 96]. Our analysis only included those position traces for which all three divisions were classified as oscillatory.

Several parameters were extracted from the position traces using software implemented in Python. The histogram of the bundle position was calculated for each of the three sections, and a kernel density estimate was applied to obtain a continuous probability distribution. The two local maxima were identified in each distribution, and the minimum between these peaks was selected to be the threshold between the open channel and closed channel states (Fig. 2.2). The amplitude of the spontaneous oscillation was defined to be half of the distance between the two peaks. The mean open probability was obtained by computing the area under the position distribution plot with a position value greater than the threshold, divided by the area under the full probability density function. Using the aforementioned open channel threshold, any excursion of the bundle beyond the threshold was designated as a positive transition to open transduction channels. The period between two consecutive, positive threshold crossings defined the instantaneous period of one cycle, from which we acquired the instantaneous frequency. All instantaneous frequencies tabulated within a section were averaged to obtain the mean oscillation frequency. Each hair cell was treated as one element of an ensemble. Thus, parameters that were extracted from cells undergoing

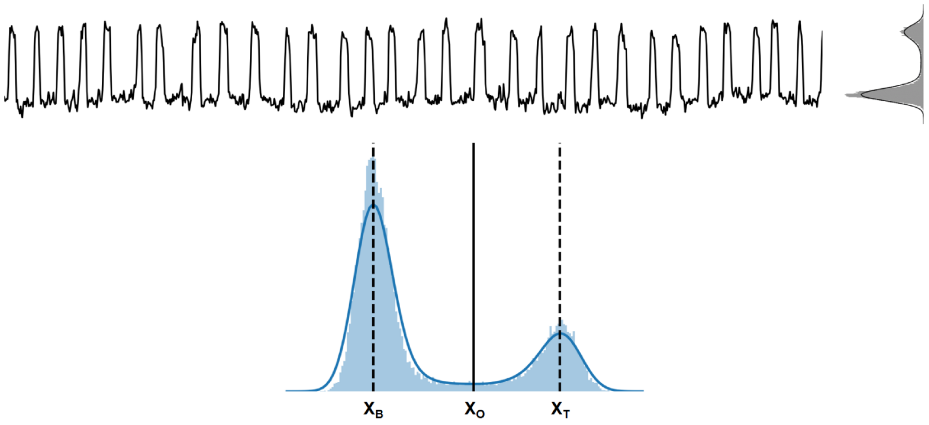


Figure 2.2: For each hair bundle's position trace, a histogram of the bundle position was calculated and a kernel density estimate was applied to obtain a continuous probability distribution. An oscillation profile was established as being oscillatory only if its Hartigans' dip statistic was greater than 0.01 and the associated $p$-value was less than 0.001, an indication of multi-modality in the position distribution. The two local maxima were identified in each distribution ($X_T$ and $X_B$), and the minimum between these peaks ($X_O$) was selected to be the threshold between the open channel and closed channel states. The amplitude of the spontaneous oscillation was defined to be half of the distance between the two peaks. The mean open probability was obtained by computing the area under the position distribution plot with a position value greater than the threshold, divided by the area under the full probability density function. Any excursion of the bundle beyond the threshold was designated as a positive transition to open transduction channels. The period between two consecutive, positive threshold crossings defined the instantaneous period of one cycle, from which we acquired the instantaneous frequency. All instantaneous frequencies tabulated within a section were averaged to obtain the mean oscillation frequency.

the same stimulus conditions were averaged together.

### 2.3.2 Statistical Analysis

All statistical analyses were performed using Python. The difference between a control and a condition for a population was assessed using a one-tailed paired t-test. The differences were considered significant if $p < 0.01$. The sample size for an experiment was considered sufficient if the resulting $p$-values met the requirement for statistical significance. The sample size was defined to be the number of hair cells measured, as the focus of this study is on the effect of efference on individual hair cells, which have been mechanically decoupled by removing the otolithic membrane. The innate activity of the hair bundles within a sacculus have previously been shown to be uncorrelated [86], as there is no known transverse coupling between hair bundles or retrograde effects on the efferent neurons.

## 2.4 Results

### 2.4.1 Efferent stimulation affects hair bundle spontaneous oscillations

We recorded the motion of spontaneously oscillating hair bundles from the sensory epithelium of the American bullfrog sacculus before, during, and after electrically stimulating the saccular nerve. There was no pre-determined location within the macula from which hair bundles were chosen, as all the hair cells in the bullfrog's sacculus have been shown to be highly innervated by efferent fibers [15]. When the efferents were actuated by application of a current to the nerve, hair bundles oscillated with a noticeably higher frequency than they did without efferent stimulation (Fig. 2.3A). This change occurred immediately after the onset of the stimulus (Fig. 2.3B) and ceased upon its termination. The temporal profile of the oscillation also changed upon the stimulus onset, showing smaller and sharper excursions of the bundle.

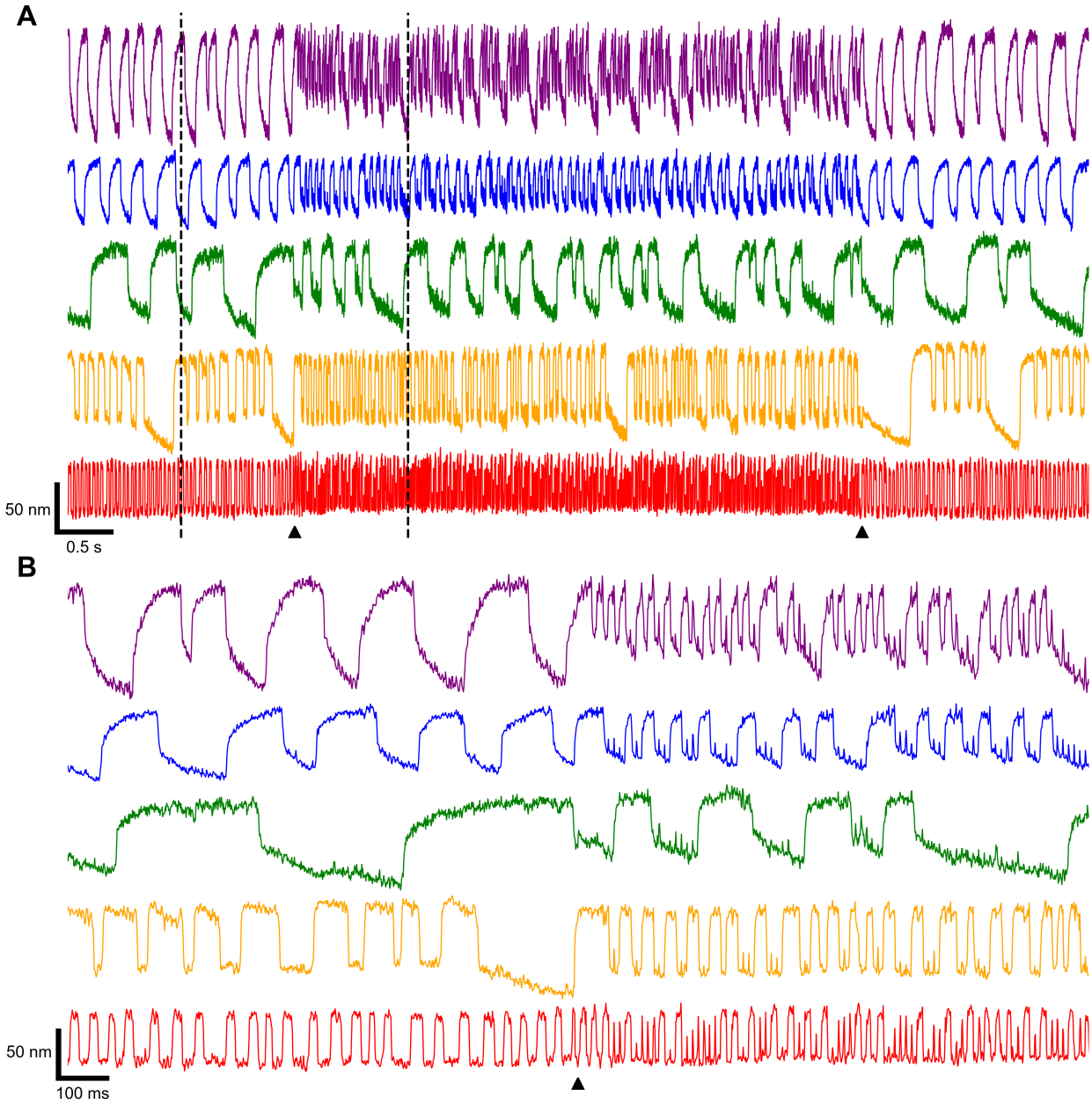


Figure 2.3: The frequency of spontaneous oscillations increased immediately upon the onset of the efferent stimulus. **A**) Spontaneous oscillations before, during, and after efferent modulation (pulse train: 200 $\mu$A, 1 ms 'on', 10 ms 'off') are displayed for five representative hair bundles procured from three different sacculi, shown in different colors, and offset for clarity. The efferent stimulus was in effect for the duration occurring between the two black triangles illustrated below the hair bundle position traces. **B**) A zoom-in of the region between the dashed lines in **A** shows that the stimulus exerts an effect rapidly upon onset.

#### 2.4.1.1 Efference causes frequency to increase and open probability to decrease

Quantitative analysis of the spontaneous oscillation frequencies of 47 hair cells confirmed the observed change and return to original value (Fig. 2.4A). The oscillation frequencies of the hair bundles increased by an average of 15.86 Hz ± 13.53 Hz (one-tailed paired t-test, $t(46)$ = 8.04, $p = 1.31 \times 10^{-10}$). Moreover, analyzing the open probabilities of these same hair cells revealed that the open probability declined during efferent activity and recovered upon cessation of the stimulus (Fig. 2.4C). The open probabilities of the hair bundles decreased by an average of -0.09 ± 0.07 (one-tailed paired t-test, $t(46)$ = -9.11, $p = 3.66 \times 10^{-12}$). While each hair bundle's frequency and open probability increased and decreased, respectively, by a different factor, the same trend was observed across all of the cells measured and by the average behavior of the sampled cells. Furthermore, by computing the individual ratios of the frequency during stimulation (F2) to the frequency prior to stimulation (F1) and averaging over the cells, we found the oscillation frequencies increased by a mean factor, $\langle$F2/F1$\rangle$, of 2.20 ± 0.84 (one-tailed paired t-test, $t(46)$ = 6.36, $p = 4.21 \times 10^{-8}$), seen in (Fig. 2.4B). A similar calculation was performed for the open probability, and it yielded a mean ratio, $\langle$O2/O1$\rangle$, of 0.83 ± 0.13 (one-tailed paired t-test, $t(46)$ = -9.35, $p = 1.67 \times 10^{-12}$).

### 2.4.2 Confirmation of the stimulation of the efferent neurons

The afferent system sends signals from the hair cells to the brain, and the efferent system sends signals from the brain to the hair cells. When the brain sends an electrical pulse to the pre-synaptic terminal, the pre-synapse depolarizes and leads to the opening of voltage-gated $Ca^{2+}$ channels. The influx of $Ca^{2+}$ causes vesicles to fuse with the membrane and release acetylcholine (ACh). The ACh binds to $\alpha 9\alpha 10$ nicotinic acetylcholine receptors (nAChRs), which are connected to $Ca^{2+}$ channels. The $Ca^{2+}$ flowing into the cell soma triggers the $Ca^{2+}$-activated SK2 $K^+$ channels, and the efflux of $K^+$ hyperpolarizes the cell [108].

In order to ensure that our novel efference setup was indeed stimulating the efferent synapses, we performed a number of control experiments. Strychnine and *d*-tubocurarine block acetylcholine receptors from binding with ACh. Thus, if hair cells exhibit a response to the efferent

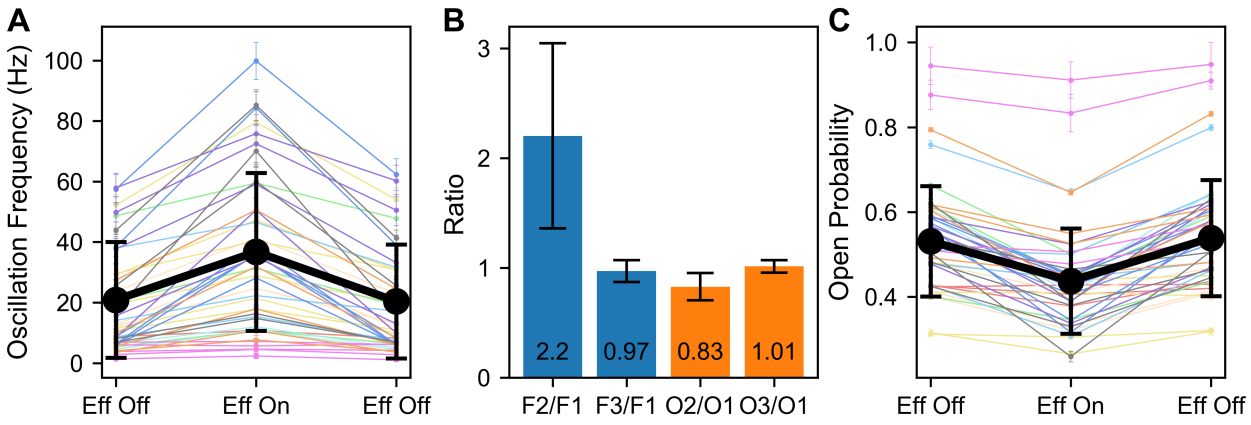


Figure 2.4: The frequency of spontaneous oscillations increased immediately upon the onset of the efferent stimulus. **A**) On average, hair bundles demonstrated an increase in oscillation frequency during stimulation and a return to their original spontaneous oscillation frequency upon cessation of the stimulus. Individual frequency data points are plotted in various colors for hair bundles undergoing the pulse train efferent stimulation described in Fig. 2.3 (pulse train: 200 $\mu$A, 1 ms 'on', 10 ms 'off'). Hair bundles from the same sacculus are plotted in the same color. The corresponding error bars were calculated from the standard deviations of the instantaneous frequencies given by the oscillation cycles during the efferent stimulus. The colored data points in each of the three sections were averaged over 47 hair cells, and the averages are displayed by the large black data points. The black error bars were calculated from the standard deviations of the individual bundle frequencies. The data shown were taken from recordings of 47 hair bundles obtained from 11 sacculi. **C**) Hair bundles displayed, on average, a decrease in open probability during efferent activity, and a return to the original open probability post-stimulus. The colored data points represent the open probabilities of individual hair bundles, and their error bars were obtained by calculating the integrated squared error of the probability density function. Hair bundles from the same sacculus are plotted in the same color. For each stimulus condition, the averages were calculated over 47 hair cells and are plotted in black. Error bars were calculated from the standard deviations of the individual bundle open probabilities. The data shown were obtained from the same hair bundles in **A**. **B**) The ratio of the frequency during efferent modulation (F2) to the frequency pre-stimulus (F1), as well as the ratio of the frequency post-stimulus (F3) to F1, were calculated for every hair bundle shown in **A**. The means of the averages $\langle$F2/F1$\rangle$ and $\langle$F3/F1$\rangle$, computed over 47 cells, are plotted in blue. Analogous open probability ratios ($\langle$O2/O1$\rangle$ and $\langle$O3/O1$\rangle$) were computed, averaged and are shown in orange. Error bars were derived from the standard deviations of the individual ratios. All cells displayed in **A**–**C** were stimulated with the same pulse train parameters detailed in Fig. 2.3.

stimulus in perilymph, but no response to the efferent stimulus with the blockers added into perilymph, then we can verify that the efferent neurons are being stimulated. Moreover, apamin is a known blocker of the SK2 $K^+$ channels and prevents the outward $K^+$ current. This control allows us to further confirm our efference setup, but also verify that the aforementioned efferent mechanism is in operation for a bullfrog saccular hair cell.

#### 2.4.2.1 Blocking nicotinic acetylcholine receptors (nAChRs)

We confirmed that the efferent synaptic activity was crucial for the observed effect by introducing 2 $\mu$M strychnine or 1 $\mu$M *d*-tubocurarine into the basolateral compartment. Both strychnine and *d*-tubocurarine block acetylcholine (ACh) from binding with nicotinic receptors (nAChRs) in the hair cell soma and thereby abolish any effect that the efferent synapses exert on the cell [101, 35]. Upon the addition of either strychnine or *d*-tubocurarine into the perilymph solution, the hair bundles' oscillation profiles remained unchanged during the efferent pulse train (200 $\mu$A, 1 ms 'on', 10 ms 'off') stimulus (Fig. 2.5A, Fig. 2.6A). This was markedly different from the increased frequencies measured in standard perilymph. We observed a full recovery of the original response to efferent actuation in the innate oscillation frequencies of the hair bundles (Fig. 2.5B, Fig. 2.6B) after completing a rinse back to standard perilymph. In standard perilymph, the hair bundles in Fig. 2.5B experienced an average frequency increase of 22.62 Hz $\pm$ 13.84 Hz (one-tailed paired t-test, $t(10) = 5.42$, $p = 0.00015$) during efferent modulation. After the addition of strychnine, the average change in frequency upon efferent stimulation was 0.12 Hz $\pm$ 1.75 Hz (two-tailed paired t-test, $t(10) = 0.23$, $p = 0.82$). In the case of Fig. 2.6B, hair bundles immersed in standard perilymph demonstrated, on average, a frequency increase of 19.32 Hz $\pm$ 9.81 Hz (one-tailed paired t-test, $t(10) = 6.53$, $p = 3.30 \times 10^{-5}$) under efferent stimulation. When *d*-tubocurarine was used to block the nAChRs, the average change in frequency was reduced to -0.11 Hz $\pm$ 0.81 Hz (two-tailed paired t-test, $t(10) = -0.45$, $p = 0.66$).

This control was also performed for a step (200 $\mu$A) stimulus and resulted in the same outcome (Fig. 2.7, Fig. 2.8), with the effects of efferents fully abolished by the blockers.

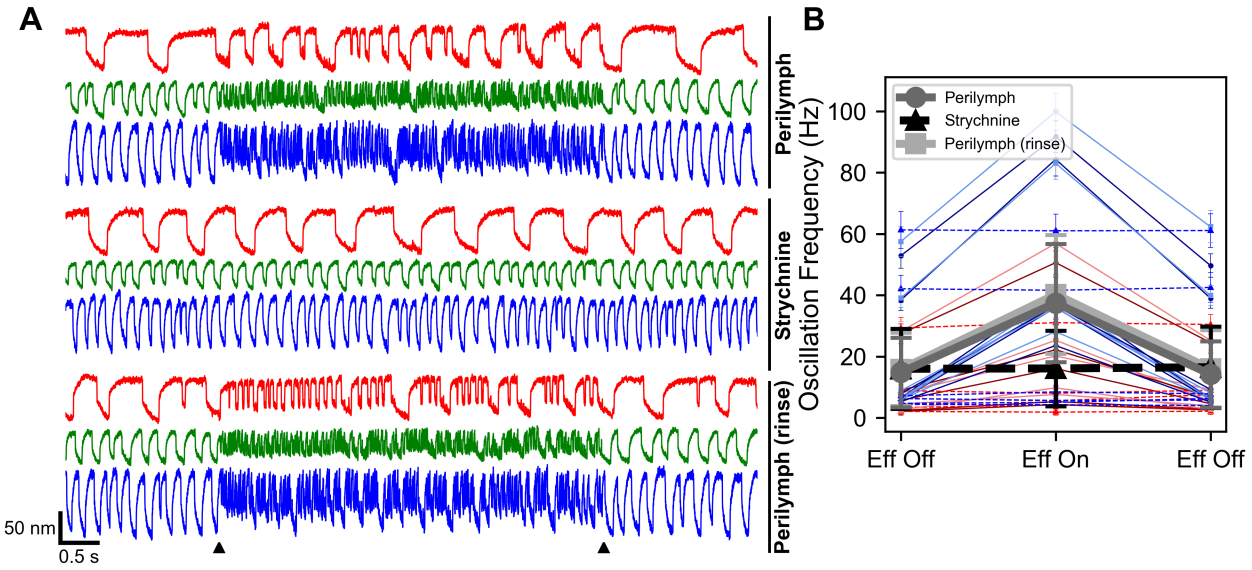


Figure 2.5: Strychnine, added into the perilymph bath solution, abolished the effects of efferent stimulation. **A**) The control was performed for a pulse train stimulus (200 $\mu$A, 1 ms 'on', 10 ms 'off'), and three different bundles are shown. Upon blockage of the receptors, the efferent stimulus exerted no visible effects on innate bundle motility. The average hair bundle oscillation frequency did not change upon efferent stimulation when strychnine (**B**) was introduced into the basal bath solution. Circles, triangles, and squares represent oscillation frequencies in standard perilymph, 2 $\mu$M strychnine perilymph, and standard perilymph (rinse), respectively. **B** was averaged from 11 bundles (2 sacculi). Hair bundles originating from the same sacculus are plotted in shades of the same color. Error bars are the standard deviations of individual hair bundle oscillation frequencies.

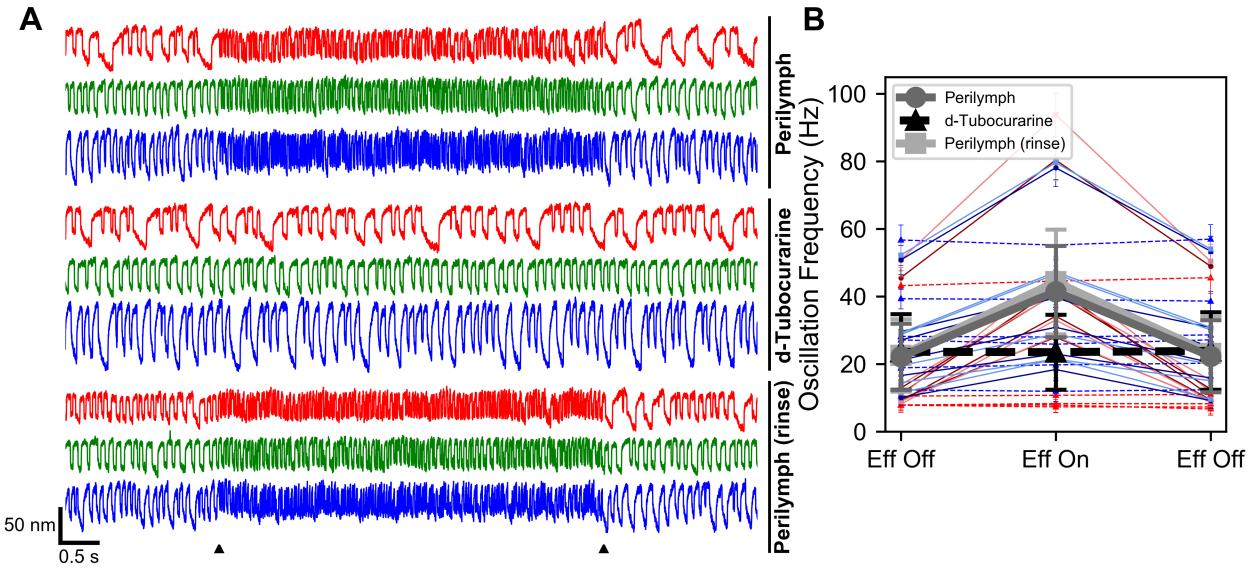


Figure 2.6: *d*-Tubocurarine also abolished the effects of efferent stimulation. **A**) The control was performed for a pulse train stimulus (200 $\mu$A, 1 ms 'on', 10 ms 'off'), and three different bundles are shown. Upon blockage of the receptors, the efferent stimulus exerted no visible effects on innate bundle motility. The average hair bundle oscillation frequency did not change upon efferent stimulation when *d*-tubocurarine (**B**) was introduced into the basal bath solution. Circles, triangles, and squares represent oscillation frequencies in standard perilymph, 1 $\mu$M *d*-tubocurarine perilymph, and standard perilymph (rinse), respectively. **B** was averaged from 11 bundles (2 sacculi). Hair bundles originating from the same sacculus are plotted in shades of the same color. Error bars are the standard deviations of individual hair bundle oscillation frequencies.

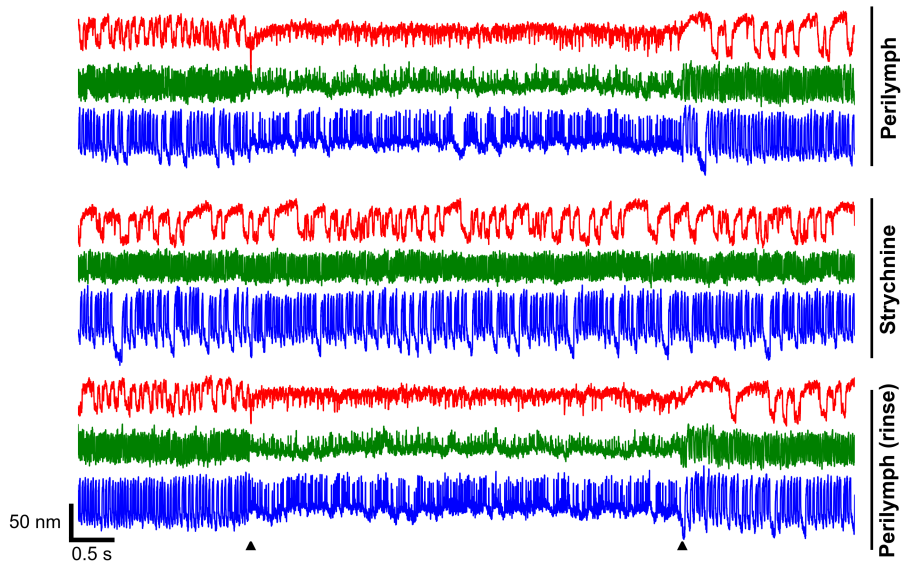


Figure 2.7: After 2 $\mu$M strychnine was added into the perilymph bath solution, the effects of efferent stimulation were eradicated. The control was performed for a step (stimulus: 200 $\mu$A) stimulus, and three different bundles are shown. As with the pulse train stimulus, the efferent step stimulus exerted no influence on hair bundle motility upon blockage of the receptors. These effects were observed in 8 bundles (2 sacculi).

The control experiments confirmed that our method of electrically stimulating the saccular nerve was exerting its effect on hair bundles by activating the efferent neurons.

#### 2.4.2.2 Blocking SK2 channels

As a further control, we applied efferent stimulation in the presence of apamin, a known blocker of the SK2 channels, which was introduced into the perilymph solution. Before the apamin was introduced, the hair bundles oscillated, on average, 7.42 Hz $\pm$ 5.81 Hz (one-tailed paired t-test, $t(9) = 4.04$, $p = 0.0015$) more quickly under efferent stimulation. After the addition of apamin into the perilymph, the difference in oscillation frequency during efferent modulation was 0.17 Hz $\pm$ 0.54 Hz (two-tailed paired t-test, $t(9) = 0.98$, $p = 0.35$). The blocker hence eliminated the effects of efferent activity (Fig. 2.9).

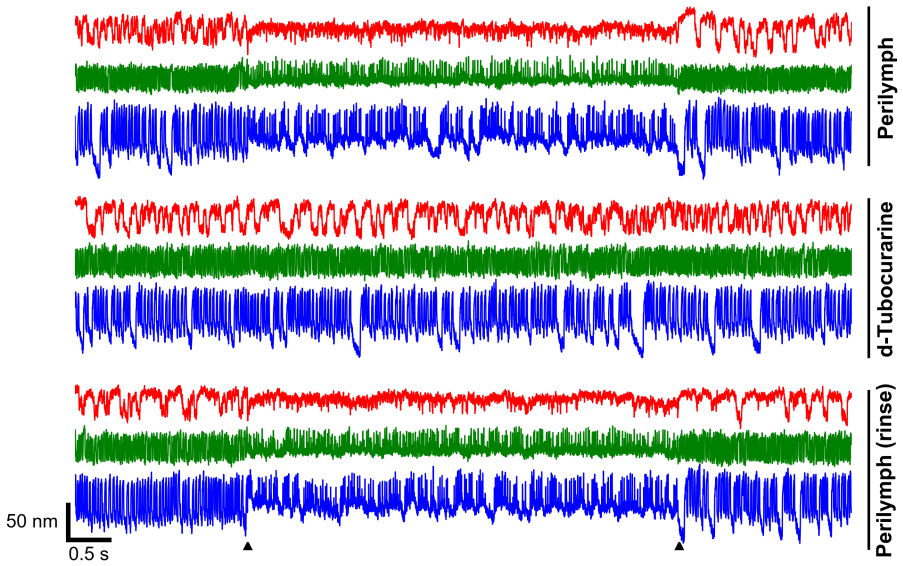


Figure 2.8: After 1 $\mu$M *d*-tubocurarine was added into the perilymph bath solution, the effects of efferent stimulation were eradicated. The control was performed for a step (stimulus: 200 $\mu$A) stimulus, and three different bundles are shown. As with the pulse train stimulus, the efferent step stimulus exerted no influence on hair bundle motility upon blockage of the receptors. These effects were observed in 8 bundles (2 sacculi).

## 2.5 Discussion

The physiology of efferent neurons has been widely explored in prior studies. A subset of the efferents synapse directly onto hair cells, releasing the neurotransmitter acetylcholine and stimulating the $\alpha 9\alpha 10$ nicotinic ACh receptors. The resulting cascade of opening ion channels in the cell soma induces changes in the membrane potential [109]. While the ramifications of these channel openings leads to a complex range of behaviors, efferent activity is inhibitory for most of the stimuli applied [56, 93, 27, 5, 83, 105, 100] and generally leads to hyperpolarization of the hair cell soma [4, 32]. In one study, hyperpolarization of the membrane potential in response to efferent stimulation was demonstrated on hair cells from the bullfrog sacculus [15]. Repeated pulses of efferent stimulus intensified the degree of hyperpolarization up to a saturating level. These electrophysiological data are in accordance with the influx of $Ca^{2+}$ current through cholinergic receptors and a subsequent outward $K^{+}$ current through SK2 channels. The hyperpolarization of the soma in response to efferent actuation

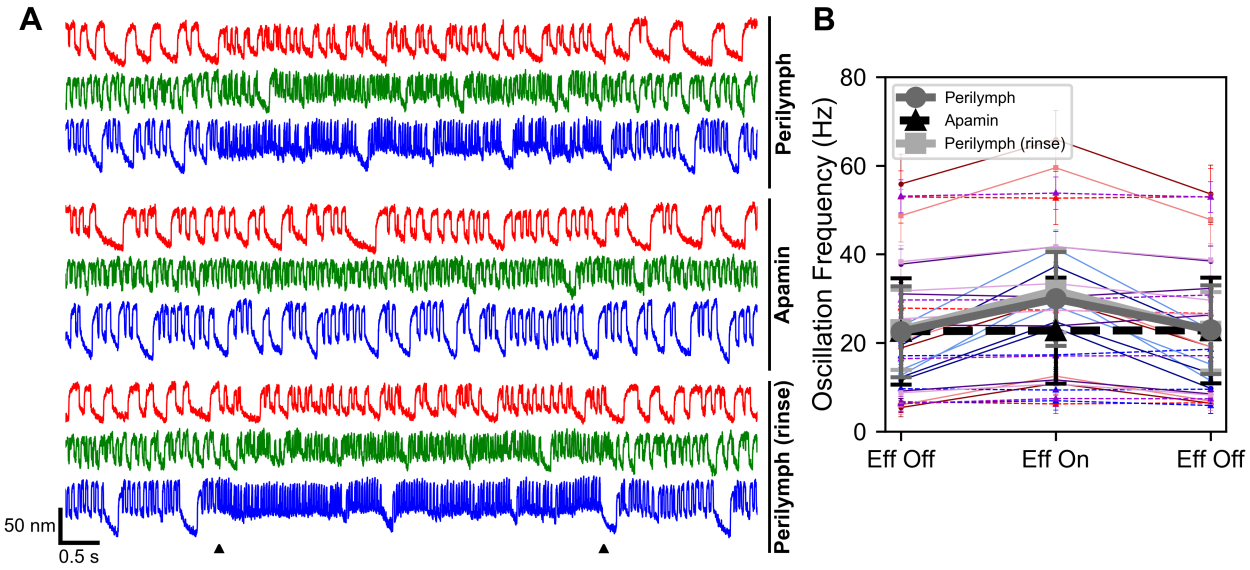


Figure 2.9: Apamin, a SK2 channel blocker, nullified the effects of efferent stimulation when added into the perilymph bath solution. The control was performed for a pulse train stimulus (**A**, stimulus: 200 $\mu$A, 1 ms 'on', 10 ms 'off'). Efferent modulation imposed no visible effects on the spontaneous bundle oscillations consequent to the blockage of the SK2 channels. **B**) The average hair bundle oscillation frequency did not change upon efferent activity when apamin was incorporated into the basal bath solution. Circles, triangles, and squares represent oscillation frequencies in standard perilymph, apamin perilymph, and standard perilymph (rinse), respectively. **B** was averaged from 10 bundles (3 sacculi). Hair bundles originating from the same sacculus are plotted in shades of the same color. Error bars are the standard deviations of individual hair bundle oscillation frequencies.

seems to be consistent across a number of species studied [4, 109]. Furthermore, a combination of cell electrophysiology and mechanical bundle manipulation likewise demonstrated that membrane potential impacts active motility [72]. Steady-state changes in the membrane potential were found to modulate the frequency, amplitude, and shape of spontaneous oscillations. Specifically, hyperpolarizing a hair cell evoked an increase in the spontaneous oscillation frequency of the hair bundle, a decrease in the amplitude, and a reduced mean opening probability. The repercussions on hair bundle mechanics that we observed with efferent stimulation are hence consistent with these prior studies.

We presented and confirmed the efficacy and robustness of our novel method for stimulating the saccular efferent neurons. While we have affirmed the activation of the efferent fibers that synapse directly onto hair cells, it is important to note that the other subset of efferents target the afferent terminals of hair cells. The stimulus protocol activates both of these efferent types, as well as afferent neurons. However, there is no known retrograde effect of afferents on hair cell activity. Hence, we assume purely efferent effects on the observed phenomena.

# CHAPTER 3

# Dependence of Innate Bundle Motility on Efferent Stimulus Parameters

## 3.1 Introduction

In this chapter, we explore the relationship between the characteristics of an efferent pulse train stimulus and the spontaneous oscillation profile of a hair bundle whose efferent synapses are being stimulated. We show that variations of the pulse train stimulus applied to the saccular nerve resulted in quantifiable changes to the spontaneous oscillation profile of the hair bundles. That is to say, varying the parameters of a pulse train stimulus affected a hair bundle's oscillation frequency, amplitude, and open probability. Hair cells were also observed to become entrained to the efferent stimulus, and the strength of the synchronization was dependent on the amplitude of the stimulus current. Lastly, we examine the long-term impact of efference on a hair cell by studying the transient changes in a hair bundle's spontaneous oscillation profile. We present our findings on hair cell efferent habituation, a new phenomenon that we observed wherein hair bundles exhibited a form of "adaptation" to efference as demonstrated by a regression back to its initial, unstimulated oscillatory motions.

## 3.2 Materials and Methods

### 3.2.1 Biological Preparation

Refer to Section 2.2.1.

### 3.2.2 Imaging and Tracking Hair Bundle Motion

Refer to Section 2.2.2.

### 3.2.3 Efferent Stimulation

Refer to Section 2.2.3. For experiments exploring the long-term impact of efferent activity, 20 seconds of efferent modulation were delivered in the form of a 200 $\mu$A pulse train with a 3 ms pulse duration and a 10 ms inter-pulse interval.

## 3.3 Data Analysis

### 3.3.1 Determination of Oscillation Frequency, Amplitude and Open Probability

Refer to Section 2.3.1. For the determination of instantaneous oscillation frequencies, amplitudes, and open probabilities, refer to Section 5.2.4.2.

### 3.3.2 Statistical Analysis

Refer to Section 2.3.2.

## 3.4 Results

### 3.4.1 Hair bundle's response to efferent modulation is dependent on stimulus parameters

When an electrical pulse is sent to the pre-synaptic terminal, the terminal becomes depolarized and releases acetylcholine [108]. The ACh binds to $\alpha 9\alpha 10$ nicotinic receptors [31, 9, 33], which enhances the influx of $Ca^{2+}$ ions into the hair cell soma. The elevated $Ca^{2+}$ level triggers the opening of $Ca^{2+}$-activated SK2 $K^+$ channels [11, 80, 91], and the efflux of $K^+$ hyperpolarizes the cell [26, 25, 50]. The extent to which the hair cell becomes hyperpolarized is hence determined by the amount of acetylcholine that is released at the synapses, which is in turn influenced by the applied electrical signal [103, 110]. We therefore varied

the parameters of the efferent stimulus pulse trains and observed the effects of this variation on the hair bundle's spontaneous oscillation profile.

#### 3.4.1.1 Variation of pulse duration (ON time)

We presented pulse train stimuli via the suction electrode, and separately varied the pulse duration ('on' time) and the interval between pulses ('off' time). For the first set of experiments, the amplitude was kept constant at 200 $\mu$A and the 'off' time at 10 ms, with the pulse duration incrementally extended from 0.5 ms to 50 ms (Fig. 3.1). Initially, the hair bundles oscillated more rapidly with increasing pulse duration. As the 'on' time was further increased, the hair bundles began to show rapid, spike-like excursions and an increasing propensity for the closed channel state. In addition, a slow cumulative offset in the negative direction was observed in the last few traces of Fig. 3.1A. This induced negative drift was detected for the majority of the hair bundles measured. Of the hair bundles that exhibited this characteristic (9 of the 10 cells recorded across 2 preparations), the magnitude of the drift positively correlated with the 'on' time. At the highest 'on' time of 50 ms, the bundles drifted by an average of 55 nm $\pm$ 35 nm in the negative direction (away from the kinocilium), with some bundles drifting up to 140 nm. All bundles were observed to recover from their negative offset, with recovery from stimuli with longer pulse durations being more protracted. Likewise, the bundles that were seen to oscillate with a lower frequency directly post stimulus were observed to return to their initial spontaneous oscillation frequencies.

To quantify the impact of varying efferent stimuli on the innate motility of hair bundles, we used oscillation analysis software implemented in Python. Three parameters were extracted to characterize the temporal profile of the bundle oscillation: oscillation frequency (Fig. 3.2A), oscillation amplitude (Fig. 3.2B), and mean channel open probability (Fig. 3.2C). The changes induced in the hair bundles' oscillations were measured with changing stimulus pulse durations ('on' time). As aforementioned, hair bundles oscillated more briskly with increasing 'on' times; however, for most bundles, their oscillation frequencies declined once they began spiking (Fig. 3.3A). However, approximately a third of the bundles we recorded

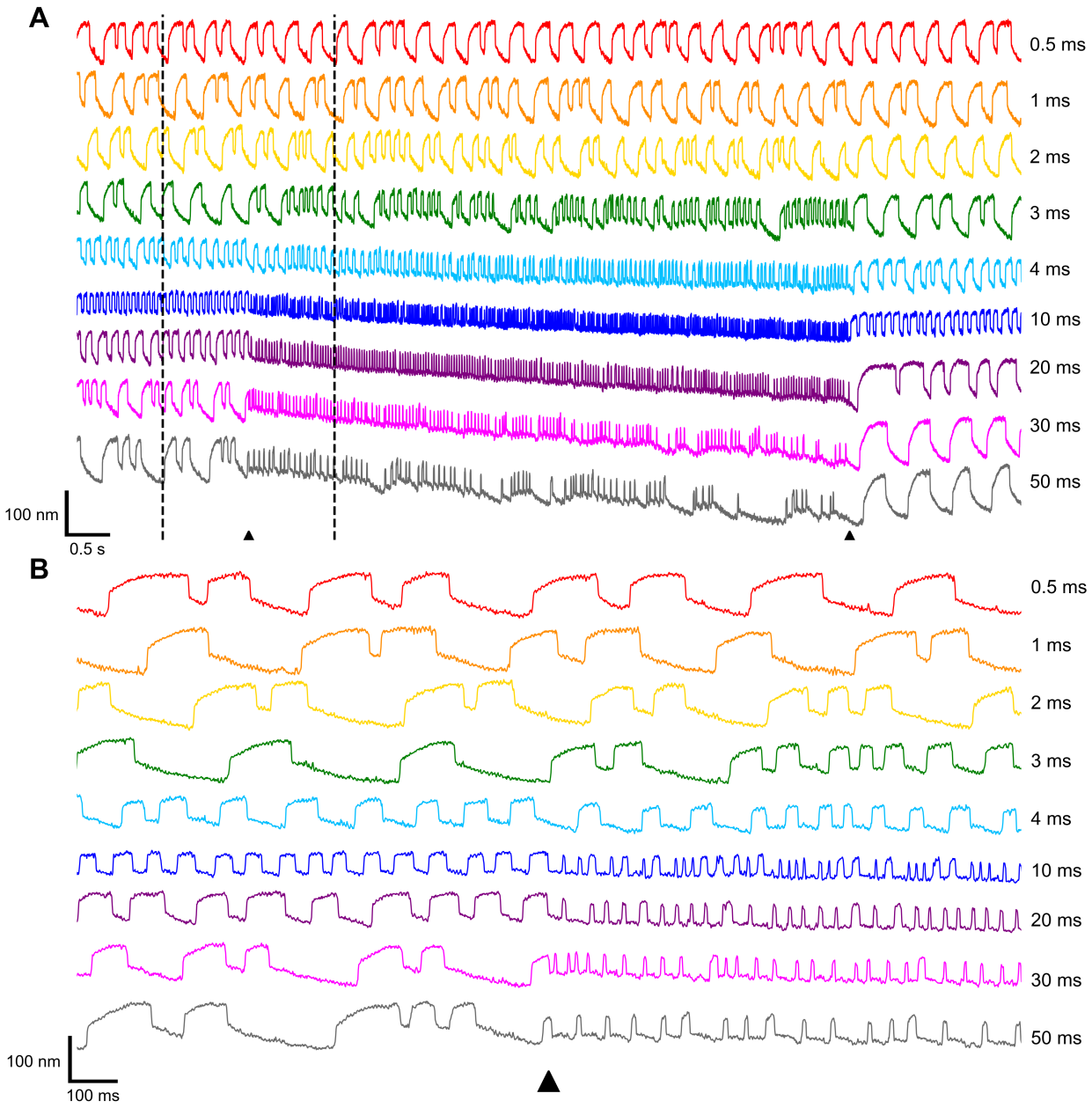


Figure 3.1: Lengthening the pulse duration of the efference pulse train led to oscillation suppression. The amplitude of the pulse train was kept constant at 200 $\mu$A, while the pulse duration ('on' time) was varied. **A**) The inter-pulse interval was kept at 10 ms while the pulse duration was systematically altered. As the pulse duration increased, the oscillation frequency of the bundle correspondingly increased until the bundle began to exhibit short spike-like excursions, seen in the zoom-in (**B**) of the region between the dashed lines in **A**. The efferent stimulus occurred between the two black triangles illustrated below the hair bundle position traces. The corresponding 'on' time of each oscillation trace is indicated on the right.

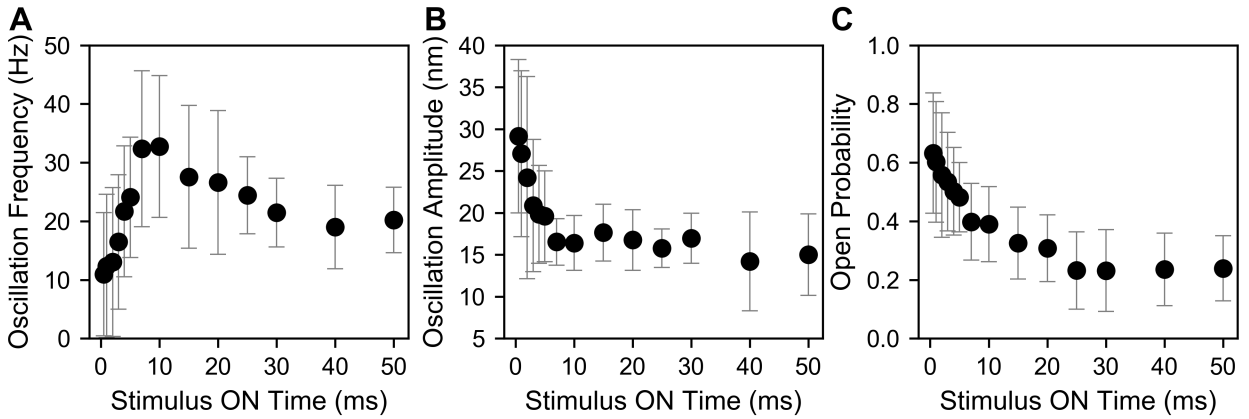


Figure 3.2: Lengthening the pulse duration of the efference pulse train affected a hair bundle's oscillation frequency, amplitude, and open probability. **A**–**C**) Increasing the 'on' time from 0.5 ms up to 50 ms led to a decrease in both the oscillation amplitude and the open probability. Averaging the behavior of both types of bundles seen in Fig. 3.3 produces a peak in the oscillation frequency with a softened falloff. **A**–**C** are the results of averaging the data from 10 bundles (2 sacculi). Error bars were computed from the standard deviations of the measurements of individual hair bundles.

did not exhibit spiking; instead, their oscillation frequencies plateaued with rising 'on' times (Fig. 3.3B). Fig. 3.2A represents the mean behavior of both of these classes. All cells showed a decrease in their oscillation amplitudes in conjunction with increasing 'on' times (Fig. 3.2B), as observed qualitatively. The change from regular oscillations to rapid, spike-like motion is reflected by the increased occurrence of the closed-channel state, and hence lower mean open probability (Fig. 3.2C). There were no observable behavioral differences between the two classes of cells for Fig. 3.2B or Fig. 3.2C. The data in Fig. 3.2 was obtained by averaging over 10 bundles (2 sacculi).

#### 3.4.1.2 Variation of inter-pulse interval (OFF time)

We presented pulse train stimuli via the suction electrode, and separately varied the pulse duration ('on' time) and the interval between pulses ('off' time). Here, the inter-pulse interval was decreased from 40 ms to 1 ms, while maintaining a constant amplitude of 200 $\mu$A and a pulse duration of 1 ms (Fig. 3.4). Decreasing the 'off' time of the pulse train elicited similar results to those observed when increasing the 'on' time of the pulse train; the frequency of

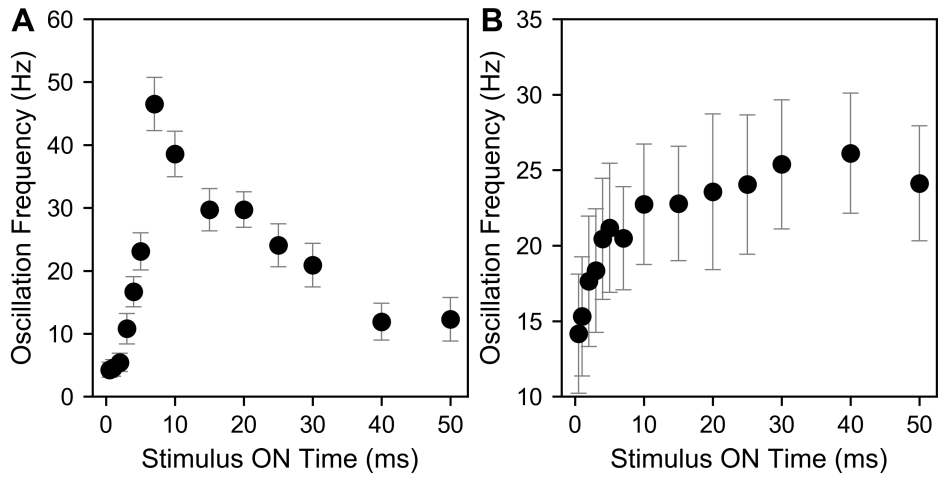


Figure 3.3: Incrementally changing a pulse train's 'on' time resulted in two categories of hair bundle responses. In both categories, increasing the pulse duration initially elevated the bundle's oscillation frequency. Afterwards, some bundles experienced a peak in their oscillation frequency, followed by a frequency decline corresponding to the exhibition of spiking behavior (**A**). The other group of bundles displayed a plateau in their oscillation frequency (**B**). Error bars were calculated in the same manner described for the individual hair bundles in Fig. 2.4A.

the bundle oscillations increased as the 'off' time decreased.

To quantify the impact of varying efferent stimuli on the innate motility of hair bundles, we used oscillation analysis software implemented in Python. Three parameters were extracted to characterize the temporal profile of the bundle oscillation: oscillation frequency (Fig. 3.5A), oscillation amplitude (Fig. 3.5B), and mean channel open probability (Fig. 3.5C). The changes induced in the hair bundles' oscillations were measured with changing stimulus inter-pulse intervals ('off' time). As aforementioned, the plots detailing the relationship between the variable 'off' time with the measured bundle oscillation frequency and oscillation amplitude (Fig. 3.5A, B) predictably followed the visible trends shown in Fig. 3.4. The mean open probability was very weakly affected by variations in the 'off' time of the stimulus train (Fig. 3.5C). The data in Fig. 3.5 was obtained by averaging over 7 bundles (2 sacculi).

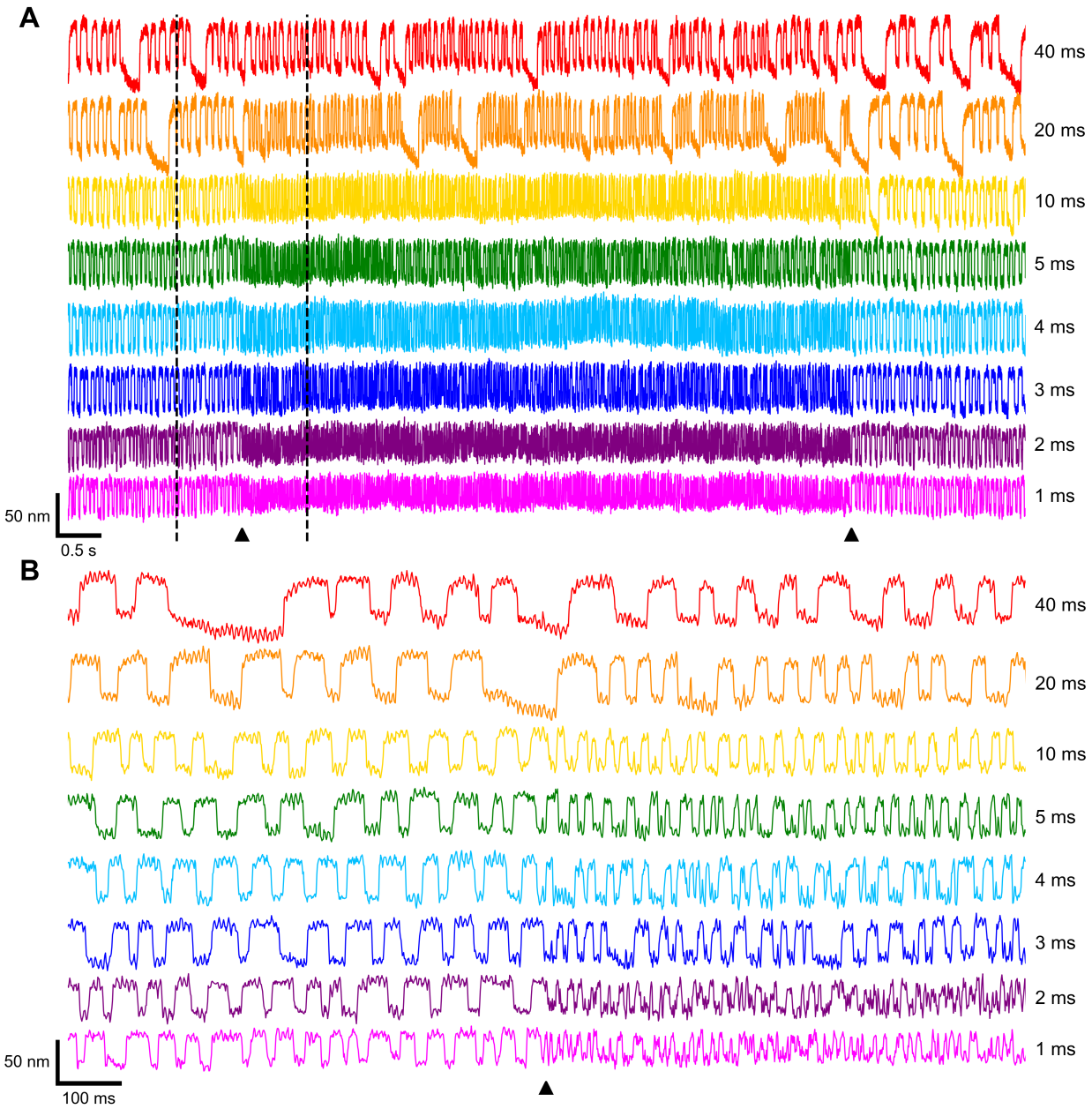


Figure 3.4: Shortening the duration between pulses led to an increase in oscillation frequency. The amplitude of the pulse train was kept constant at 200 $\mu$A, while the interval between pulses ('off' time) was varied. **A**) The inter-pulse interval was systematically varied, with the pulse duration held constant at 1 ms. The hair bundle's oscillation frequency increased with decreasing inter-pulse interval, seen clearly in the zoom-in (**B**) of the region between the dashed lines in **A**. The efferent stimulus occurred between the two black triangles illustrated below the hair bundle position traces. The corresponding 'off' time of each oscillation trace is indicated on the right.

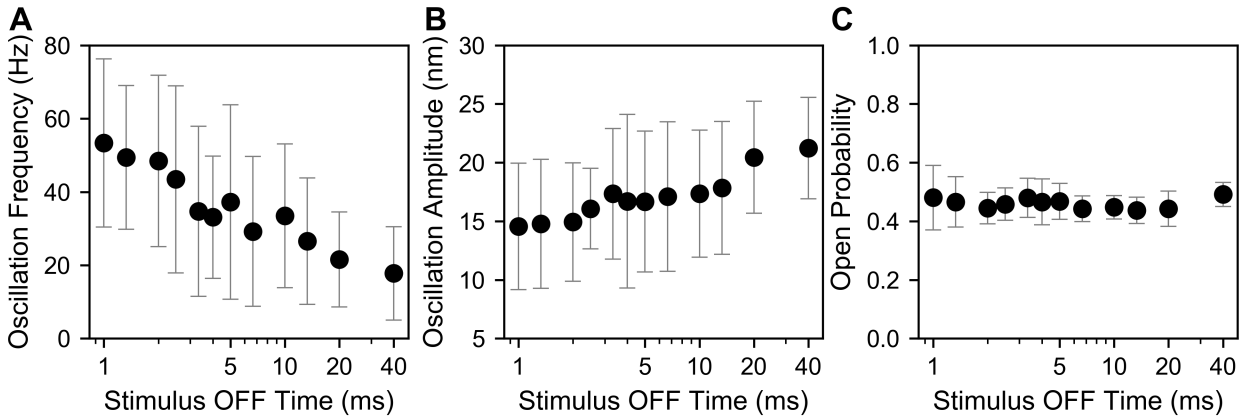


Figure 3.5: Shortening the duration between pulses affected a hair bundle's oscillation frequency, amplitude, and open probability. **A**–**C**) Decreasing the 'off' time from 40 ms to 1 ms led to an increase in the oscillation frequency. As with increasing the 'on' time, the oscillation amplitude declined, while the open probability was fairly unaffected. **A**–**C** were derived with data from 7 bundles (2 sacculi). Error bars were computed from the standard deviations of the measurements of individual hair bundles.

#### 3.4.1.3 Variation of pulse amplitude

Lastly, we investigated the dependence of the hair bundles' oscillation profiles on the amplitude of the applied efferent stimulus. We increased the amplitude of the pulse train (3 ms 'on' time and 10 ms 'off' time) from 10 $\mu$A to 250 $\mu$A. The bundle traces shown in Fig. 3.6 demonstrate that the rising current amplitude elevated the impact of the efferent activity. A similar outcome was achieved when the experiment was repeated with a current step applied instead of a pulse train (Fig. 3.7). Oscillation suppression was attained more readily with the step stimulus than with the pulse train stimulus. Additionally, half (6 of the 12 hair cells recorded across 3 preparations) of the hair bundles were observed to negatively drift during the step stimulus.

To quantify the impact of varying efferent stimuli on the innate motility of hair bundles, we used oscillation analysis software implemented in Python. Again, three parameters were extracted to characterize the temporal profile of the bundle oscillation: oscillation frequency (Fig. 3.8A), oscillation amplitude (Fig. 3.8B), and mean channel open probability (Fig. 3.8C). The changes induced in the hair bundles' oscillations were measured with changing

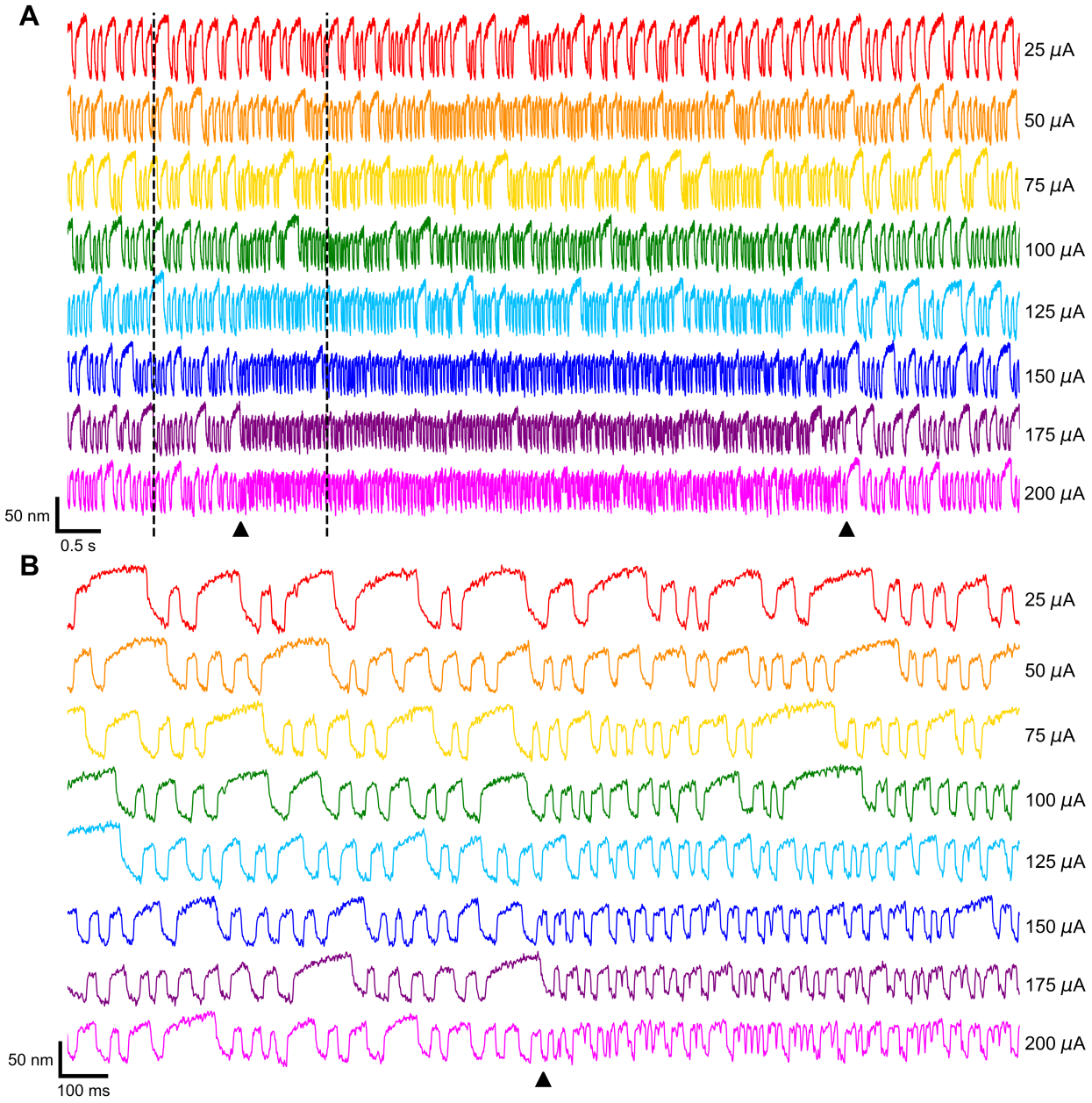


Figure 3.6: Increasing the stimulus amplitude of a pulse train intensified the effect of the efferent stimulation. In **A**, the pulse duration and inter-pulse interval of the pulse train applied to the saccular nerve were kept constant (3 ms 'on' and 10 ms 'off' time), while the current amplitude was systematically varied. When the amplitude was increased, the frequency of the spontaneous oscillations increased, as seen in the zoom-in (**B**) of the region between the dashed lines in **A**. The efferent stimulus occurred between the two black triangles illustrated below the hair bundle position traces. The corresponding current amplitudes of each oscillation trace is labeled on the right.

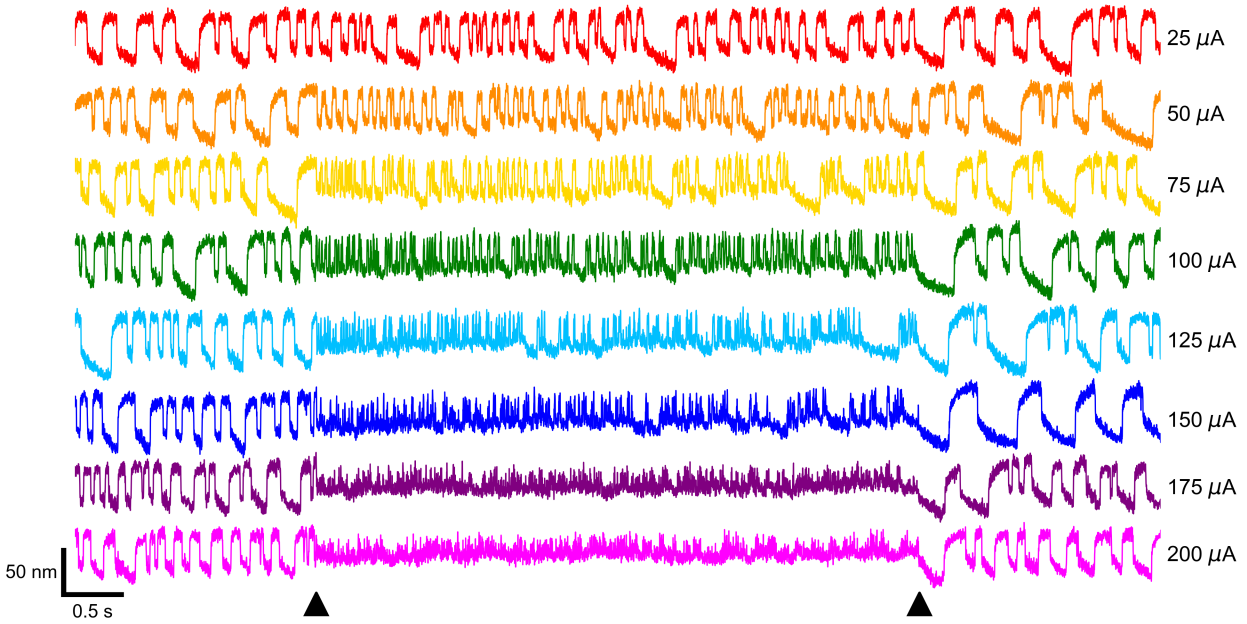


Figure 3.7: Increasing the stimulus amplitude of a step efferent stimulus also escalated the effect of the efferent modulation. A continuous step stimulus was applied to the saccular nerve, and the frequency of the spontaneous oscillations increased. The oscillations were suppressed at high amplitudes of the current. The efferent stimulus occurred between the two black triangles illustrated below the hair bundle position traces. The corresponding current amplitudes of each oscillation trace is labeled on the right.

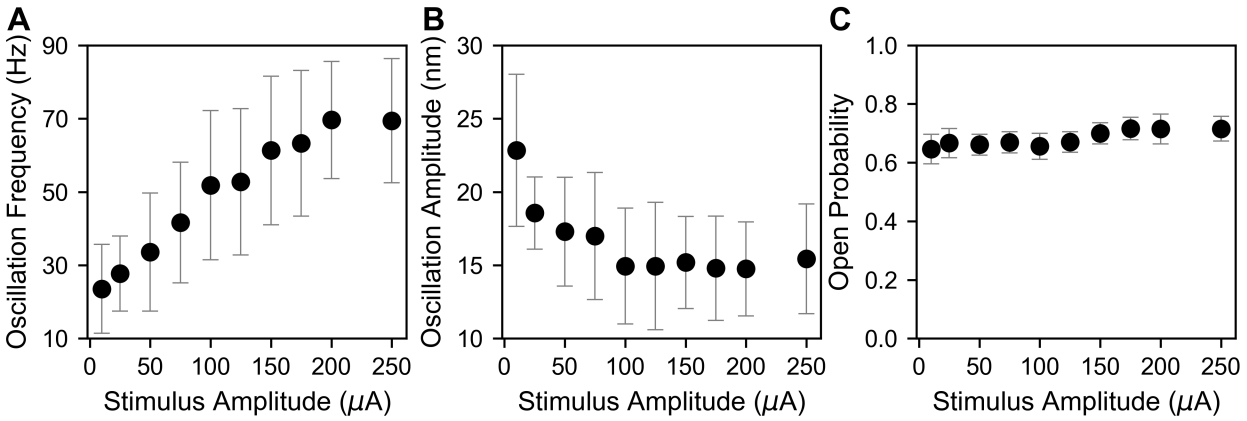


Figure 3.8: Increasing the stimulus amplitude of a pulse train affected a hair bundle's oscillation frequency, amplitude, and open probability. **A**–**C**) Predictably, increasing the amplitude of the pulse train raised the oscillation frequency and reduced the oscillation amplitude. However, the open probability remained relatively constant. **A**–**C**s are the results of averaging the data from 9 bundles (2 sacculi). Error bars were computed from the standard deviations of the measurements of individual hair bundles.

stimulus amplitudes. As aforementioned, the effect of increasing current amplitude was to enhance the frequency (Fig. 3.8A) and decrease the amplitude of the bundle oscillation (Fig. 3.8B); the impact on the mean open probability was similarly weak (Fig. 3.8C). The data in Fig. 3.8 was obtained by averaging over 9 bundles (2 sacculi).

#### 3.4.1.4 Synchronization of the hair bundle to the efferent stimulus

Looking at Fig. 2.3B, it is noticeable that the efferent stimulation transformed the hair bundle spontaneous oscillations in a manner such that the position traces appear like superimpositions of a spiking pattern on top of regular bundle oscillations. In order to examine this observation, we analyzed the power spectral densities (PSDs) of the hair bundle's innate oscillations, which allows us to examine the impact of efference on a hair cell's active motility in the frequency domain. Fig. 3.9 illustrates how a bundle's PSD transforms in response to efferent modulation. The PSDs displayed in Fig. 3.9A and Fig. 3.9B are calculated from the red and blue traces in Fig. 2.3, respectively. The beginning and ending thirds of the oscillation trace – without efferent actuation – are plotted in gray and blue, respectively. The PSD of the middle, stimulated section is displayed in red. As a reminder, the efferent

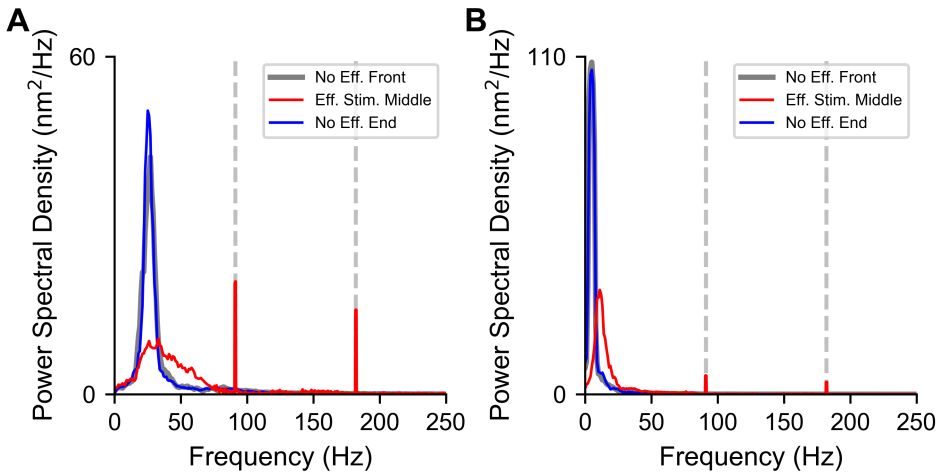


Figure 3.9: Pulse train efferent stimulation resulted in entrainment at the frequency of the pulse train. When the efferent neurons are activated by a pulse train stimulus, the power spectral density (PSD) of a hair bundle's spontaneous oscillations exhibits peaks at the frequency of the efference pulse train and its harmonics. The PSDs displayed in **A** and **B** were calculated from the red and blue traces in Fig. 2.3, respectively. The front and end (efference-off) sections of the oscillation trace are plotted in gray and blue, respectively. The PSD of the middle, efference-on section is displayed in red. The efferent neurons of both hair cells were actuated by a 91 Hz pulse train stimulus (pulse train: 200 $\mu$A, 1 ms 'on', 10 ms 'off'). Gray dashed lines pinpoint the frequency of the efference pulse train and its harmonics.

neurons of both hair cells were actuated by a 91 Hz pulse train stimulus (pulse train: 200 $\mu$A, 1 ms 'on', 10 ms 'off'). The gray dashed lines identify the locations of the frequency of the efference pulse train and its harmonics. When the efferent neurons were activated by a pulse train stimulus, the power spectral density (PSD) of a hair bundle's spontaneous oscillations exhibited peaks at the frequency of the efference pulse train and its harmonics. We found that the pulse train efferent stimulation resulted in entrainment at the frequency of the pulse train, in addition to a clear rehabilitation of the initial PSD.

Furthermore, the strength of this entrainment was dependent on the amplitude of the efferent stimulus. We found the power spectral densities of spontaneous oscillations under concurrent efferent actuation were dependent on the amplitude of the efferent stimulus. In Fig. 3.10, the PSDs of a hair bundle's innate oscillations with simultaneous efferent stimulation are

plotted in violet, blue, green, gold, and red for a stimulus amplitude of 0 $\mu$A, 50 $\mu$A, 100 $\mu$A, 150 $\mu$A, and 200 $\mu$A. The data presented reflects recordings collected from four hair bundles sourced from two sacculi. The pulse duration and inter-pulse interval of the applied efferent pulse train were kept constant (3 ms 'on', 10 ms 'off'), and the stimulus amplitude was varied. The inset plot displays a zoom-in of the peak at the efference pulse train frequency, 77 Hz. The gray dashed lines identify the frequency of the efference pulse train and its harmonics. Increasing the current amplitude resulted in a greater degree of phase-locking, as evinced by the notable growth in the peak at the frequency of the pulse train efferent stimulus coupled with a flattening of the lower frequency, broader peak under 0 $\mu$A. As expected, the height of the peak at the frequency of the pulse train stimulus was strongly dependent on the amplitude of the efferent stimulus.

We quantified this relationship between the efference amplitude and the height of the peak at the stimulus frequency (77 Hz) in Fig. 3.11. Increasing the current amplitude of the efferent stimulus generally led to enhanced phase-locking at the frequency of the efferent pulse train. On average, the height of the peak at the frequency of the pulse train grew in magnitude with elevated stimulus amplitudes. Individual frequency data points are plotted in various colors for hair bundles undergoing the same 77 Hz pulse train efferent stimulation (pulse train: 200 $\mu$A, 3 ms 'on', 10 ms 'off'). Data points from the same hair bundle are connected together. The colored data points were averaged over 15 hair cells, and the averages are displayed by the large black data points. The black error bars were calculated from the standard deviations of the individual bundle peak heights. The data shown were taken from recordings of 15 hair bundles obtained from 5 sacculi.

### 3.4.2 Hair bundles may exhibit habituation during extended efferent activation

In the previous section, we explored the temporary shifts in innate bundle dynamics effectuated by short-term efferent actuation. Given the significant impact observed even upon brief efferent stimulation, further investigation into the effect of long-term efferent actuation is warranted.

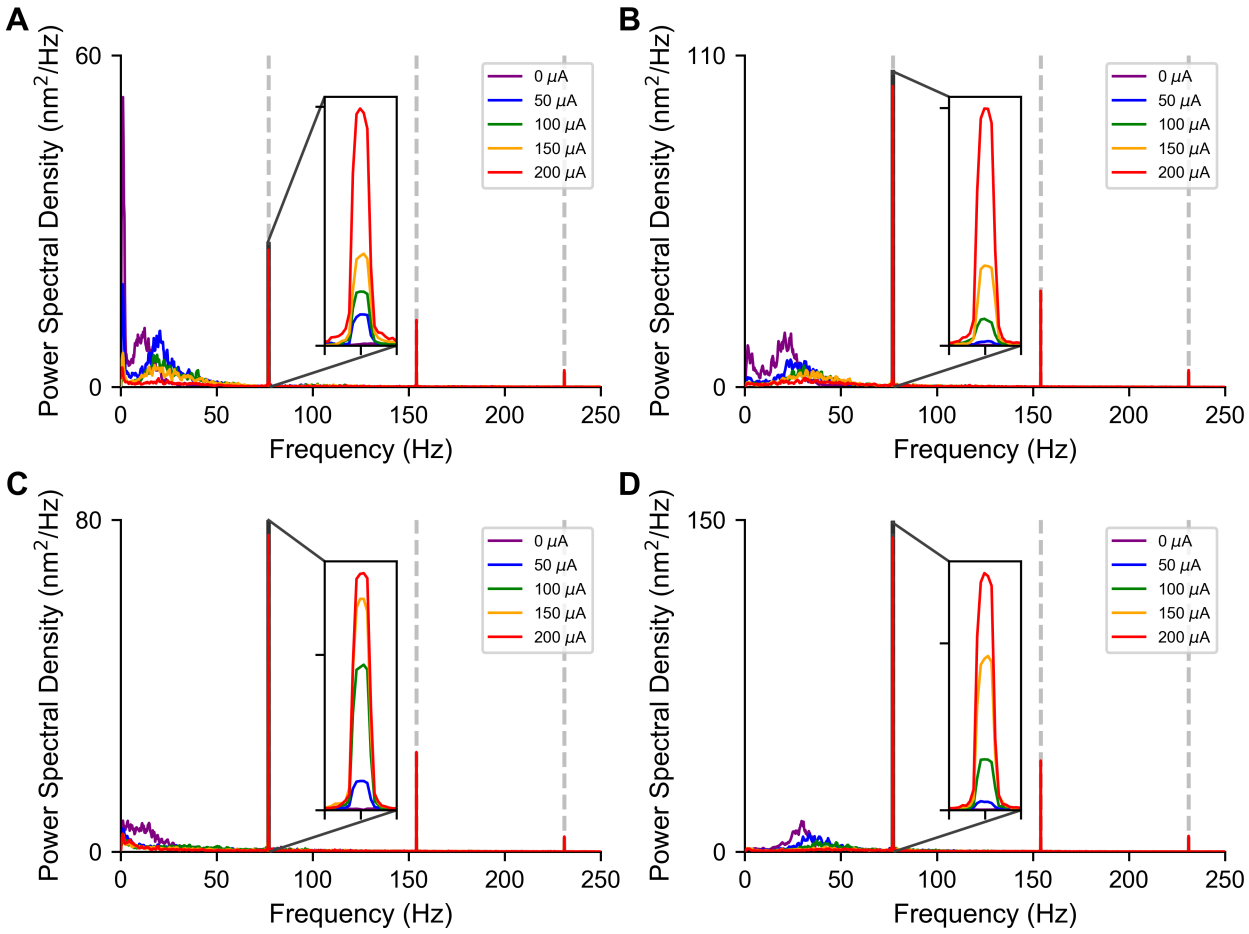


Figure 3.10: The power spectral densities (PSDs) of spontaneous oscillations under concurrent efferent actuation were dependent on the amplitude of the efferent stimulus. Power spectral densities of a hair bundle's innate oscillations with simultaneous efferent stimulation are plotted in violet, blue, green, gold, and red for a stimulus amplitude of 0 $\mu$A, 50 $\mu$A, 100 $\mu$A, 150 $\mu$A, and 200 $\mu$A. The pulse duration and inter-pulse interval of the pulse train applied to the saccular nerve were kept constant (3 ms 'on', 10 ms 'off'), and the stimulus amplitude was varied. The inset plot displays a zoom-in of the peak at the efference pulse train frequency, 77 Hz. Gray dashed lines identify the frequency of the efference pulse train and its harmonics. As expected, the height of the peak at the frequency of the pulse train stimulus was strongly dependent on the amplitude of the efferent stimulus. The height of the 77 Hz peak experienced significant growth with larger current amplitudes. The data presented reflects recordings collected from four hair bundles sourced from two sacculi.

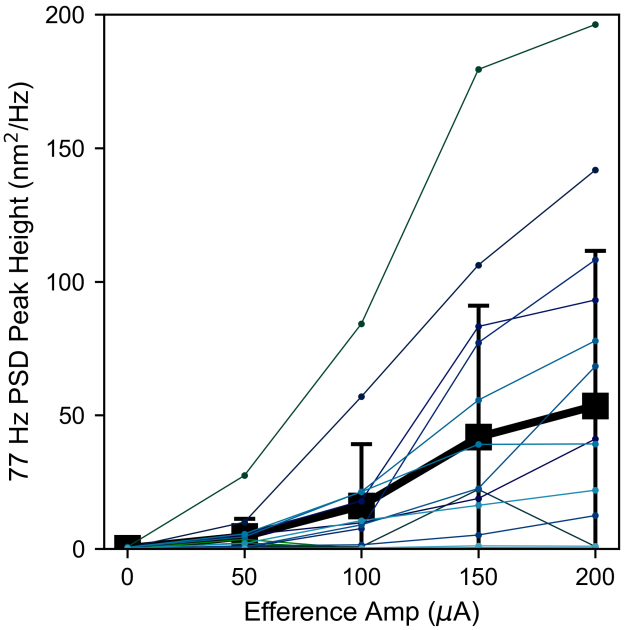


Figure 3.11: Increasing the current amplitude of the efferent stimulus led to enhanced phase-locking at the frequency of the efferent pulse train. On average, the height of the peak at the frequency of the pulse train grew in magnitude with elevated stimulus amplitudes. Individual frequency data points are plotted in various colors for hair bundles undergoing the same 77 Hz pulse train efferent stimulation (pulse train: 200 $\mu$A, 3 ms 'on', 10 ms 'off'). The colored data points were averaged over 15 hair cells, and the averages are shown by the large black data points. The black error bars were calculated from the standard deviations of the individual bundle peak heights. The data shown were taken from recordings of 15 hair bundles obtained from 5 sacculi.

#### 3.4.2.1 Oscillation profiles of habituating and non-habituating hair cells

In order to investigate the long-term impact of efferent activity on a hair bundle's innate motility, the motion of spontaneously oscillating hair bundles was recorded while simultaneously electrically stimulating the saccular nerve for 20 s with a 200 $\mu$A (3 ms 'on', 10 ms 'off') pulse train. A dichotomy emerged in the ensemble of hair bundles measured, with one set of bundles showing oscillation profiles that changed over time (habituating hair cells) and one set whose oscillatory motion remained the same (non-habituating hair cells) upon prolonged efferent stimulation. The common feature shared between cells that habituated to efference was a gradual re-emergence of the bundle's original spontaneous oscillation profile. Fig. 3.12 display one second motion trace excerpts for five representative bundles demonstrating efferent habituation. Fig. 3.12A captures the bundles during the first second of efferent stimulation. Fig. 3.12B and Fig. 3.12C show the same bundle traces at the tenth second and twentieth second of the recordings, respectively. Comparing the leftmost and rightmost panels reveals a noticeable slowing down of hair bundle movement in response to continued efferent activity. Occasionally, this habituation presented itself as a superimposition of rapid spike-like twitches (exhibiting the same frequency as the efference pulse train) onto a bundle's unstimulated oscillation, as seen in the red and gold traces of Fig. 3.12C. Fig. 3.13 provides bundle trace excerpts, with sectioning commensurate to Fig. 3.12, respectively, of five representative hair bundles that did not experience efference habituation.

#### 3.4.2.2 Frequency, amplitude, and open probability trendlines of habituating and non-habituating hair cells

In order to further examine this phenomenon, we looked at the time-series trendlines of the instantaneous frequencies (Fig. 3.14A, Fig. 3.15A), amplitudes (Fig. 3.14B, Fig. 3.15B), and open probabilities (Fig. 3.14C, Fig. 3.15C) of the two sets of hair cells represented in Fig. 3.12 and Fig. 3.13, respectively. As we had visually observed from the oscillation profiles in Fig. 3.12, habituating hair cells manifest an appreciable decline in oscillation frequency over long periods of efferent modulation (Fig. 3.14A). The hair bundle for which

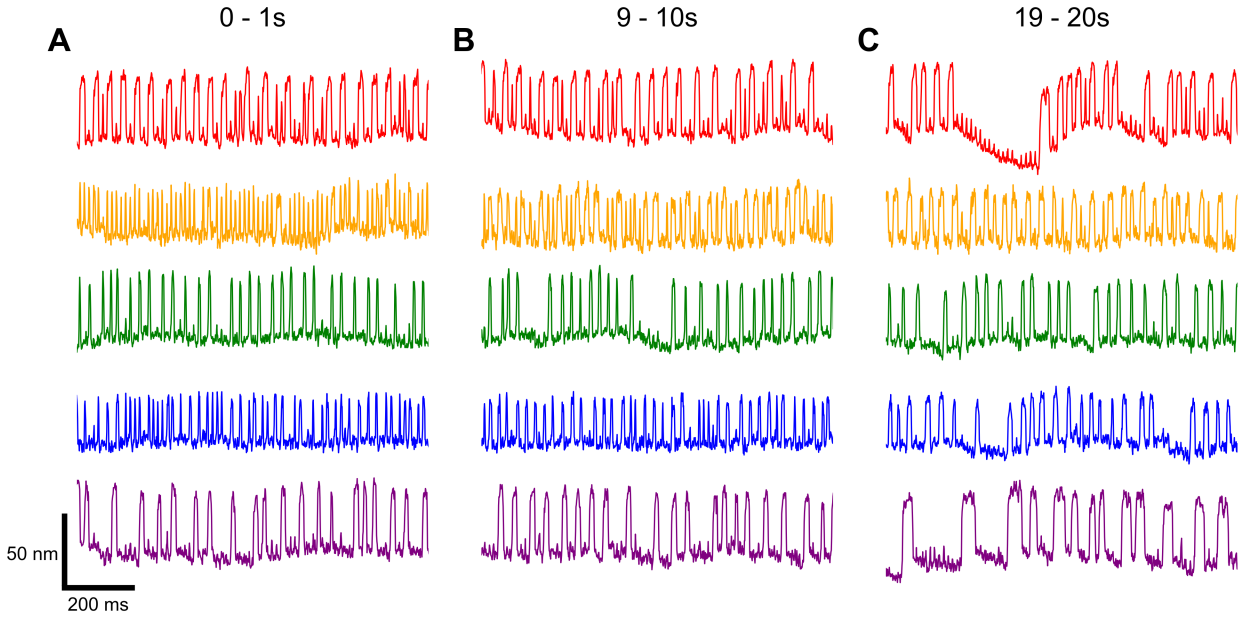


Figure 3.12: Hair bundles may exhibit habituation to long-term efferent stimulation. **A**–**C**) Spontaneous oscillation traces are shown for five representative hair bundles displaying efferent habituation in response to 20 s of efferent modulation (pulse train: 200 $\mu$A, 3 ms pulse duration, 10 ms inter-pulse interval). Oscillation profiles are displayed for 0 – 1 s (**A**), 9 – 10 s (**B**), 19 – 20 s (**C**) after the start of the efferent stimulus. The five bundles were procured from four different sacculi, shown in different colors, and offset for clarity. Scale bars in **A** are applicable for **B** & **C**.

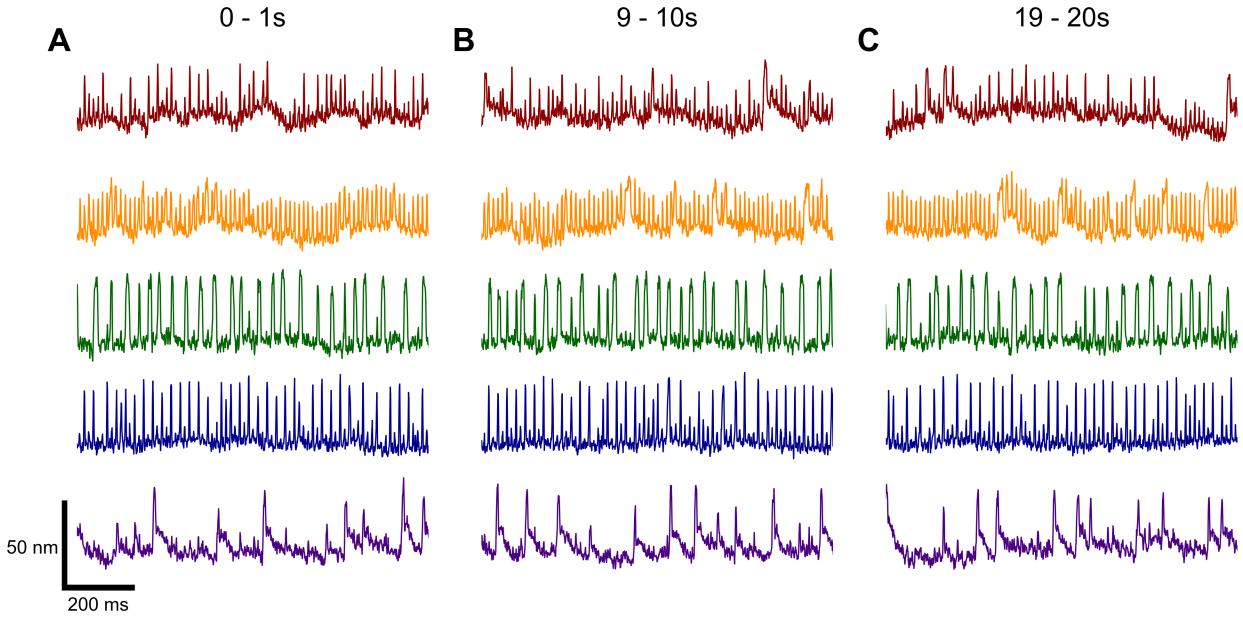


Figure 3.13: Hair bundles may exhibit habituation to long-term efferent stimulation. **A**–**C**) Spontaneous oscillation traces are shown for five representative hair bundles not exhibiting efferent habituation in response to 20 s of efferent modulation (pulse train: 200 $\mu$A, 3 ms pulse duration, 10 ms inter-pulse interval). Hair bundle oscillation profiles are shown for 0 – 1 s (**A**), 9 – 10 s (**B**), 19 – 20 s (**C**) after the onset of efferent actuation. The five bundles were procured from three different sacculi, shown in different colors, and offset for clarity. Scale bars in **A** are applicable for **B** & **C**.

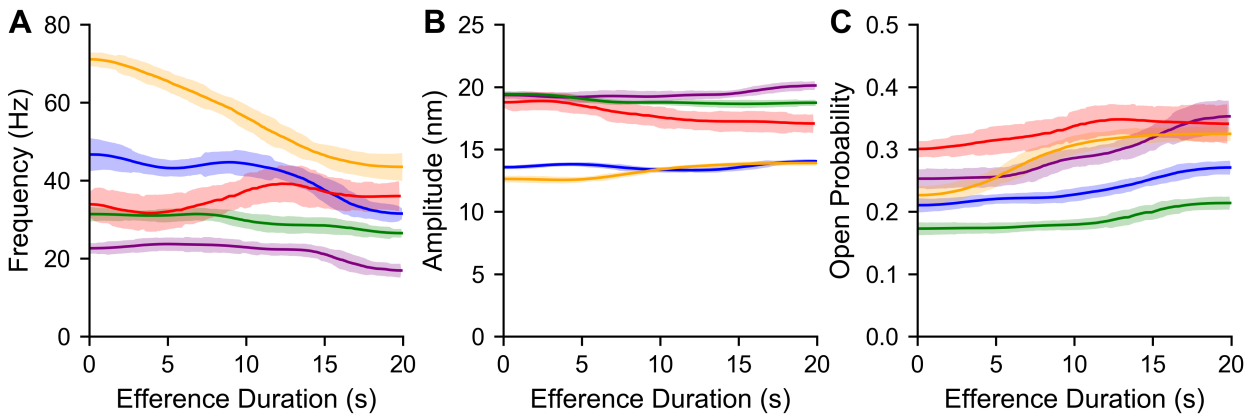


Figure 3.14: Characteristic parameters of habituating hair cells' oscillation profiles experienced a temporal evolution under continued efferent stimulation. Time-series trendlines of the instantaneous frequencies (**A**), amplitudes (**B**), and open probabilities (**C**) are displayed for the five habituating bundles shown in Fig. 3.12. The hair bundles' frequencies trended downwards while the open probabilities trended upwards. Trendlines are plotted with the same color as the corresponding bundles in Fig. 3.12. The efferent neurons of the hair cells were actuated by a pulse train stimulus (pulse train: 200 $\mu$A, 3 ms 'on', 10 ms 'off'). Error bands represent the standard deviations of data points in a one second moving window.

this was not the case transformed from being a regular oscillator to one exhibiting bursts of oscillation interspersed with quiescent intervals. Similar to our expectations, the frequencies of non-habituating bundles remained relatively stable over the same duration (Fig. 3.15A). Likewise, the non-habituating hair cells' amplitude (Fig. 3.15B) and open probability (Fig. 3.15C) trendlines stayed comparatively flat. Habituating cells' open probability trendlines curved upwards, indicating increased fractions of time in the open state (Fig. 3.14C). There was no apparent change in the oscillation amplitude trendlines of the habituating hair bundles (Fig. 3.14B).

A broad survey of 26 hair cells across 12 sacculi yielded the instantaneous frequency, amplitude, and open probability trendlines shown in Fig. 3.16A, Fig. 3.16B, and Fig. 3.16C, respectively. The hair bundles in Fig. 3.16A are color-coded in ascending order by their initial instantaneous frequency. The color given to a cell in Fig. 3.16A is used for the same cell in Fig. 3.16B and Fig. 3.16C. Trendlines normalized by their characteristic, unstimulated values obtained prior to efferent stimulation, are shown in Fig. 3.16D–F. Bundles in

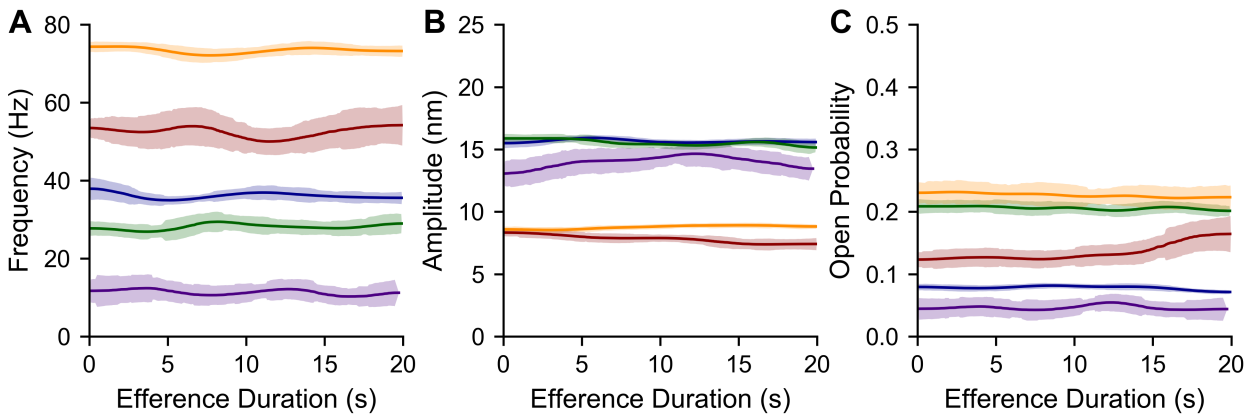


Figure 3.15: Characteristic parameters of non-habituating hair cells' oscillation profiles did not experience a temporal evolution under continued efferent stimulation. Time-series trendlines of the instantaneous frequencies (**A**), amplitudes (**B**), and open probabilities (**C**) are displayed for the five non-habituating bundles shown in Fig. 3.13. Trendlines are plotted with the same color as the corresponding bundles in Fig. 3.13. The efferent neurons of the hair cells were actuated by a pulse train stimulus (pulse train: 200 $\mu$A, 3 ms 'on', 10 ms 'off'). Error bands represent the standard deviations of data points in a one second moving window.

Fig. 3.16D are assigned colors in the same manner as in Fig. 3.16A, and the equivalent color schematic is utilized in Fig. 3.16E and Fig. 3.16F. Hair bundles that initially showed a stronger efferent effect showed more prominent habituation. The color schema established that there was no clear pattern amongst the three extracted components of a hair bundle's long-term behavior under efferent stimulation.

Lastly, we explored the possibility that the amplitude of the efferent stimulus contributes to the likelihood of a hair bundle experiencing efferent habituation. The temporal evolution of the characteristic parameters of a hair bundle's oscillation profile seemed to be influenced by the amplitude of the efferent pulse train stimulus. Time-series trendlines of the instantaneous frequencies (Fig. 3.17A, Fig. 3.17D), amplitudes (Fig. 3.17B, Fig. 3.17E), and open probabilities (Fig. 3.17C, Fig. 3.17F) are shown in Fig. 3.17 for two distinct hair cells originating from the same sacculus. Trendlines corresponding to a stimulus amplitude of 0 $\mu$A, 50 $\mu$A, 100 $\mu$A, 150 $\mu$A, or 200 $\mu$A are plotted in red, gold, green, blue, and violet, respectively. The pulse duration and inter-pulse interval of the applied efferent pulse train were kept constant

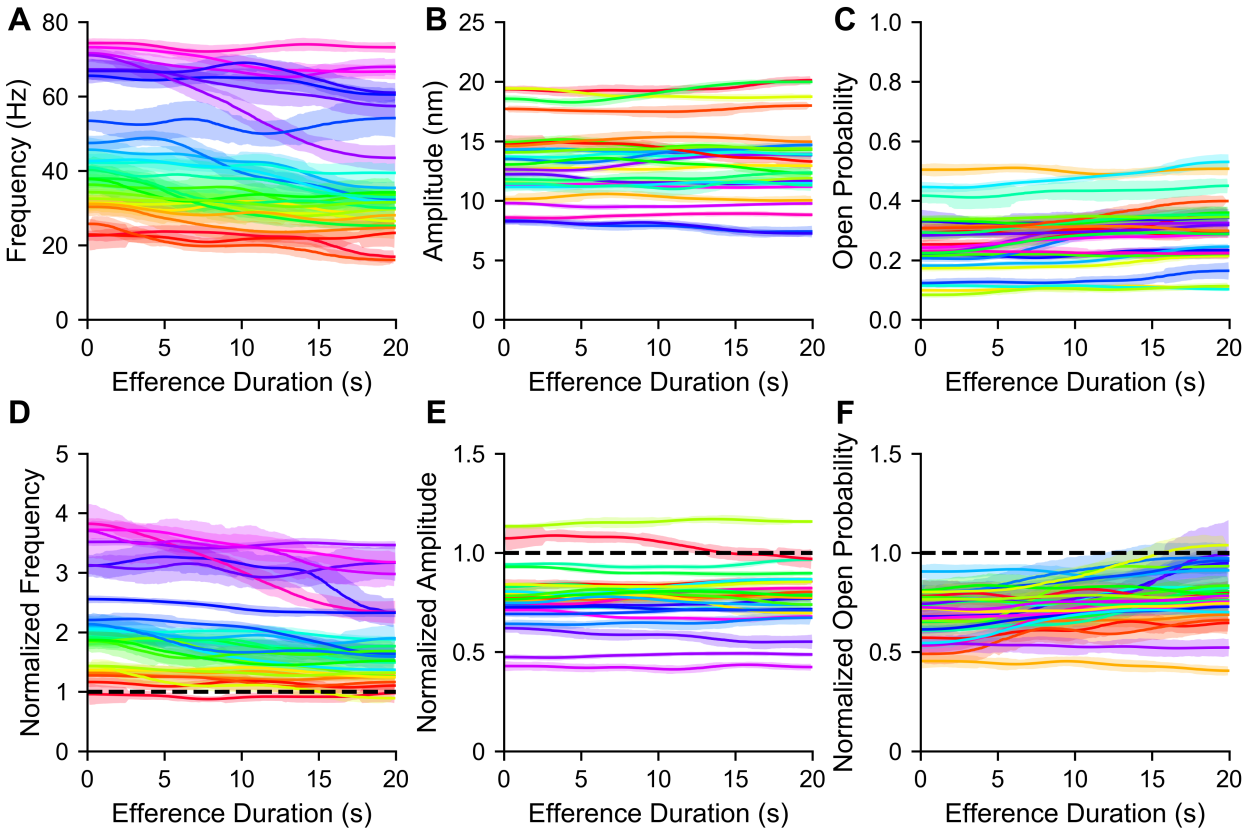


Figure 3.16: A large sample of hair cells demonstrated a wide variety of responses to long-term efferent stimulation. Time courses of the instantaneous frequencies (**A**), amplitudes (**B**) and open probabilities (**C**) of 26 bundles across 12 sacculi are displayed. The trendlines in **A**–**C** were normalized by their measured characteristic values, obtained from the same bundle prior to efferent stimulation, and are shown in **D**–**F**. Each bundle in **A** and **D** is color-coded in ascending order by its initial frequency and normalized frequency value, respectively. The color representing an individual hair bundle in **A** and **D** is used for the same hair bundle in **B** & **C** and **E** & **F**, respectively. For panels showing normalized trendlines, complete recovery to the characteristic unstimulated value is indicated by the black dashed line at 1.0. The efferent neurons of all the hair cells were actuated by a pulse train stimulus (pulse train: 200 $\mu$A, 3 ms 'on', 10 ms 'off'). Error bands represent the standard deviations of data points in a one second moving window.

(3 ms 'on', 10 ms 'off'), and the stimulus amplitude was varied. The main impact of the stimulus amplitude appeared to be in shaping the oscillation profile immediately upon efferent modulation, and thus its evolution over time. Elevated stimulus amplitudes appeared to increase the likelihood of a hair cell exhibiting habituation in response.

#### 3.4.2.3 Power spectral densities of habituating and non-habituating hair cells

To demonstrate how efference habituation manifests itself in the frequency domain, we explored the time-evolution of a hair bundle's power spectral density (PSD) during efferent actuation. Fig. 3.18 displays the power spectral densities of four habituating hair bundles. Fig. 3.19 illustrates the PSDs of four non-habituating hair bundles. Each bundle's unstimulated PSD is plotted in gray, and the locations of the efferent stimulus frequency (77 Hz) and its harmonics are identified by gray dashed lines. Power spectral densities of four consecutive five-second sections of a bundle's stimulated spontaneous oscillations are plotted in red, gold, green, and blue, respectively. The inset plots reveal further details about the first peak at the efferent pulse train frequency. For all cells, the stimulated PSDs exhibit significant peaks at the stimulus frequency and its harmonics. However, the time-lapsed PSDs of the habituating bundles experienced an unmistakable evolution while those of the non-habituating cells persisted for the full duration of efferent activity. The two main developments evinced by Fig. 3.18 are a dramatic reduction in the height of the 77 Hz peak and a regression to the original, broader, low frequency peak.

## 3.5 Discussion

The physiology of efferent neurons has been widely explored in prior studies. A subset of the efferents synapse directly onto hair cells, releasing the neurotransmitter acetylcholine and stimulating the $\alpha 9\alpha 10$ nicotinic ACh receptors. The resulting cascade of opening ion channels in the cell soma induces changes in the membrane potential [109]. While the ramifications of these channel openings leads to a complex range of behaviors, efferent activity is inhibitory for most of the stimuli applied [56, 93, 27, 5, 83, 105, 100] and generally leads

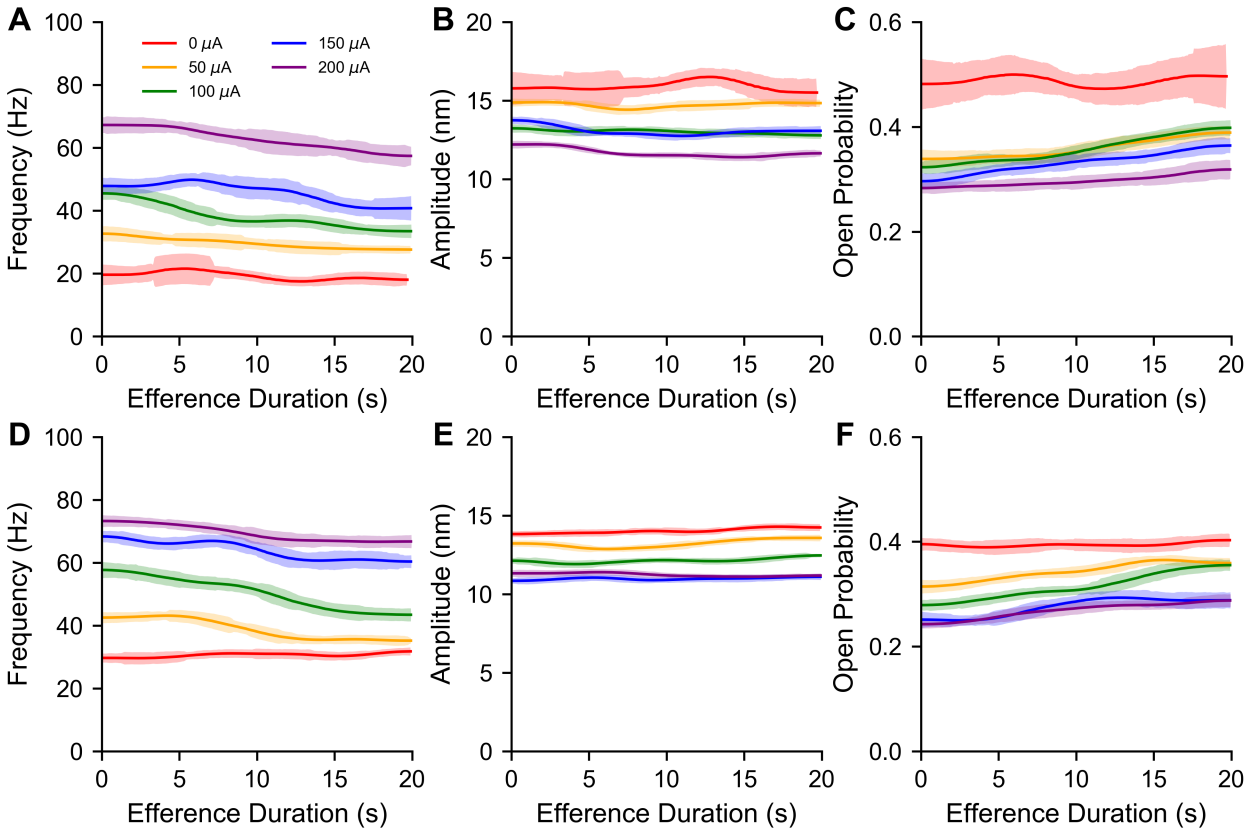


Figure 3.17: The temporal evolution of the characteristic parameters of a hair bundle's oscillation profile were influenced by the amplitude of an efferent pulse train stimulus. Time-series trendlines of the instantaneous frequencies (**A**, **D**), amplitudes (**B**, **E**), and open probabilities (**C**, **F**) are displayed for two distinct hair cells originating from the same sacculus. Trendlines corresponding to a stimulus amplitude of 0 $\mu$A, 50 $\mu$A, 100 $\mu$A, 150 $\mu$A, or 200 $\mu$A are plotted in red, gold, green, blue, and violet, respectively. The pulse duration and inter-pulse interval of the pulse train applied to the saccular nerve were kept constant (3 ms 'on', 10 ms 'off'), and the stimulus amplitude was varied. The main impact of the stimulus amplitude appeared to be in shaping the oscillation profile immediately upon efferent modulation, and thus its evolution over time. Elevated stimulus amplitudes appeared to increase the likelihood of a hair cell exhibiting habituation in response. Error bands represent the standard deviations of data points in a one second moving window.

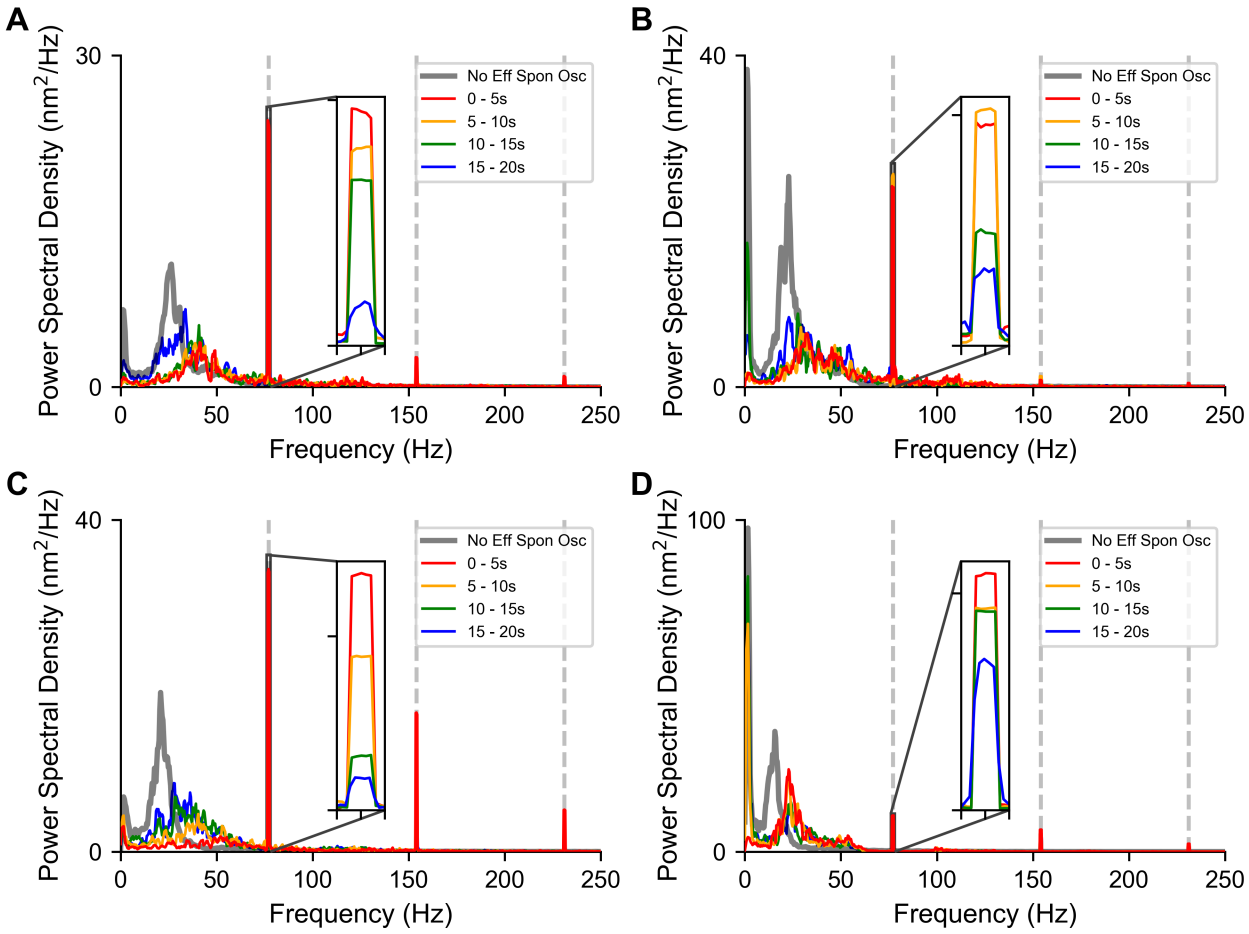


Figure 3.18: The power spectral densities (PSDs) of habituating hair bundles drifted back to their original, unstimulated PSDs over time. Power spectral densities of a hair bundle's innate oscillations with simultaneous efferent stimulation are plotted in red, gold, green, and blue for each five second segment up to 20 s, respectively, following the onset of efferent actuation. The power spectral density of a bundle's unstimulated spontaneous oscillations is plotted in gray. The inset plot provides a zoom-in of the peak at the efference pulse train frequency, 77 Hz. Gray dashed lines identify the frequency of the efference pulse train and its harmonics. Habituating bundles experienced a significant decrease in the height of the peak at the location of the frequency of the pulse train stimulus. Each sub-figure represents the calculated PSDs of oscillation profiles illustrated in Fig. 3.12, with **A**, **B**, **C**, and **D** reflecting the blue, green, gold, and red traces, respectively. The efferent neurons of the hair cells were actuated by a pulse train stimulus (pulse train: 200 $\mu$A, 3 ms 'on', 10 ms 'off').

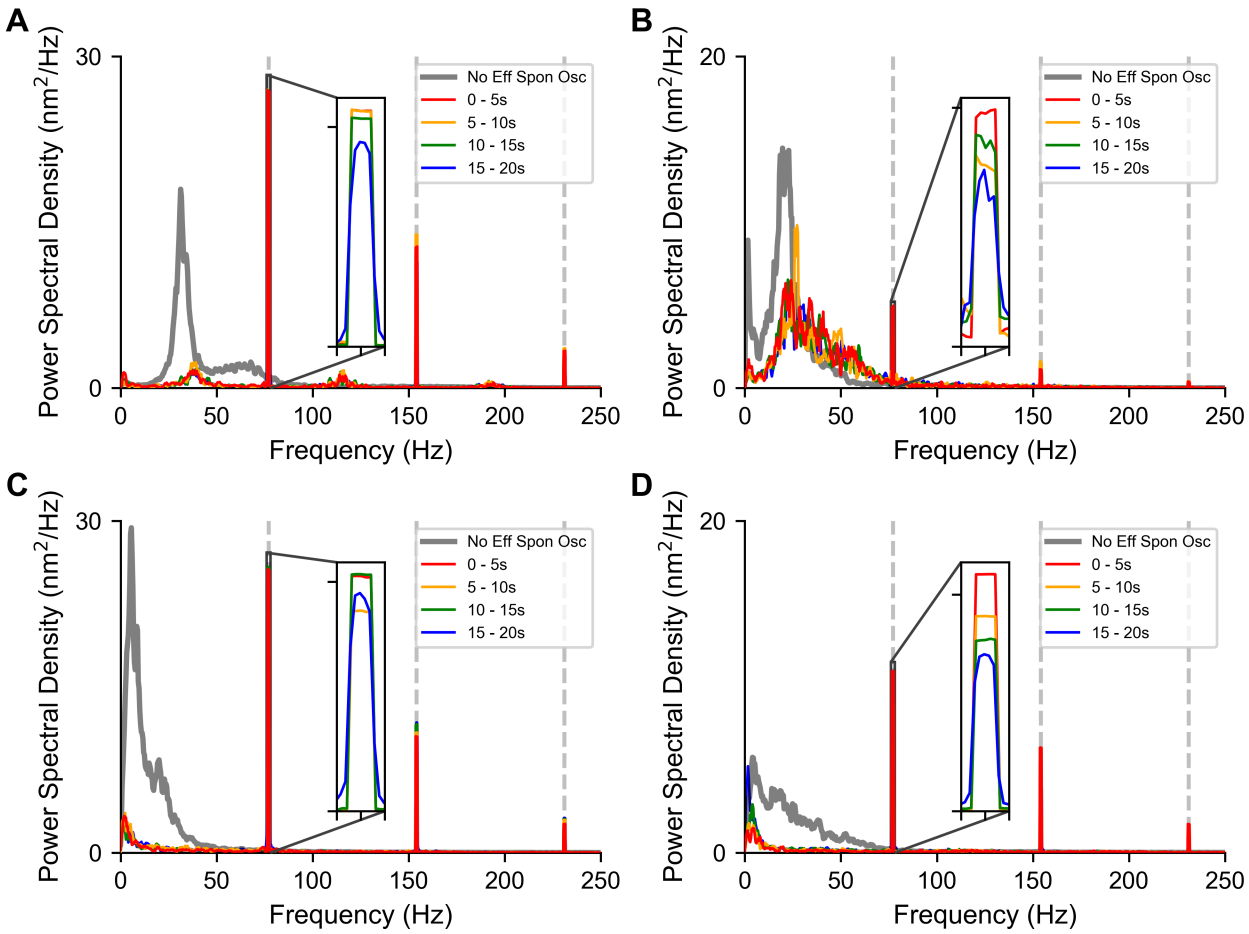


Figure 3.19: The power spectral densities (PSDs) of non-habituating hair cells remained relatively unchanged for the full 20 s of efferent actuation. Power spectral densities of a hair bundle's innate oscillations with simultaneous efferent stimulation are plotted in red, gold, green, and blue for each five second segment up to 20 s, respectively, following the onset of efferent actuation. The power spectral density of a bundle's unstimulated spontaneous oscillations is plotted in gray. The inset plot provides a zoom-in of the peak at the efference pulse train frequency, 77 Hz. Gray dashed lines identify the frequency of the efference pulse train and its harmonics. The non-habituating bundles did not exhibit a significant decline in the height of the peak at the location of the frequency of the pulse train stimulus. Each sub-figure represents the calculated PSDs of oscillation profiles illustrated in Fig. 3.13, with **A**, **B**, **C**, and **D** reflecting the blue, green, gold, and red traces, respectively. The efferent neurons of the hair cells were actuated by a pulse train stimulus (pulse train: 200 $\mu$A, 3 ms 'on', 10 ms 'off').

to hyperpolarization of the hair cell soma [4, 32]. In one study, hyperpolarization of the membrane potential in response to efferent stimulation was demonstrated on hair cells from the bullfrog sacculus [15]. Repeated pulses of efferent stimulus intensified the degree of hyperpolarization up to a saturating level. These electrophysiological data are in accordance with the influx of $Ca^{2+}$ current through cholinergic receptors and a subsequent outward $K^{+}$ current through SK2 channels. The hyperpolarization of the soma in response to efferent actuation seems to be consistent across a number of species studied [4, 109]. Concurrent with hyperpolarization, stimulation of the efferent axons was shown to generate both a reduction in sensitivity to tones at the characteristic frequency and a loss of frequency selectivity, as measured by the evoked response in afferent neurons and the somatic voltage [2, 3].

It is not fully understood how changes in the membrane potential of the hair cell affect active bundle mechanics. However, a number of studies have established that such an effect exists. Transepithelial electrical stimulation was shown to trigger and entrain active bundle motility [13]. A combination of cell electrophysiology and mechanical bundle manipulation likewise demonstrated that membrane potential impacts active motility [72]. Steady-state changes in the membrane potential were found to modulate the frequency, amplitude, and shape of spontaneous oscillations. Specifically, hyperpolarizing a hair cell evoked an increase in the spontaneous oscillation frequency of the hair bundle, a decrease in the amplitude, and a reduced mean opening probability.

The repercussions on hair bundle mechanics that we observed with efferent stimulation are hence consistent with these prior studies. Efferent modulation typically raised the frequency and reduced the amplitude of spontaneous oscillations, concurring with the effect of hyperpolarizing the cell electrophysiologically. Moreover, the shape of the oscillation changed in a manner consistent with hyperpolarization, with bundles spending increasing fractions of time in the channel-closed state. This response was quantified for different levels of efferent stimulation and found to exhibit similar dependencies to those observed with increasing hyperpolarization of the hair cell. These parallels are compatible with the correlation between efferent activity and modulation of the membrane potential of the hair cell soma. Moreover,

the application of apamin (SK2 channel blocker) and subsequent elimination of the effects of efferent activity, discussed in Section 2.4.2.2, further support our assertion that the observed effects of efferent activity on active hair bundle mechanics are effectuated through the hyperpolarization of the cell soma.

### 3.5.1 Control of $Ca^{2+}$ entry is a plausible mediator for the membrane potential's influence on active bundle mechanics

The most plausible hypothesis for how the membrane potential alters bundle mechanics is that it does so indirectly by modulating the electrodiffusion of $Ca^{2+}$ into the stereocilia [72]. The consequences of varying $Ca^{2+}$ concentration on active spontaneous motility, as well as direct measurements of transduction currents, have indicated that raised $Ca^{2+}$ levels reduce the opening probability of the ion channels [61, 66, 70]. $Ca^{2+}$ could affect the channel conformation directly, or it may modulate the stiffness of the internal elements in series with the tip link [66, 88, 10]. Additionally, experimental data indicate that $Ca^{2+}$ plays a role in determining the rate of adaptation motors [66, 60, 13, 70]. Under all of these interpretations, the net effect of increasing $Ca^{2+}$ is to boost the oscillation frequency, reduce the amplitude of oscillation, and decrease the mean opening probability of the transduction channels.

Interpreting our results in the context of prior studies, we assume that efferent stimulation hyperpolarizes the hair cell soma, enhancing the electrodiffusion of $Ca^{2+}$ into the stereocilia. The elevated $Ca^{2+}$ influx lowers the mean opening probability of the transduction channels, modulating the profile of the innate oscillation. Taking this into account, it is uncertain what the principal causal mechanism is behind efferent habituation. It is not clear whether the source of this phenomenon is pre-synaptic or post-synaptic. For the former, it is possible that habituation is a repercussion of ACh depletion in the pre-synaptic terminal due to the *in vitro* nature of our experimental set-up. As for the latter, recent work has shed some light on the synaptic $Ca^{2+}$ dynamics generated by efferent stimulation [76]. In this study, hair cell $Ca^{2+}$ levels were observed to saturate within 300 ms and decline even before the efferent actuation ceased – possibly due to the ignition of cisternal modulation. Thus, efferent

habituation might be a repercussion of declining internal $Ca^{2+}$ concentration. Investigating the origin of this phenomenon through pre-synaptic ACh measurements and post-synaptic $Ca^{2+}$ measurements is a possible avenue for future work.

# CHAPTER 4

# Effect of Efferent Activity on Hair Cell Sensitivity

## 4.1 Introduction

We investigate how efferent activity altered the mechanical properties of a hair cell by observing how a hair bundle responded to a mechanical stimulus both with and without concurrent efferent stimulation. In conjunction with the efferent stimulation utilized in the previous chapters, we provided a mechanical stimulus to the hair bundle through a flexible glass probe. By sweeping through 24 stimulus frequencies (3 – 50 Hz) and 10 stimulus amplitudes (4 – 80 nm), we measured Arnold Tongues and sensitivity curves of individual hair bundles across multiple sacculi. The Arnold Tongues and sensitivity curves of hair cells undergoing efferent actuation demonstrated an overall desensitization with respect to those of unstimulated cells. Hence, we demonstrate that a hair bundle is desensitized by efference.

## 4.2 Materials and Methods

### 4.2.1 Biological Preparation

Refer to Section 2.2.1.

### 4.2.2 Imaging and Tracking Hair Bundle Motion

Refer to Section 2.2.2.

### 4.2.3 Efferent Stimulation

Refer to Section 2.2.3.

### 4.2.4 Mechanical Stimulation

A glass fiber approximately 1 $\mu$m in diameter was created with a modified microforge to fabricate an additional rod perpendicular to the tip of a borosilicate glass capillary that had been pulled with a micropipette puller (Sutter Instruments). The stiffness and viscous drag coefficient of the glass probe were measured by recording the Brownian motion of the tip of the glass fiber in water and fitting its power spectral density to a Lorentzian function [40]. The stiffness and drag coefficients of the glass probes used in these experiments were 75 – 150 $\mu$N/m and 100 – 150 nN·s/m, respectively. With these specifications, a 10 nm probe displacement corresponds to, approximately, a 1 pN force on the bundle. Probes were mounted on a piezoelectric actuator (Piezosystem Jena PA 4/12) at an angle of approximately 30 degrees with respect to the preparation and positioned to attach to either the kinocilium or the tallest row of stereocilia. The probe was micromanipulated to adjoin a single hair bundle, and visual confirmation was utilized to ensure that the glass fiber was in contact with only one hair bundle (Fig. 4.1B). Prior to attachment, the fiber tip was dipped into 5 mg/mL concanavalin-A, a highly charged polymer, to enhance the adhesion. Synchronously with efferent stimulation and video acquisition, 3 – 50 Hz sinusoidal signals with amplitudes ranging from 4 – 80 $\mu$m were sent to the piezoelectric amplifier via LabView (National Instruments). Mechanical stimuli of varying frequencies and amplitudes were applied sequentially, without any intervals between the signals. Unless indicated otherwise, the sinusoidal amplitude is reported as the amplitude applied to the base of the probe. Displacements to the base of the probe generated lateral sinusoidal displacements of the hair bundle, mimicking the mechanical stimulation produced by sound *in vivo*.

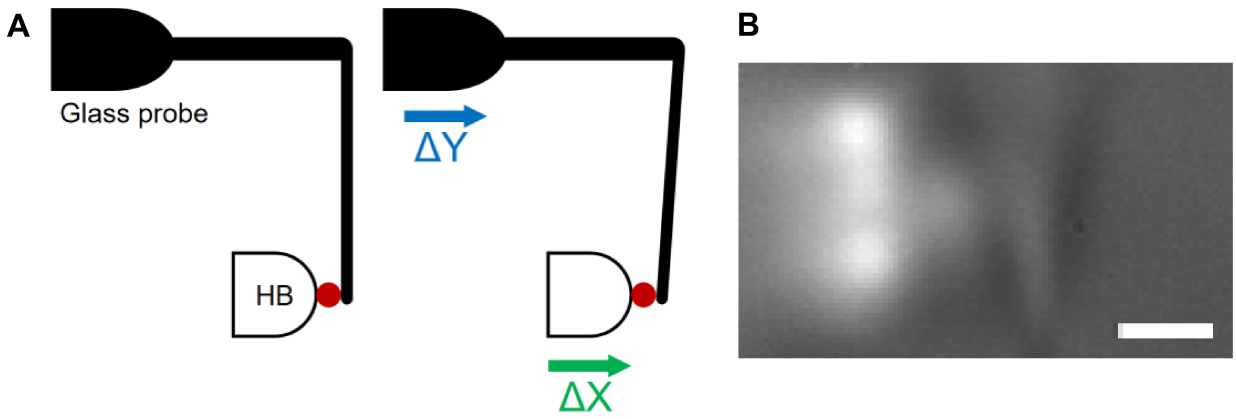


Figure 4.1: **A**) A flexible glass probe (stiffness $\approx 100$ $\mu$N/m) was attached to the kinocilium (red dot) of the hair bundle (HB). A displacement at the base of the probe caused a displacement in the position of the hair bundle. **B**) Bright field image of a single hair bundle with a glass fiber attached to the kinocilium. The width of the scale bar is 1 $\mu$m.

## 4.3 Data Analysis

### 4.3.1 Arnold Tongue Background

A hair cell's mechanical responsiveness over a range of frequencies and stimulating amplitudes can be visualized by an Arnold Tongue.

For a weak forcing stimulus, with amplitude $F$, frequency $\omega_f$, and phase $\phi_f$:

$$F_{stim}(t) = Fsin(\omega_f t + \phi_f), \tag{4.1}$$

a driven oscillator will have a response with amplitude $A$, frequency $\omega_{osc}$, and phase $\phi_{osc}$:

$$A_{osc}(t) = Asin(\omega_{osc} t + \phi_{osc}). \tag{4.2}$$

Then, the difference between the frequency of the stimulus and the frequency of the oscillator is:

$$\Delta\Omega = \omega_{osc} - \omega_f. \tag{4.3}$$

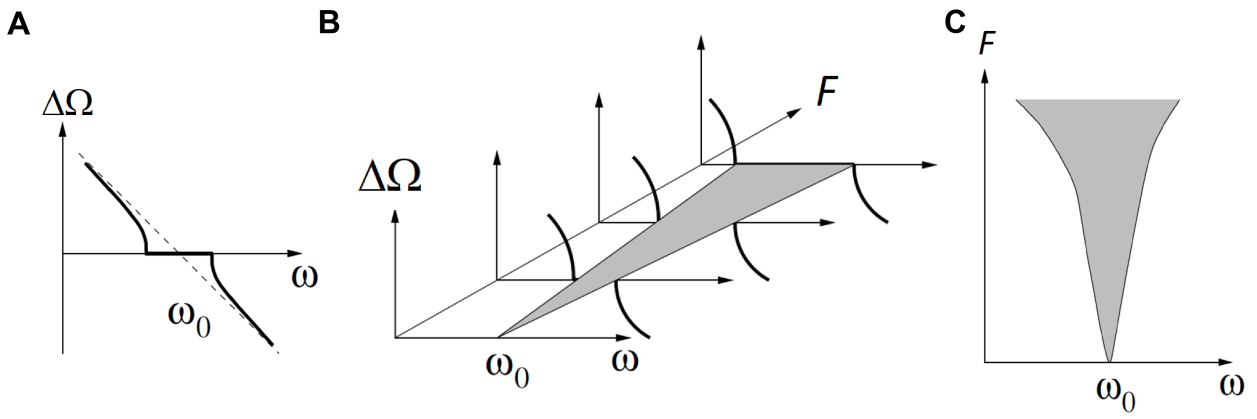


Figure 4.2: An Arnold Tongue visualizes a hair cell's mechanical responsiveness over a range of frequencies and stimulating amplitudes. At some stimulus amplitude, a nonlinear oscillator phase-locks with the stimulus for a certain frequency range but becomes detuned outside of this region (**A**). This region is usually centered around the characteristic frequency of the oscillator. As the stimulus amplitude increases, the width of the phase-locked region grows wider (**B**). Putting it all together, an Arnold Tongue is constructed, which shows the phase-space for which the nonlinear oscillator is entrained to the stimulus and most sensitive (**C**) [82].

A hair cell is a nonlinear oscillator and, thus, has a nonlinear response to stimuli. For some stimulus amplitude, a nonlinear oscillator phase-locks with the stimulus for a certain frequency range, but becomes detuned outside of this region (Fig. 4.2A). This region is usually centered around the characteristic frequency of the oscillator. As the stimulus amplitude increases, the width of the phase-locked region grows wider (Fig. 4.2B). Putting it all together, an Arnold Tongue is constructed, which shows the phase-space for which the nonlinear oscillator is entrained to the stimulus and most sensitive (Fig. 4.2C) [82].

### 4.3.2 Measuring Arnold Tongues and Sensitivity Curves

Arnold Tongues were measured by calculating the phase-locked component of a hair bundle's response to sinusoidal deflection over a range of mechanical drive frequencies. The applied frequency spanned the range 3 – 50 Hz in 2 Hz increments. Ten cycles were presented for each stimulus frequency. The full sweep was administered at stimulus amplitudes varying from 4 to 80 nm. For a particular stimulus frequency and stimulus amplitude, the corresponding

bundle position trace was divided into ten segments and averaged. A single sine wave with the corresponding stimulus frequency was fit to the averaged response, and its amplitude was extracted to obtain the phase-locked component.

At a specific stimulus amplitude, a hair bundle's sensitivity, $\chi(\omega_S)$, was computed from

$$\chi(\omega_S) = \frac{A_{pl}(\omega_S)}{f(\omega_S)}, \tag{4.4}$$

where $\omega_S$ is the stimulus frequency, $A_{pl}(\omega_S)$ is the phase-locked amplitude of the bundle oscillation, and the force $f(\omega_S)$ is given by

$$f(\omega_S) = (K_F + i\omega_S\xi)A_S, \tag{4.5}$$

where $K_F$ is the glass fiber's stiffness, $\xi$ is its viscous drag coefficient and $A_S$ is the stimulus amplitude [67].

## 4.4 Results

### 4.4.1 Efferent actuation alters the mechanical responsiveness of individual hair cells

We explored how efferent modulation changes the mechanical properties of a hair cell by observing how a hair bundle responds to a mechanical stimulus both with and without simultaneous efferent stimulation. In conjunction with the efferent stimulation described in the previous chapters, we provided a mechanical stimulus to the hair bundle through a flexible glass probe. As evident from Fig. 4.3, the bundle's motions are significantly less phase-locked with the mechanical stimulus in the presence of efferent stimulation.

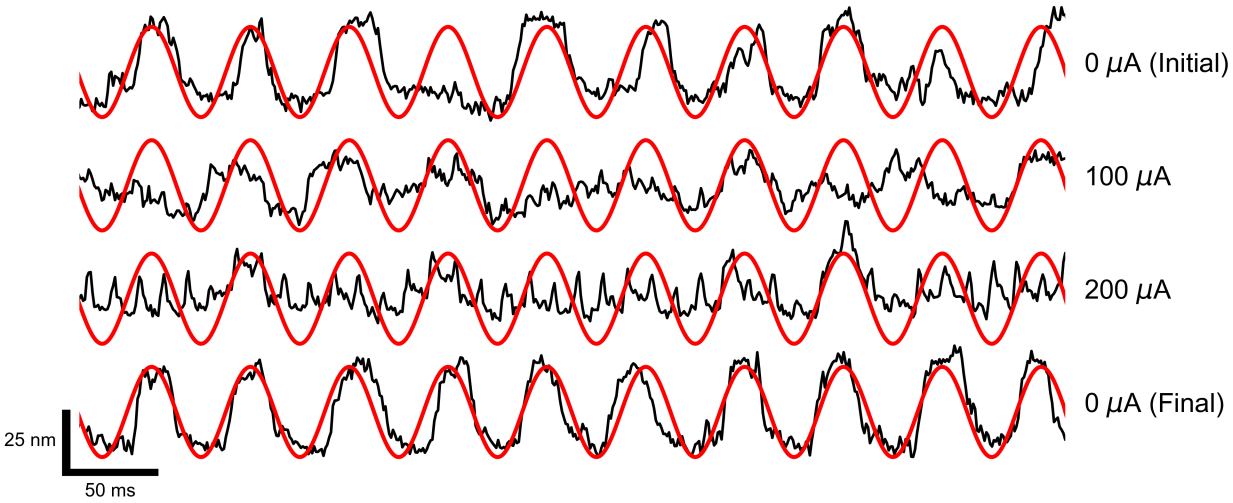


Figure 4.3: A hair bundle's response to sinusoidal mechanical stimuli differed greatly depending on the presence and level of efferent modulation (stimulus: 1 ms 'on', 10 ms 'off'). The bundle visibly phase-locked with the mechanical stimulus in the top and bottom traces. This characteristic was lost with the introduction of efferent stimulation. All four traces were recorded from the same hair bundle. The scale bars are applicable to both the bundle traces (black) and the stimulus (red).

#### 4.4.1.1 Pulse train stimulus

To fully explore this phenomenon, we applied a drive to the hair bundle at frequencies 3 – 50 Hz, sampled in 2 Hz increments, with amplitudes (measured as displacements at the base of the probe) of 4, 8, 12, 16, 20, 30, 40, 50, 80 nm. Each frequency and amplitude pair was presented for ten cycles. Fig. 4.4A illustrates the synchronization dynamics of a hair bundle, without any efferent modulation, in the form of an Arnold Tongue. At low mechanical stimulus amplitudes, the hair bundle showed entrainment only over a limited frequency range. However, the extent of the phase-locking grew with mechanical stimulus amplitude and created the triangular formation seen in the graph.

The hair bundle's Arnold Tongue was drastically altered by the application of a pulse train efferent stimulus with amplitudes of 100 $\mu$A and 200 $\mu$A, shown in Fig. 4.4B and Fig. 4.4C, respectively. As these two panels demonstrate, the hair bundle showed much weaker phase-locking than it had in the absence of an efferent stimulus and only did so for the highest

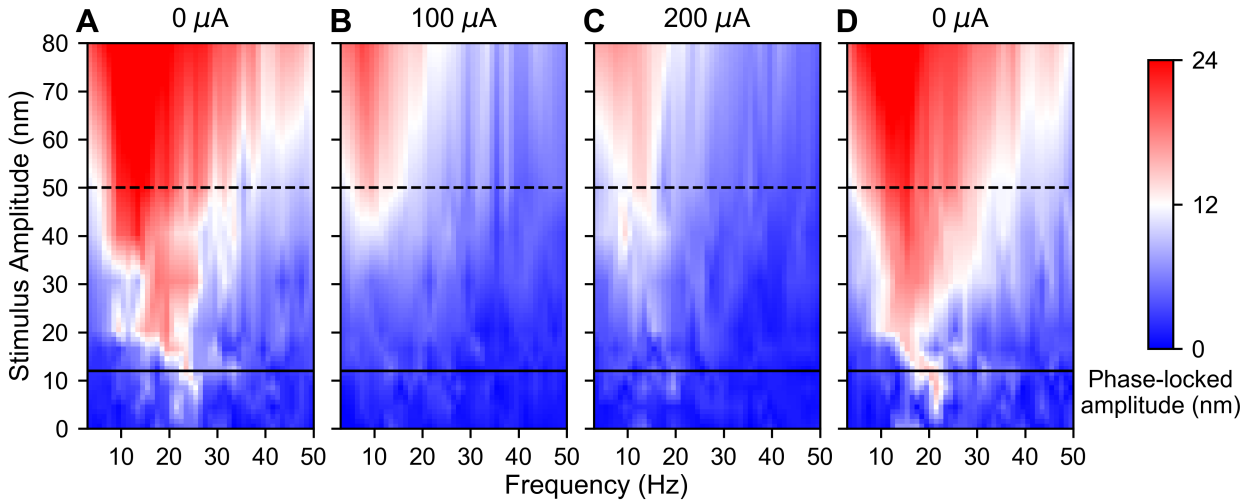


Figure 4.4: Arnold Tongues of a hair cell were obtained with and without efferent stimulation. Each plot was constructed by mechanically driving the bundle at 24 frequencies (3 – 50 Hz in 2 Hz increments) with ten mechanical stimulus amplitudes (0, 4, 8, 12, 16, 20, 30, 40, 50, 80 nm). **A** and **D** show measurements obtained in the absence of efferent stimulation. **B** and **C** show the mechanical response of the bundle measured while the efferent neurons were stimulated with pulse trains (3 ms 'on', 10 ms 'off') of 100 $\mu$A and 200 $\mu$A amplitudes, respectively. Each combination of mechanical stimulus frequency and amplitude was presented for ten cycles. Linear interpolation was applied along the stimulus amplitude direction to yield the color maps. The bundle showed decreased phase-locking and frequency selectivity with efferent stimulation.

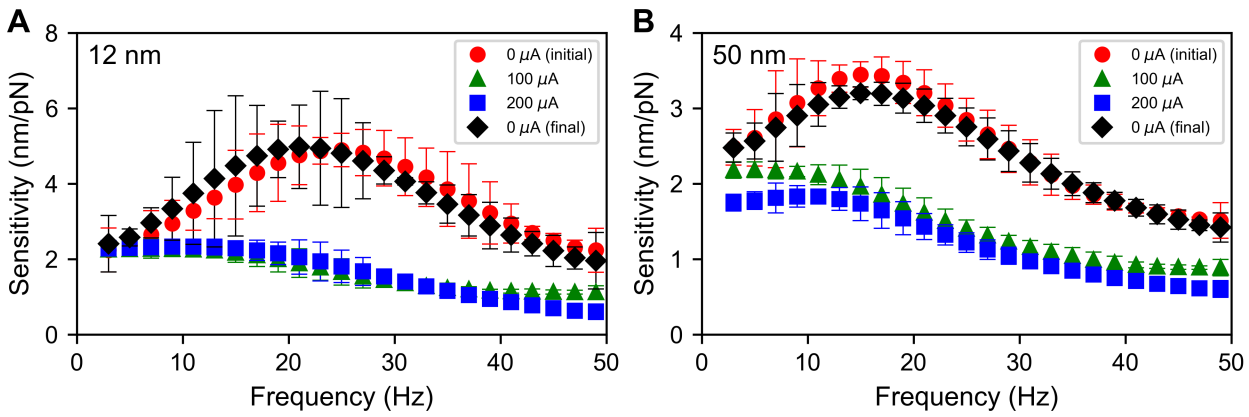


Figure 4.5: The sensitivity curves at glass probe base displacements of **A**) 12 nm (corresponding to the solid lines in Fig. 4.4) and **B**) 50 nm (corresponding to the dashed lines in Fig. 4.4) demonstrate that the cell's sensitivity decreased upon efferent actuation. Circles, triangles, squares, and diamonds correspond to sensitivity curves with efferent stimulus amplitudes of 0 $\mu$A (initial), 100 $\mu$A, 200 $\mu$A, and 0 $\mu$A (final), respectively. The sensitivity curves were smoothed by applying a running average of three data points. The error bars specify the standard deviations from these means.

stimulus amplitudes. Although some synchronization still occurred, the phase-locked region dramatically decreased, indicating that the hair bundle became significantly less sensitive while the efferents were activated. After the efferent stimulus was switched off, the hair bundle sensitivity showed a full return, exhibiting its original mechanical response. The sensitivity curves in Fig. 4.5 further demonstrate that efferent modulation mechanically desensitized a hair cell.

#### 4.4.1.2 Step stimulus

We repeated the measurements with a step stimulus substituted for the pulse train (Fig. 4.6). As a step stimulus exerts a stronger effect than a pulse train (equivalent to 0 ms 'off' time), the efferent stimulus was set to amplitudes of 50 $\mu$A and 100 $\mu$A. The results are shown Fig. 4.6B and Fig. 4.6C, respectively. At 50 $\mu$A, the phase-locked region of the bundle's Arnold Tongue was considerably reduced. At 100 $\mu$A, the bundle exhibited only weak entrainment and showed no frequency selectivity. This supports an increased effect on the hair bundle with increasing efferent stimulus level. Moreover, there was a discernible difference in the

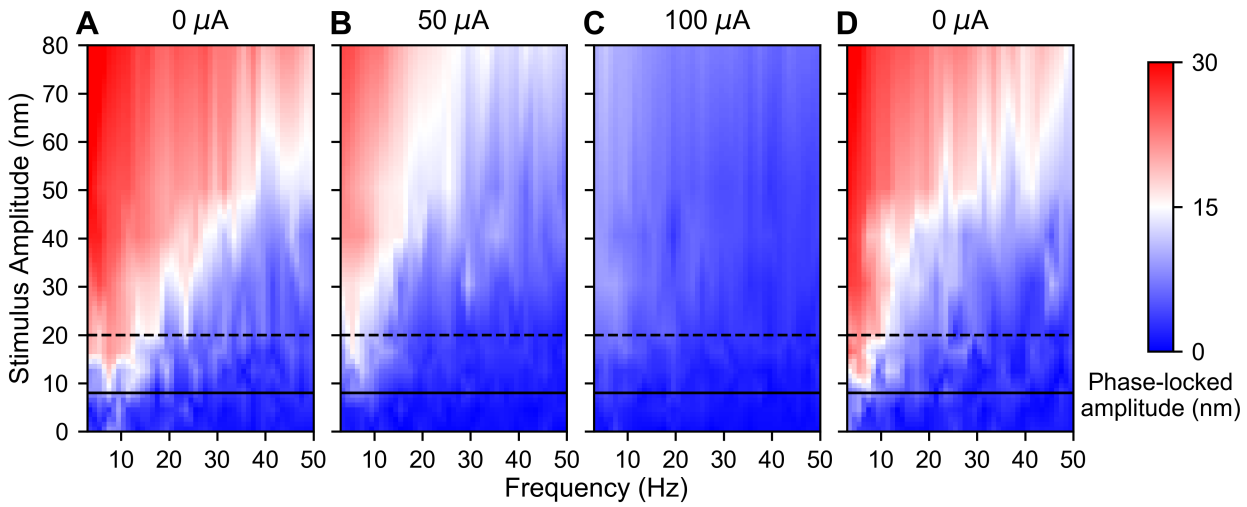


Figure 4.6: Arnold Tongues of a hair cell were measured for varying current step amplitudes (50$\mu$A and 100 $\mu$A) of efferent stimulation. Each plot was constructed by mechanically driving the bundle at 24 frequencies (3 – 50 Hz in 2 Hz increments) with ten mechanical stimulus amplitudes (0, 4, 8, 12, 16, 20, 30, 40, 50, 80 nm). Linear interpolation was applied along the stimulus amplitude direction. As with the pulse train stimulus, the hair bundle showed reduced phase-locking with efferent modulation.

sensitivity curves (Fig. 4.7A, B) between the two levels of efferent modulation. These two figures reveal that a hair bundle's mechanical sensitivity diminished with increasing amplitude of a step current applied to the efferent neurons.

### 4.4.2 Efferent activity leads to hair bundle desensitization

The stated observations for pulse train and step stimuli were noted across eight hair bundles. By shifting the x-axis to reflect the amount of detuning from the bundle's characteristic frequency, we were able to capture the mean effect of efferent activity on a hair bundle's mechanical responsiveness. The visualization of this mean effect in Fig. 4.8 and Fig. 4.9 mirrors the findings attained from individual bundles. Fig. 4.8 and Fig. 4.9 were both averaged over four bundles, with each bundle originating from a different sacculus. Each bundle was subjected to only one of the two forms of efferent stimulation. The averaged sensitivity curves (Fig. 4.10A, B) obtained from the Arnold Tongues confirmed the observed sensitivity reduction during efferent stimulation.

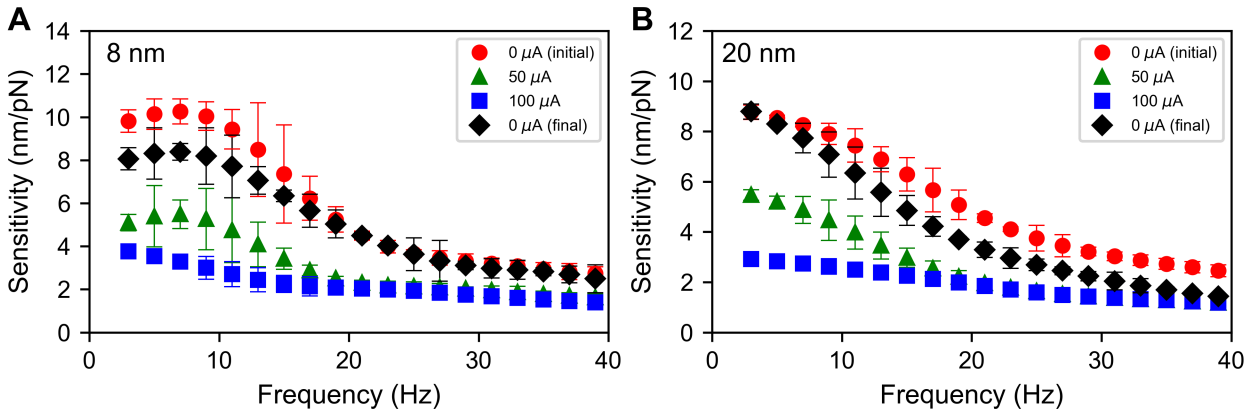


Figure 4.7: The sensitivity curves at glass probe base displacements of **A**) 8 nm (corresponding to the solid lines in Fig. 4.6) and **B**) 20 nm (corresponding to the dashed lines in Fig. 4.6) show that the cell became desensitized with efferent activity. Circles, triangles, squares, and diamonds correspond to sensitivity curves with efferent stimulus amplitudes of 0 $\mu$A (initial), 50 $\mu$A, 100 $\mu$A, and 0 $\mu$A (final), respectively. The sensitivity curves were smoothed by applying a running average of three data points. The error bars specify the standard deviations from these means.

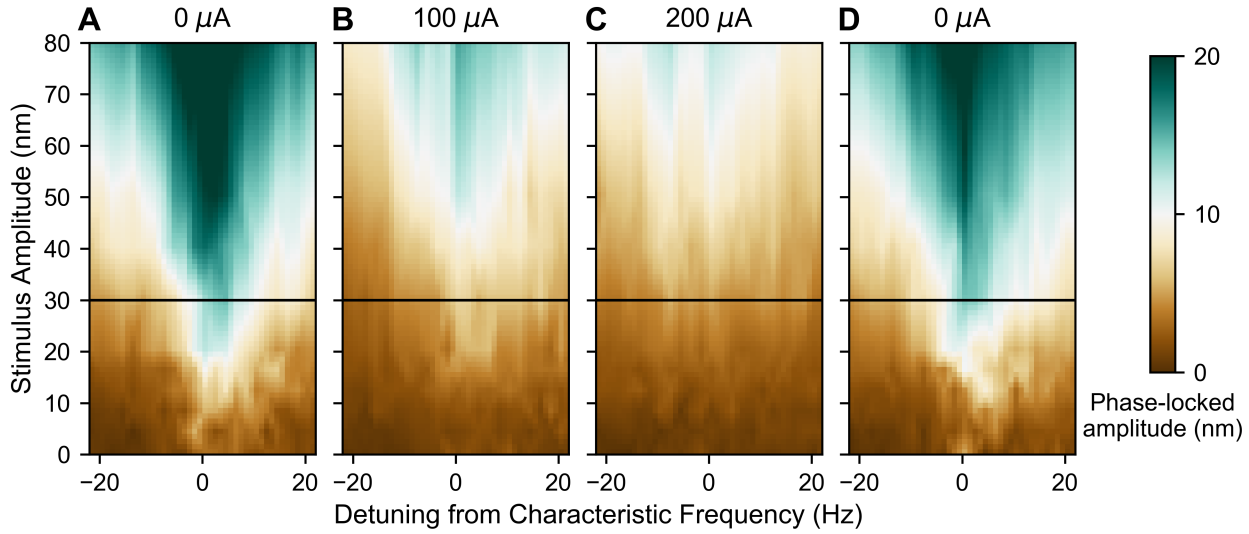


Figure 4.8: The Arnold Tongues in Fig. 4.4 were offset along the x-axis to represent the detuning relative to a hair bundle's characteristic frequency. **A**–**D**) These modified maps were averaged and plotted for pulse train stimuli. The characteristic frequency of each hair bundle was determined from its spontaneous oscillations. The mean Arnold Tongues were averaged from four bundles coming from four sacculi.

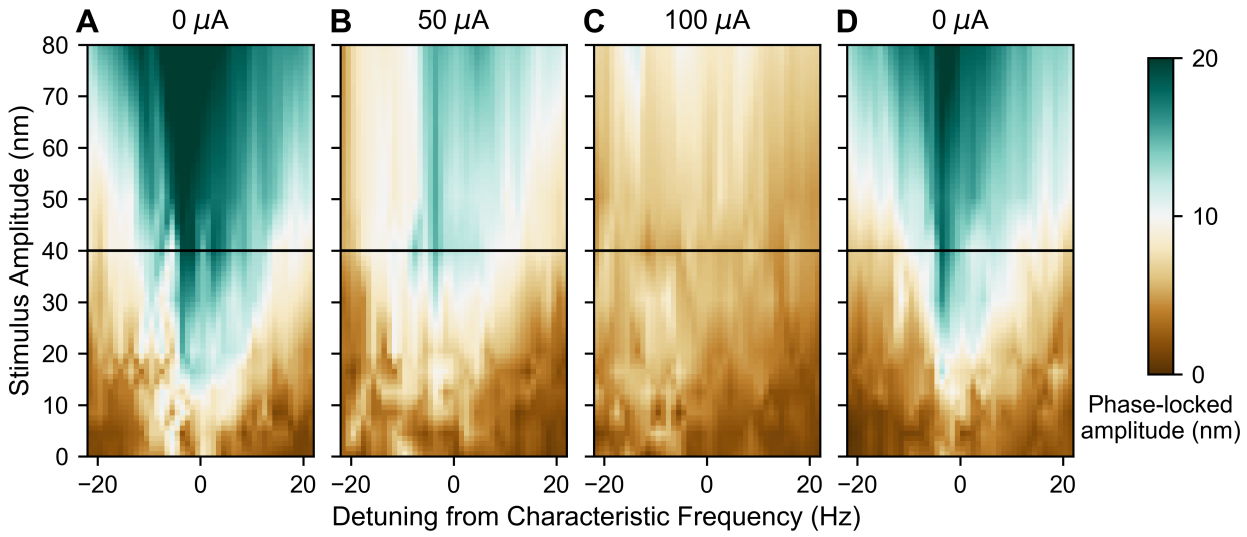


Figure 4.9: The Arnold Tongues in Fig. 4.6 were offset along the x-axis to represent the detuning relative to a hair bundle's characteristic frequency. **A**–**D**) These modified maps were averaged and plotted for step stimuli. The characteristic frequency of each hair bundle was determined from its spontaneous oscillations. The mean Arnold Tongues were averaged from four bundles coming from four sacculi.

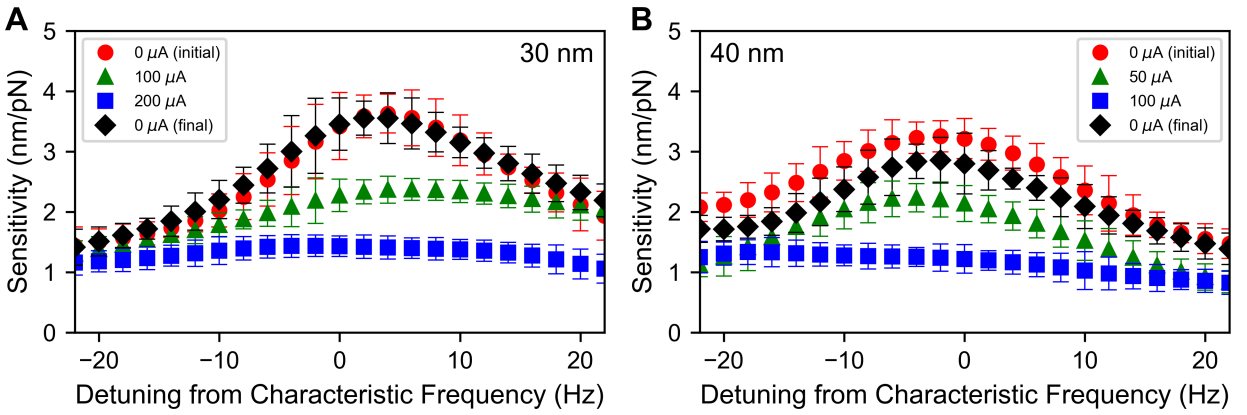


Figure 4.10: **A** and **B** show the averaged sensitivity curves at glass probe base displacements of 30 nm and 40 nm, respectively, corresponding to the solid lines in Fig. 4.8 and Fig. 4.9, respectively. Circles, triangles, squares, and diamonds correspond to averaged sensitivity curves with efferent stimulus amplitudes of 0 $\mu$A (initial), 100 $\mu$A, 200 $\mu$A, and 0 $\mu$A (final), respectively, for **A**, and 0 $\mu$A (initial), 50 $\mu$A, 100 $\mu$A, and 0 $\mu$A (final), respectively, for **B**. The sensitivity curves were smoothed by applying a running average of three data points. **A** and **B** were averaged from 4 bundles each, coming from 8 sacculi. The error bars specify the standard deviations from the means.

## 4.5 Discussion

In prior studies, stimulation of the efferent axons was shown to generate both a reduction in sensitivity to tones at the characteristic frequency and a loss of frequency selectivity, as measured by the evoked response in afferent neurons and the somatic voltage [2, 3]. The findings of our experiments are consistent with these prior studies. Upon efferent stimulation, hair bundles became mechanically desensitized and their frequency selectivity vanished. We hypothesize that these observations are a result of the efferents shifting the hair bundle dynamics to a low-sensitivity spiking regime, wherein the bundles mostly do not entrain in a frequency dependent manner [24]. Although our experiments focused on the efferent impact manifested by individual bundles, we note that *in vivo* many species exhibit mechanical coupling from overlying structures, as well as efferent coupling from divergent innervation patterns, with each neuron synapsing onto multiple hair cells. Hence, activation of one efferent fiber is likely to have an inhibitory effect on many hair cells in parallel. In the presence of mechanical coupling between cells, there may exist a regime in which the efferents improve the sensitivity of the system.

### 4.5.1 The efferent system provides a biological mechanism for controlling the mechanical sensitivity of hair bundles

Hair bundles exhibit remarkable sensitivity, which can be at least partly explained by several characteristics of its mechanics. First, its response is highly nonlinear, with a power-law dependence on the applied stimulus [22, 44, 69, 67]. This feature has been measured *in vitro* and is consistent with *in vivo* nonlinearities observed across many species [65]. Secondly, the hair bundle response contains internal active mechanisms [68, 88, 78]. In certain species, the bundles can even exhibit innate oscillations, driven by internal ATP-consuming processes [65]. These spontaneous oscillations are phase-locked by an applied stimulus of much smaller amplitude, leading to an amplified response [71, 69].

There are many indications that the efferent pathway could serve as a complex gain control

mechanism for both hair cells and hearing. Studies performed on the mammalian auditory system have shown that the olivocochlear efferent system plays an important role in maintaining the integrity of hearing and in fine-tuning its detection properties [99, 34, 57]. Prior work has shown that efferent activity reduces the voltage-dependent tuning of the hair cell soma [2]. Our research adds the finding that bundle mechanics likewise show a reduction in tuning, suggesting that these could be different manifestations of the same phenomenon. Furthermore, despite obvious physiological differences, the otoprotective role of efferents seems to be consistent across the species measured. Additionally, prior electrophysiological studies of hair cells and efferent neurons performed *in vitro* have shown that efference modulates the somatic membrane potential. This effect has also been seen in different end organs, indicating that some aspects of the efferent pathway are consistent across the species.

In the current chapter, we demonstrated that the activation of efferent neurons leads to changes in mechanical responsiveness at the level of the hair bundle. Visible changes in the innate motility of the bundle showed that its internal active processes are significantly impacted. Further, the sensitivity of the mechanical response, characterized across a range of stimulus frequencies and amplitudes, was drastically reduced. This reduction in the evoked motility of the bundle could be an important contribution to the mechanisms that underlie the otoprotective capabilities of the efferent architecture. The efferent system may therefore be viewed as a biological control mechanism that tunes the mechanical responsiveness of the hair bundle.

# CHAPTER 5

# Long-term Hair Bundle Recovery Dynamics following Mechanical Overstimulation

## 5.1 Introduction

In this chapter, we tackle understanding the long-term trajectory of a hair cell's recovery to its original oscillatory state. This work is a continuation of the research performed by Kao et al. [46] and is in preparation for exploring the role of efference in otoacoustic protection. The method of mechanically overstimulating a hair bundle using a stiff glass probe allows us to mimic the mechanical deflection experienced by a hair bundle *in vivo* as a repercussion of a loud sound. Here, we first start with an examination of the temporal evolution of a hair bundle's oscillation profile after it has experienced a large mechanical deflection. We specifically delve into the influence of the duration of mechanical overstimulation on a hair cell's active dynamic state, and demonstrate that longer overstimulation durations shift a hair cell further away from its original dynamic state. In the subsequent chapter, we couple this mechanical overstimulation protocol with our method for efferent actuation in order to investigate the impact of efferent stimulation on a hair cell's recovery from a high-amplitude mechanical displacement. Comparisons against the findings in this chapter elucidate the effects of efference on a hair cell's dynamic state.

## 5.2 Materials and Methods

### 5.2.1 Biological Preparation

Research was conducted following animal-handling and euthanasia protocols approved by the University of California, Los Angeles Chancellor's Animals Research Committee, in accordance with federal and state regulations. Experiments were performed on *in vitro* preparations of sacculi extracted from adult North American bullfrogs (*Rana catesbeiana*) of both genders [55]. In order to mimic the physiological conditions of the *in vivo* environment, saccular maculae were affixed in a two-compartment chamber. The basolateral and apical membranes were submerged in artificial perilymph (in mM: 110 $Na^+$, 2 $K^+$, 1.5 $Ca^{2+}$, 113 $Cl^-$, 3 D-(+)-glucose, 1 $Na^+$ pyruvate, 1 creatine, 5 HEPES) and artificial endolymph (in mM: 2 $Na^+$, 118 $K^+$, 0.25 $Ca^{2+}$, 118 $Cl^-$, 3 D-(+)-glucose, 5 HEPES), respectively. Solutions were freshly oxygenated prior to use. The otolithic membrane was gently lifted from the epithelium subsequent to nine minutes of enzymatic dissociation with 50 $\mu$g/mL collagenase IA-S (Sigma Aldrich). After the otolithic membrane was decoupled, spontaneous oscillations were observed in hair bundles and could be sustained for several hours following dissection.

### 5.2.2 Imaging and Tracking Hair Bundle Motion

Experiments were performed with an upright optical microscope (Olympus BX51WI) mounted on a vibration-isolation table (Technical Manufacturing Corporation) and imaged with a water immersion objective (Olympus XLUMPlanFL N, 20×, 1.00 NA). Images were optically magnified (∼400× total magnification) and recorded with a high-speed CMOS camera (Photron FASTCAM SA1.1) at 1000 frames per second. A hair bundle's movement was tracked utilizing software written in MATLAB (The MathWorks), and its position was determined by the center of gravity of the bundle's intensity profile along a row of pixels [55]. The time-dependent position trace of a hair bundle's motion was acquired by plotting the mean position for each frame of the recording.

### 5.2.3 Mechanical Overstimulation

Prolonged mechanical overstimulation was applied with a glass probe approximately $1-2$ $\mu$m in diameter (Fig. 5.1A). Glass fibers were initially pulled from borosilicate glass capillaries in a micropipette puller (Sutter Instruments P-97). Then, an additional rod was fabricated perpendicular to the tip of the pulled capillary with a modified microforge. In order to depress the natural adhesion that occurs between a hair bundle and a glass fiber, the fiber tips were coated with a layer of hydrophobic silane (Gelest SII6453.0). Probes were mounted on a piezoelectric actuator (Piezosystem Jena PA 4/12) and positioned $\sim$2 $\mu$m away from the tallest row of stereocilia. Step signals corresponding to an $\sim$1 $\mu$m deflection were generated and digitally filtered (eight-pole Bessel filter at 300 Hz) in Python. Prior to experimentation, visual confirmation ensured that the glass fiber deflected the hair bundle by $\sim$1 $\mu$m. Step deflections were sent to the piezoelectric amplifier concurrently with video acquisition via LabView (National Instruments). In order to account for the glass probe's hydrodynamic effects in our analysis, surveillance of the bundle's recovery response initiated only once the probe was fully withdrawn. Large-scale displacements of the hair bundle (in the direction of the kinocilium) provided mechanical overstimulation that detuned the hair cells away from their natural dynamic state [46]. Prior work indicated that a sustained steady-state deflection elicited the same effects as a prolonged high-amplitude sinusoidal deflection, thus mimicking the effects of loud sound *in vitro* [98].

### 5.2.4 Data Analysis

#### 5.2.4.1 Baseline Extraction from Overstimulation Recovery

Recovery of active bundle motility following mechanical overstimulation involves both a return to the bundle's initial equilibrium position and a reemergence of bundle oscillations [46]. To disentangle these two components from the original recovery trace, we calculated the baseline trend in two steps. First, a rough estimation of the baseline was computed by passing the original recovery trace through a moving average filter (5 points window) five times, and the time at which the slope of the rough baseline estimation surpassed -

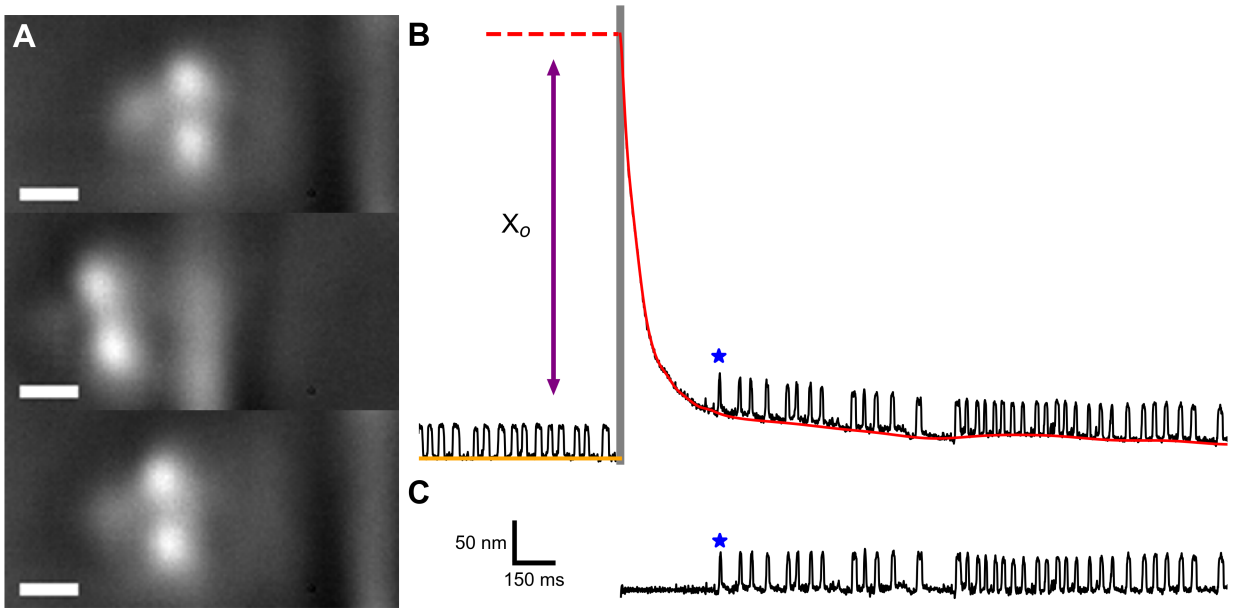


Figure 5.1: **A**) Bright field images showing the application of a large-amplitude ($\sim 1$ $\mu$m) mechanical deflection to an individual hair bundle via a stiff glass probe. The top, middle, and bottom panels depict the hair bundle prior to, during, and immediately after the mechanical overstimulation, respectively. The width of the scale bar is 1 $\mu$m. **B**) Hair bundle position traces (black) were extracted from high-speed recordings of hair cells undergoing mechanical overstimulation. Hair bundles experienced an induced offset before relaxing back to their initial oscillatory dynamic state. The gray vertical bar represents the interval during which the deflection was applied. The baseline (red) of a hair bundle's relaxation trace (black) was subtracted from the original trace to obtain a flattened recovery trace (**C**). The blue star annotates the location of the first detected oscillation. The initial (induced) offset, $X_o$, is the height difference between the position of the hair bundle directly after the withdrawal of the glass probe (red dotted line) and the baseline of the pre-stimulus spontaneous oscillations (orange line). Scale bars in **C** are applicable for **B**.

0.02 nm/ms was determined. Then, a narrow moving average filter (11 points window) was implemented three times for position values prior to this threshold time, and a 1000 points window size was adopted for the subsequent data points and applied three times. The final baseline trend was obtained by stitching the two parts together at the threshold point so as to eliminate any discontinuity (Fig. 5.1B). Isolating the slow component of the recovery and subtracting it from the original recording resulted in a "flattened" recovery trace (Fig. 5.1C), which allowed for ready visualization of the oscillation onset. We note that this approach yielded similar results to the two-exponent fit used previously [46].

#### 5.2.4.2 Determination of Instantaneous Oscillation Frequency, Amplitude and Open Probability

Throughout this manuscript, a positive displacement in a trace corresponds to motion towards the kinocilium, which is consistent with the standard convention in the literature. Our analysis included only those position traces (flattened or otherwise) for which the hair bundle's activity was classified as oscillatory by satisfying the criteria of multi-modality in the position distribution [37, 95, 96, 55]. For all position traces, the open-channel threshold was computed in the same manner detailed in our previous work [55]. Then, the instantaneous frequency was acquired by inverting the period between two consecutive, positive transitions from the closed-channel state to the open-channel state. For the composite data points of a single cycle, those points above and below the threshold were separately averaged to give a top and bottom mean. The instantaneous amplitude of the cycle was defined to be half of the difference between the two means. The instantaneous open probability was obtained by dividing the amount of position data points with values exceeding the threshold by the total number of data points in an individual cycle. Instantaneous parameters tabulated for an analyzed trace were averaged to obtain the mean oscillation parameters. Trendlines were generated by way of a moving average filter.

#### 5.2.4.3 Determination of Quiescent Time and Initial Offset

Two additional parameters, quiescent time and initial offset, were extracted from the overstimulation recovery position traces. The quiescent time, $T_q$, is the length of time between the cessation of the overstimulation and the first oscillation, as determined by the process detailed in the previous section. The initial offset, $X_o$, is defined as the height difference between the apex of the original recovery trace and the baseline of the spontaneous oscillations prior to mechanical overstimulation (Fig. 5.1B).

## 5.3 Results

### 5.3.1 Hair bundles express gradual recuperation following mechanical overstimulation

Hair bundles of the amphibian sacculus have been shown to exhibit spontaneous oscillations, active motion observed in the absence of stimulus, which are indicative of an interplay between mechanical transduction and internal adaptation processes [70, 65]. This active motility is sensitive to changes in $Ca^{2+}$ concentration, membrane potential of the soma, and other manipulations, and thus provides us with a useful experimental readout of the dynamic state of the hair bundle [13, 70, 53, 85, 92, 72, 95, 55]. While loud sounds would naturally occur at specific frequencies, our prior studies of overstimulation showed that the effect on saccular hair bundles was not dependent on the frequency of the stimulus, but rather on the duration of the applied signal [46]. For simplicity, we henceforth focus on steady state deflections of the bundle and vary only the length of the stimulus.

Here, we report on the findings of experiments on saccular hair cells solely experiencing mechanical overstimulation, and examine its impact on the innate oscillations of the bundle. We applied large ($\sim$1 $\mu$m) mechanical deflections to hair bundles via a silane-coated, stiff glass probe. The deflections were applied for an overstimulation duration (OD) of 5 s, 10 s, 20 s or 40 s. Bundles were deflected in the positive direction (towards the kinocilium), which corresponds with opening transduction channels. Recordings began two seconds prior to the

application of the stimulus and concluded 20 seconds after the probe was retracted. All of the examined hair cells exhibited robust spontaneous bundle oscillations prior to mechanical overstimulation. Fig. 5.2A and Fig. 5.3A portray the hair bundle time courses of recovery of two individual hair cells (from distinct sacculi) following each of the four overstimulation durations. The same sets of positions traces are plotted in Fig. 5.10A and Fig. 5.11A for two additional hair cells (separate sacculi) and can be viewed in the Supplemental Information and Figures (Section 5.5). We observed both a transitory suppression of spontaneous oscillations and a temporary offset in bundle position, consistent with observations by Kao et al. [46].

#### 5.3.1.1 Extracted baselines (Slow component of recovery)

The extracted baselines (red) shown in Fig. 5.2A and Fig. 5.11A are chromatically visualized in Fig. 5.4A and Fig. 5.4C, respectively. The baseline displacements were normalized by their respective initial offsets. Thus, the range of the colorbars in Fig. 5.4 extend from 1.0 to 0.0 – with 1.0 corresponding to the bundle at its peak displacement, and 0.0 corresponding to the bundle having fully returned to its steady state level. Increasing the overstimulation duration caused the hair bundle to withdraw more slowly back to its steady state position, with a typical return halfway back to original position occuring within the first 150 ms. A more marked change between the 10 s OD and 20 s OD tiers can be seen in Fig. 5.4D, compared to the subtle difference pictured in Fig. 5.4B. Averaging baselines collected from 13 bundles (6 sacculi) produced Fig. 5.5, which suggests that the shape of a bundle's baseline recovery from 10 s OD and 20 s OD were generally comparable.

#### 5.3.1.2 Frequency, amplitude, and open probability trendlines (Fast component of recovery)

To quantify the effects of mechanical deflections on the temporal profiles of hair bundle oscillations, we examined the trendlines of the instantaneous frequencies, amplitudes, and open probabilities of flattened traces and investigated the time dependence of recovery to

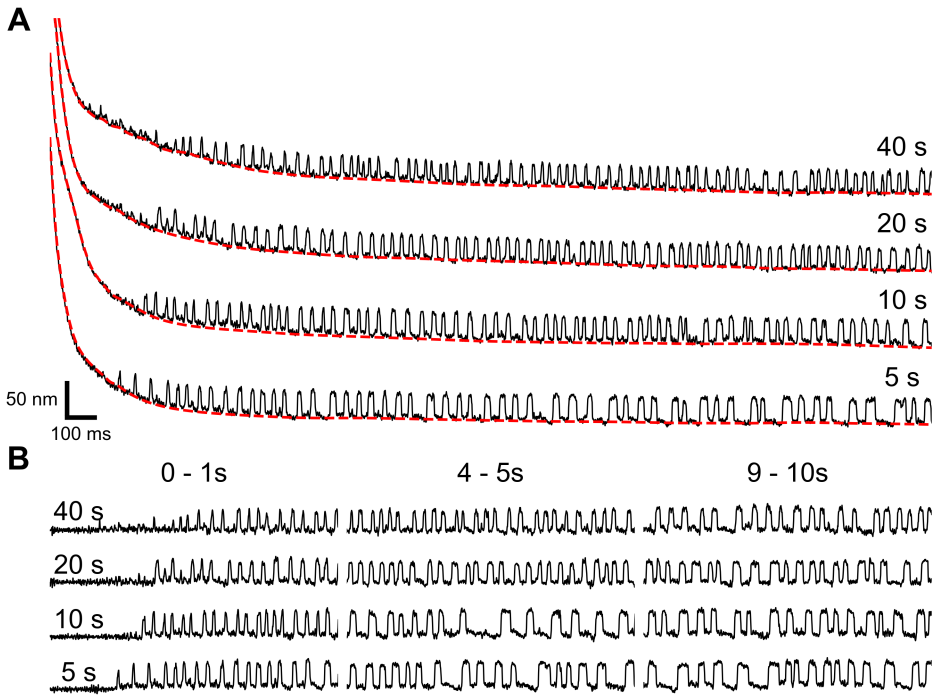


Figure 5.2: A hair bundle's relaxation trajectory was dependent on the duration of mechanical overstimulation. **A**) A series of traces recorded from a single hair cell (Hair Cell 1) is shown. Each trace depicts hair bundle recovery following mechanical overstimulation of duration (in seconds) indicated on the right. The hair bundle remained in a quiescent state longer with increasing stimulus duration. The recording order was from bottom to top. **B**) A series of flattened recovery traces, extracted from the recordings displayed in **A**, is shown. Three, chronologically subsequent segments are displayed in the first (0 – 1 s), second (4 – 5 s), and third (9 – 10 s) panels. Longer overstimulation durations led to slower recovery of the original oscillation profile. Scale bars in **A** are applicable for **B**.

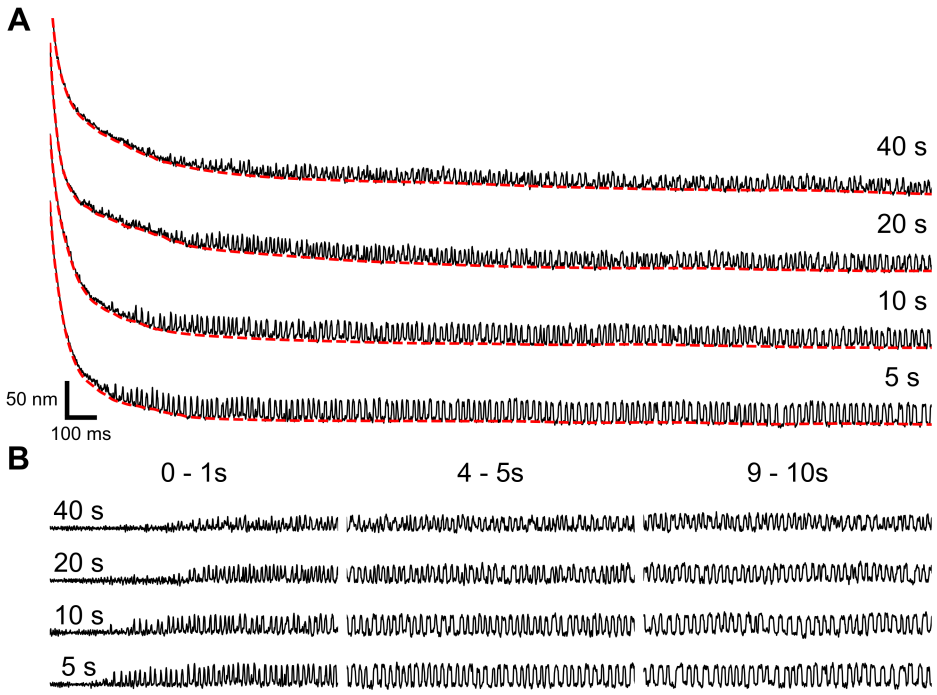


Figure 5.3: A hair bundle's relaxation trajectory was dependent on the duration of mechanical overstimulation. **A**) A series of traces recorded from a single hair cell (Hair Cell 2) is shown. Each trace depicts hair bundle recovery following mechanical overstimulation of duration (in seconds) indicated on the right. The hair bundle remained in a quiescent state longer with increasing stimulus duration. The recording order was from bottom to top. **B**) A series of flattened recovery traces, extracted from the recordings displayed in **A**, is shown. Three, chronologically subsequent segments are displayed in the first (0 – 1 s), second (4 – 5 s), and third (9 – 10 s) panels. Longer overstimulation durations led to slower recovery of the original oscillation profile. Scale bars in **A** are applicable for **B**.

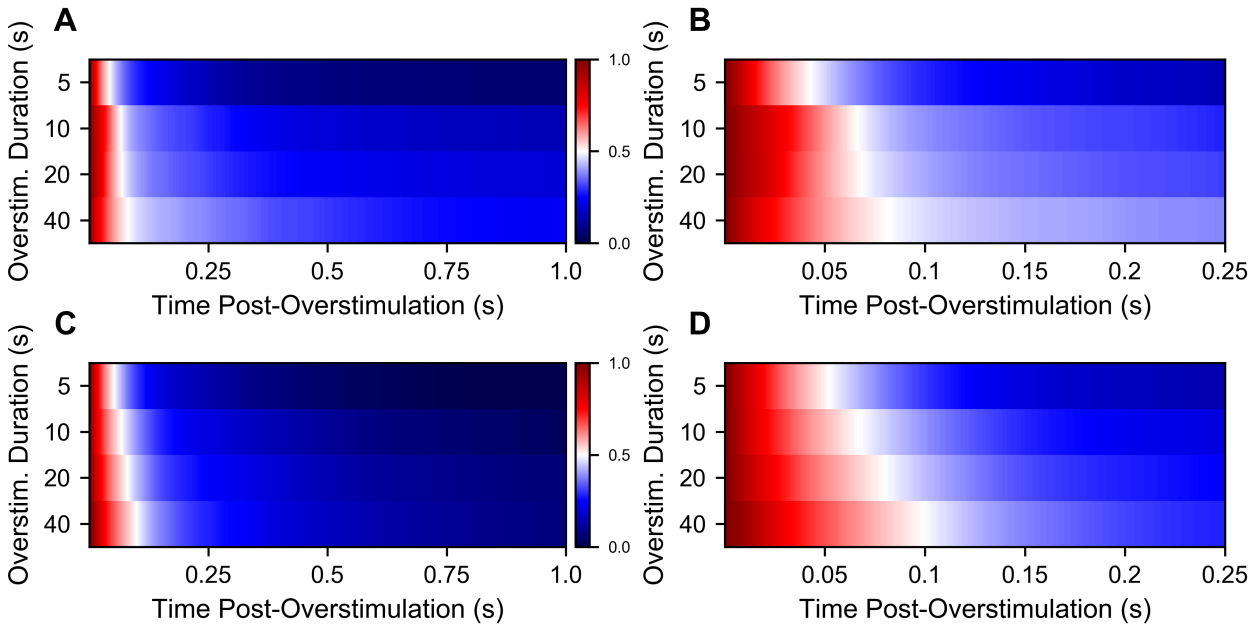


Figure 5.4: The duration of overstimulation significantly affected the slow-component of a hair bundle's recovery from mechanical overstimulation. The normalized chromatic representations of the relaxation baselines in **A** and **C** are reflective of those plotted in Fig. 5.2A and Fig. 5.11A, respectively. Baselines were normalized by their respective initial offsets, with 1.0 on the colorbar corresponding to the bundle being at its highest offset and 0.0 corresponding to the bundle having fully returned to its steady state level. **B** and **D** provide a zoom-in of the first 250 ms of **A** and **C**, respectively. A longer overstimulation duration led to a slower resumption of the steady state position.

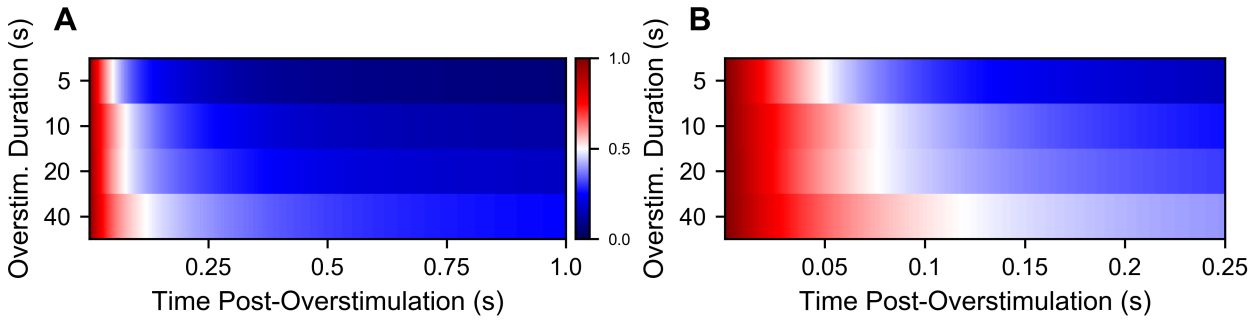


Figure 5.5: The duration of overstimulation significantly affected the slow-component of a hair bundle's recovery from mechanical overstimulation. **A**) Baselines recorded from 13 bundles (6 sacculi) were averaged together and the resulting mean baselines are chromatically visualized. Before averaging, baselines were initially normalized by their respective initial offsets, with 1.0 on the colorbar corresponding to the bundle being at its highest offset and 0.0 corresponding to the bundle having fully returned to its steady state level. **B** provides a zoom-in of the first 250 ms of **A**. On average, the normalized chromatic representations of the mean recovery baselines show that increasing the overstimulation duration led to a slower resumption of the steady state position.

the original oscillatory state. The trendlines presented in Fig. 5.6A–C and Fig. 5.6D–F were calculated from the traces in Fig. 5.2B and Fig. 5.3B, respectively. Frequency, amplitude, and open probability trendlines extracted from 13 bundles (6 sacculi) were averaged, and the mean trendlines for each overstimulation duration are depicted in Fig. 5.7A (frequency), Fig. 5.7B (amplitude), and Fig. 5.7C (open probability). In Fig. 5.6 and Fig. 5.7, trendlines associated with a 5 s OD, 10 s OD, 20 s OD, and 40 s OD are plotted in red, gold, blue, and violet, respectively. Fig. 5.7A indicates that the initial frequency of spontaneous oscillation for a hair cell recovering from quiescence was dependent on the overstimulation duration – longer ODs gave rise to higher initial frequencies. In all cases, the frequency trendlines progressed towards a plateau. Fig. 5.7B shows the pattern obtained for amplitude recovery – longer ODs led to smaller initial amplitudes. The trendlines of the four conditions gradually regressed towards a common point. Finally, Fig. 5.7C shows a negative correlation between a bundle's nascent open probability and its overstimulation duration. Similar to Fig. 5.7B, the four mean trendlines arched upwards until leveling off. The conclusions drawn from the mean plots can also be inferred from the individual bundle plots. Fig. 5.7 indicates that

longer overstimulation durations shifted a hair cell further away from its original dynamic state.

Focusing on a 20 s overstimulation duration, we show the findings of an ensemble of 33 hair cells sampled across 14 sacculi in Fig. 5.8. Their individual instantaneous frequency, amplitude, and open probability trendlines are illustrated in Fig. 5.8A, Fig. 5.8B, and Fig. 5.8C, respectively; their respective normalized trendlines are recreated in Fig. 5.8D–F. Normalization was obtained by taking the ratio of instantaneous frequency, amplitude, and open probability, by their respective mean values that were obtained from their pre-stimulus spontaneous oscillations. As with Fig. 3.16, the hair bundles in Fig. 5.8A and Fig. 5.8D are color-coded in ascending order by their initial (normalized) frequency. The color assigned to a cell in Fig. 5.8A or Fig. 5.8D is employed for the same cell in Fig. 5.8B & Fig. 5.8C or Fig. 5.8E & Fig. 5.8F, respectively. The color schema showed no apparent relationship between the initial values of the three oscillation traits. Fig. 5.8D–F show the consistent prevailing trends of the bundles' recoveries to their original oscillatory states.

#### 5.3.1.3 Power spectral densities

Lastly, we examined the time-evolution of a hair bundle's power spectral density during its recovery from mechanical overstimulation. Fig. 5.9A and Fig. 5.9B demonstrate the PSDs of the flattened recovery position traces in Fig. 5.10B and Fig. 5.3B, respectively. The first, second, third, and fourth panels of each sub-figure correspond to a 5 s OD, 10 s OD, 20 s OD, and 40 s OD, respectively. The power spectral density of each cell's fundamental spontaneous oscillations is plotted in gray. PSDs of four successive five-second sections of a bundle's flattened position trace are plotted in red, gold, green, and blue, respectively. Consistent with our preceding findings, the power spectral density of a recuperating hair cell displayed an initial rightward shift in the direction of higher frequencies. Longer overstimulation durations induced increasingly depressed magnitudes before migrating leftward and growing in magnitude. These observations were persistent amongst the 13 hair cells surveyed.

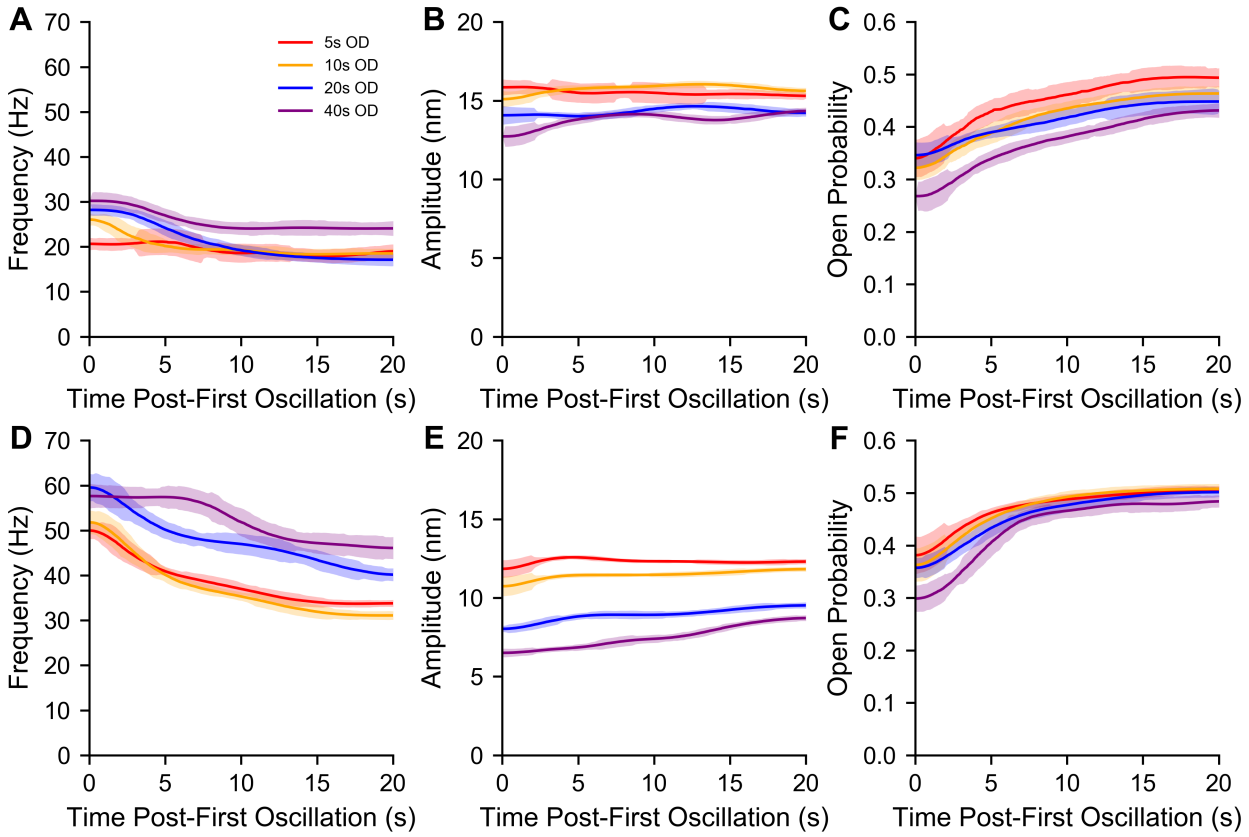


Figure 5.6: Varying the duration of hair bundle deflection affected the induced shifts in the oscillation parameters. Time-series trendlines of instantaneous frequencies, amplitudes, and open probabilities are plotted for the hair cell in Fig. 5.2B (**A**, **B**, **C**) and Fig. 5.3B (**D**, **E**, **F**), respectively. The four overstimulation durations (5 s, 10 s, 20 s, 40 s) are plotted in red, gold, blue, and violet, respectively. A hair bundle re-entered the oscillatory regime displaying different characteristics from its initial state. The oscillation parameters reflected this difference before gradually transitioning back to its characteristic values. As the OD increased, the initial frequency increased, while the amplitude and open probability decreased. This increased detuning from the original state correlated with a slower recovery from longer mechanical overstimulation. Error bands represent the standard deviations of data points in a one second moving window.

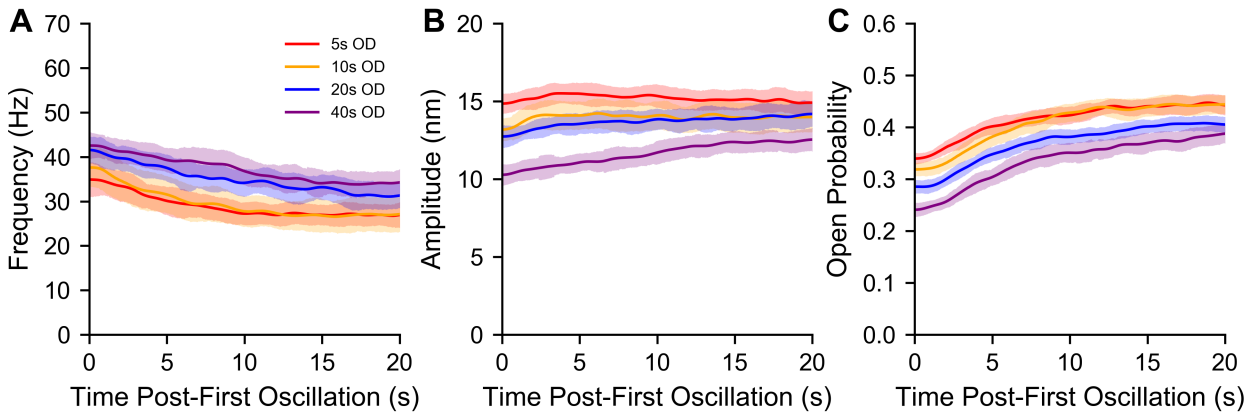


Figure 5.7: Varying the duration of hair bundle deflection affected the induced shifts in the oscillation parameters. Frequency, amplitude, and open probability trendlines of the same overstimulation duration were averaged together to obtain the mean trendlines in **A**, **B**, and **C**, respectively. The four overstimulation durations (5 s, 10 s, 20 s, 40 s) are plotted in red, gold, blue, and violet, respectively. A hair bundle re-entered the oscillatory regime displaying different characteristics from its initial state. The oscillation parameters reflected this difference before gradually transitioning back to its characteristic values. As the OD increased, the initial frequency increased, while the amplitude and open probability decreased. This increased detuning from the original state correlated with a slower recovery from longer mechanical overstimulation. The averaged trendlines reflect data from 13 bundles (6 sacculi). Error bands represent the standard deviations of data points in a one second moving window.

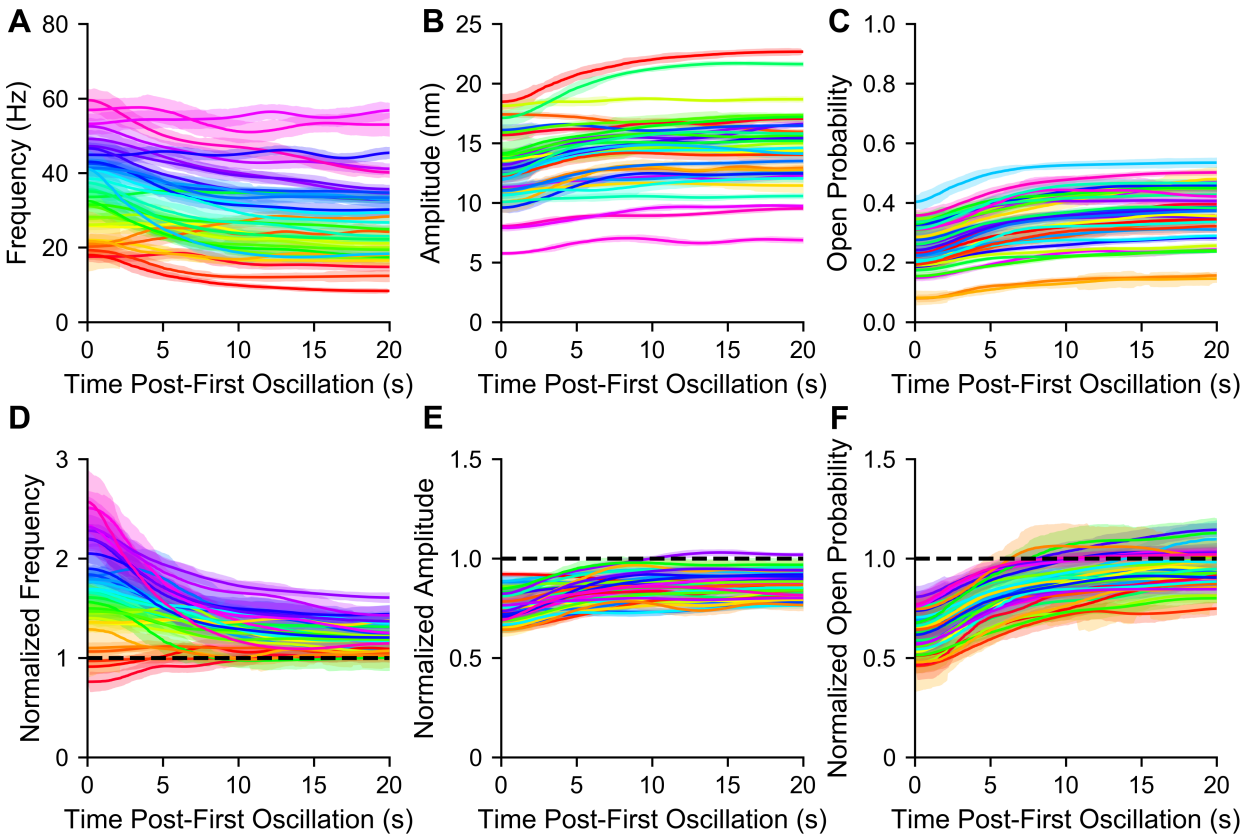


Figure 5.8: A large sample of hair cells demonstrated a wide variety of responses and recoveries to mechanical overstimulation. Time courses of the instantaneous frequencies (**A**), amplitudes (**B**) and open probabilities (**C**) of 33 bundles across 14 sacculi are displayed. The trendlines in **A**–**C** were normalized by their measured characteristic values, obtained from the same bundle prior to efferent stimulation, and are shown in **D**–**F**. Each bundle in **A** and **D** is color-coded in ascending order by its initial frequency and normalized frequency value, respectively. The color representing an individual hair bundle in **A** and **D** is used for the same hair bundle in **B** & **C** and **E** & **F**, respectively. For panels showing normalized trendlines, full recuperation to the characteristic value is indicated by the black dashed line at 1.0. Error bands represent the standard deviations of data points in a one second moving window.

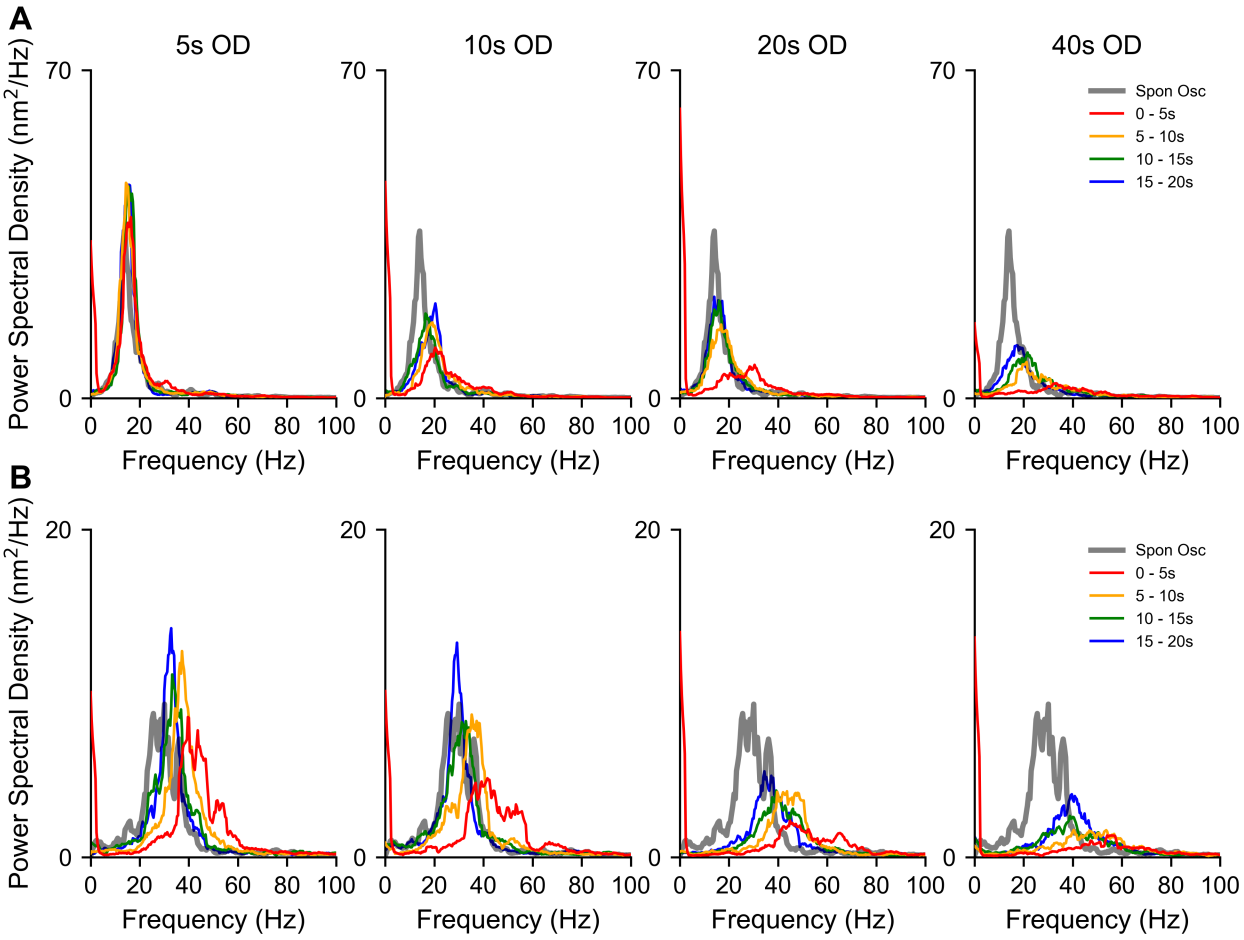


Figure 5.9: Hair bundles exhibited slower recoveries in the frequency domain as a response to increased overstimulation durations. **A**, **B**) Sets of time-lapsed power spectral densities of two hair bundles from two distinct sacculi are displayed. The PSDs were computed from the flattened recovery traces of each respective hair cell. Time-lapsed PSDs corresponding to a 5 s, 10 s, 20 s, and 40s OD are displayed in the first, second, third, and fourth panels, respectively. Power spectral densities of a bundle's flattened return are plotted in red, gold, green, and blue for each five second segment up to 20s, respectively, following the cessation of mechanical overstimulation. The PSD of a hair bundle's spontaneous oscillations is plotted in gray. PSDs in **A** and **B** reflect the hair bundle position traces in Fig. 5.10B and Fig. 5.3B, respectively. Longer overstimulation durations increased the hair cell's detuning from the original state, which is consistent with our visual observations.

## 5.4 Discussion

The hair bundle exhibits a complex temporal profile as it relaxes back to its equilibrium position following the cessation of mechanical overstimulation. Our findings indicate that, with lengthening deflection durations, the hair cell's burgeoning spontaneous oscillation frequency generally increased, while the amplitude and open probability typically decreased. The strong dependency of the hair bundle's incipient oscillation frequency, amplitude, and open probability on the overstimulation duration point to a cumulative effect that seems to integrate over the presentation of mechanical stimulus.

When the hair bundle is deflected, the mechanoelectrical transduction (MET) channels are held in a preferentially open state, allowing for the influx of cations, which are predominantly $K^+$ but with a fraction of the current carried by $Ca^{2+}$ [59, 61, 44]. In conjunction, $Ca^{2+}$ pumps located in the stereovilli continuously extrude $Ca^{2+}$ in order to restore a low internal resting concentration [60]. The impact of prolonged deflection on the dynamics of the hair bundle has not been fully explained and likely involves a combination of internal mechanisms. As adaptation of the channel opening probability has been shown to be incomplete [21], a deflection applied at a large amplitude is likely to lead to a prolonged ionic influx, which possibly overwhelms the extrusion pumps and leads to an accumulation of $Ca^{2+}$ within the stereovilli. Studies involving manipulations of external $Ca^{2+}$ concentration and blockers of extrusion pumps were consistent with this possibility [60, 10, 46]. Another set of studies showed that depolarization of the hair cell soma strongly impacts the oscillations of the bundle [72, 47], again likely by modulating the internal $Ca^{2+}$. While a direct effect of voltage on the bundle mechanics cannot be excluded, voltage-mediated effects on bundle position have thus far been found to be transient [7], and hence unlikely to play a role in the slow recovery. Finally, the myosin motors which tune the optimal set point of the hair bundle are likely to be strongly offset by the deflection. The full biophysical effect, therefore, likely involves an interplay between depolarization of the soma, possible $Ca^{2+}$ accumulation in the stereovilli, and myosin motor offsets.

### 5.4.1 Mechanical overstimulation induces a transition in the dynamic state of the hair bundle

In the formalism of nonlinear dynamics theory, however, the effect is fairly simple. A number of active nonlinear systems have been described using equations that exhibit two different dynamic states: a quiescent and an oscillatory state – with a critical point separating the two regimes. Spontaneous hair bundle oscillations have been shown to constitute active limit cycles, which are very well described by these simple models [14, 78, 104]. Our results show that the application of a strong mechanical signal, which triggers a complex set of internal biophysical processes, ultimately modulates a control parameter that temporarily shifts the hair bundle into the quiescent state. Theoretical work on hair cell dynamics has long speculated that a control mechanism serves to tune its response [16, 14, 98]. The findings reported in Chapter 6 (Section 6.3) indicate that the efferent neurons may serve as this biological control mechanism.

## 5.5 Supplemental Information and Figures

### 5.5.1 Supplemental hair bundles' mechanical overstimulation recovery position traces

Here, we present mechanical overstimulation recovery traces of two additional hair cells sourced from separate sacculi (Fig. 5.10 and Fig. 5.11).

### 5.5.2 Consistency of measured quiescent times and initial offsets with previous studies

We extracted quiescent times ($T_q$) and induced initial offsets ($X_o$) as a confirmation of our protocol for mechanically overstimulating hair bundles (Fig. 5.12). Our results are consistent with those recorded by Kao et al. [46].

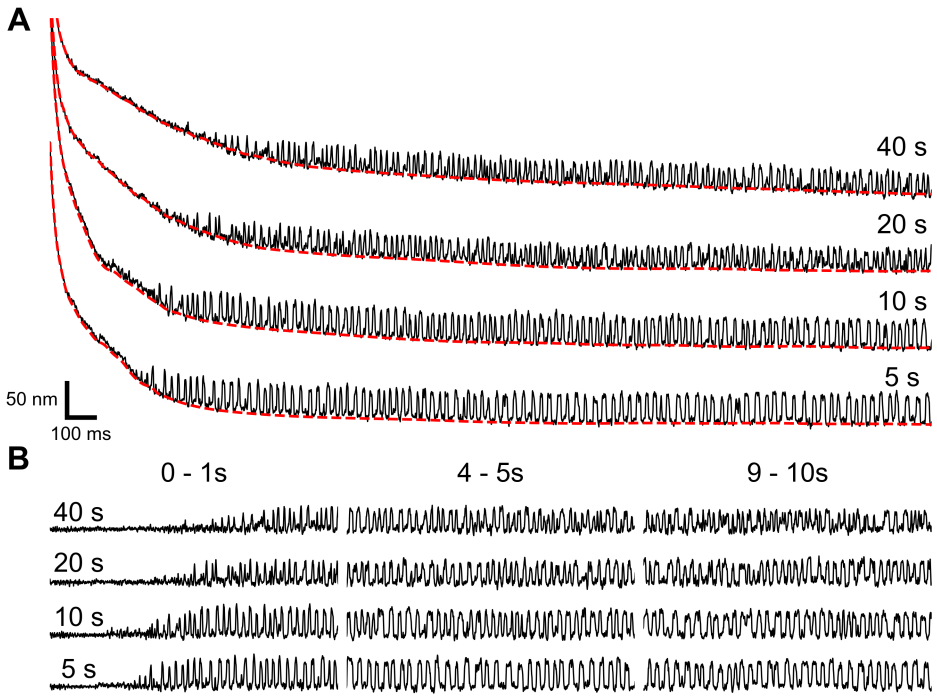


Figure 5.10: A hair bundle's relaxation trajectory was dependent on the duration of mechanical overstimulation. **A**) A series of traces recorded from a single hair cell (Hair Cell 3) is shown. Each trace depicts hair bundle recovery following mechanical overstimulation of duration (in seconds) indicated on the right. The hair bundle remained in a quiescent state longer with increasing stimulus duration. The recording order was from bottom to top. **B**) A series of flattened recovery traces, extracted from the recordings displayed in **A**, is shown. Three, chronologically subsequent segments are displayed in the first (0 – 1 s), second (4 – 5 s), and third (9 – 10 s) panels. Longer overstimulation durations led to slower recovery of the original oscillation profile. Scale bars in **A** are applicable for **B**.

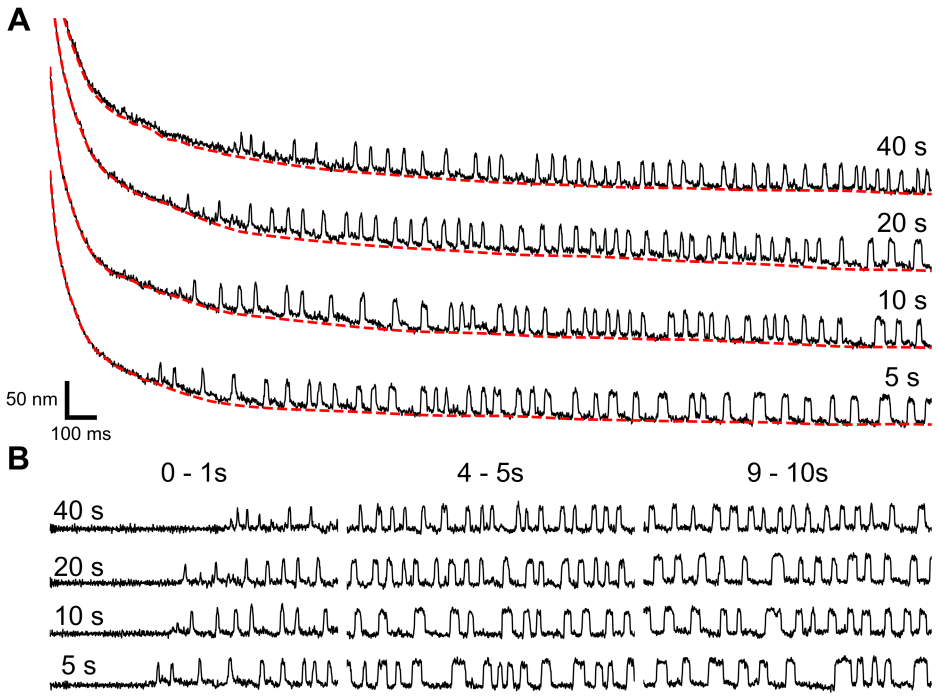


Figure 5.11: A hair bundle's relaxation trajectory was dependent on the duration of mechanical overstimulation. **A**) A series of traces recorded from a single hair cell (Hair Cell 4) is shown. Each trace depicts hair bundle recovery following mechanical overstimulation of duration (in seconds) indicated on the right. The hair bundle remained in a quiescent state longer with increasing stimulus duration. The recording order was from bottom to top. **B**) A series of flattened recovery traces, extracted from the recordings displayed in **A**, is shown. Three, chronologically subsequent segments are displayed in the first (0 – 1 s), second (4 – 5 s), and third (9 – 10 s) panels. Longer overstimulation durations led to slower recovery of the original oscillation profile. Scale bars in **A** are applicable for **B**.

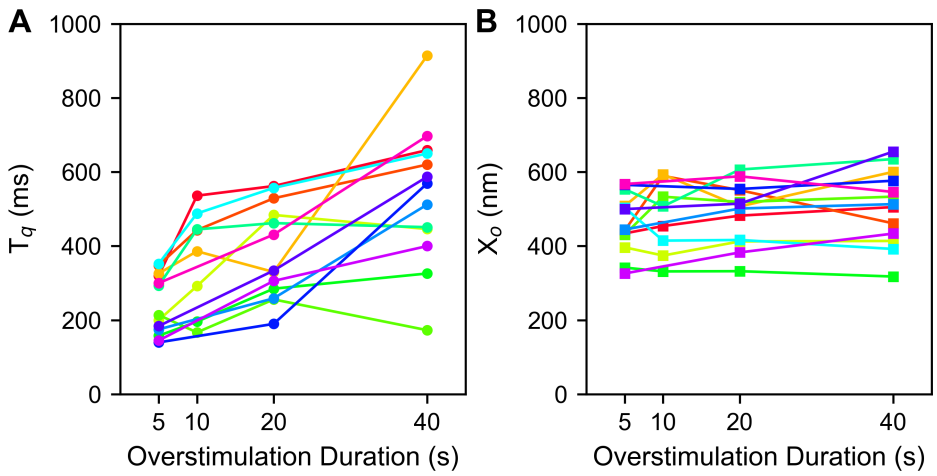


Figure 5.12: **A**) Quiescent times ($T_q$) and **B**) initial offsets ($X_o$) corresponding to four different ODs are displayed. The two quantities were extracted from the recordings of 13 hair bundles obtained from 6 sacculi. Data points from the same hair bundle are plotted in the same color and connected together. These results are consistent with the findings of Kao et al. [46].

### 5.5.3 Reversibility of mechanical overstimulation

Mechanically overstimulating a hair cell did not generate a cumulative change in the slow component of a hair bundle's recovery dynamics. A hair bundle's baseline response to a high-amplitude mechanical deflection was reversible, even for such extended overstimulation durations (Fig. 5.13). This is also consistent with observations made by Kao et al. [46].

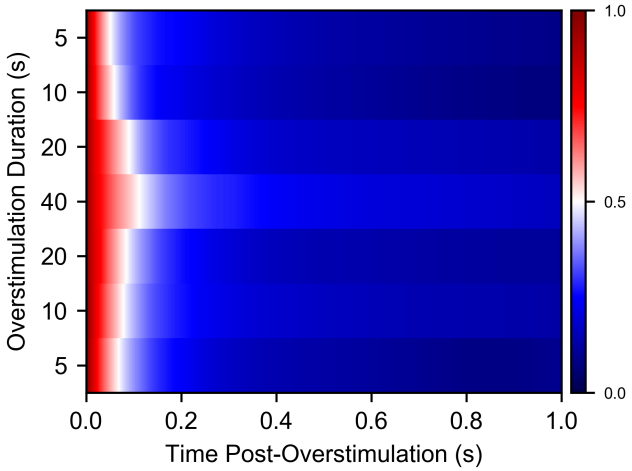


Figure 5.13: Mechanically overstimulating a hair cell did not generate a cumulative change in the slow component of a hair bundle's recovery dynamics. Baselines were normalized by their respective initial offsets, with 1.0 on the colorbar corresponding to the bundle being at its highest offset and 0.0 corresponding to the bundle having fully returned to its steady state level. Recordings were made from the top to the bottom. A hair bundle's baseline response to a high-amplitude mechanical deflection was reversible, even for such extended overstimulation durations.

# CHAPTER 6

# Impact of Efferent Modulation on Hair Cell Response to Mechanical Overstimulation

## 6.1 Introduction

The efferent system has been directly implicated in mitigating noise-induced deterioration in the inner ear. Specifically, acoustic trauma generated more advanced levels of hair cell extinction and synaptic damage in subjects with impaired efferent innervation. However, it is still not known how efferent stimulation effectuates its protective role at the level of an individual hair cell. The results presented in the previous chapter showed that a high-amplitude mechanical deflection detunes a hair bundle from its innately oscillatory regime and renders it quiescent for intervals dependent on the applied stimulus. In the current chapter, we investigate the influence of efferent modulation on a hair bundle's active recovery dynamics following mechanical overstimulation. We approach this task by examining the time evolution of a hair bundle's oscillatory profile as it recovers from a large-amplitude mechanical displacement while incorporating different modes of efferent activity. We demonstrate that efferent activation drastically changes the dynamics of hair bundle recovery following mechanical overstimulation. Simultaneous efferent actuation with the hair bundle's relaxation from a high-amplitude mechanical deflection significantly altered the recovery profile and often entirely eliminated a protracted transition from quiescence. This finding indicates that the efferent system provides a biological feedback mechanism that controls the dynamic state of a hair cell.

## 6.2 Materials and Methods

### 6.2.1 Biological Preparation

Refer to Section 5.2.1.

### 6.2.2 Imaging and Tracking Hair Bundle Motion

Refer to Section 5.2.2.

### 6.2.3 Efferent Stimulation

The saccular nerve was stimulated using a bipolar suction electrode (A-M Systems) [55] and electrically connected to the positive electrode via a 0.5 mm diameter silicon tube [15]. The reference electrode was positioned in the basolateral compartment. Current was supplied to the suction electrode via a linear stimulus isolator (World Precision Instruments A395), and stimulus protocols were sent to the isolator via LabView (National Instruments). Throughout this work, efferent modulation was delivered in the form of a 200 $\mu$A pulse train with a 3 ms pulse duration and a 10 ms inter-pulse interval. In experiments featuring dual mechanical and electrical stimulation of the hair cell, a five class efference paradigm was utilized (Fig. 6.1). The efferents were not actuated in Class 0, and thus Class 0 was treated as the control against which comparisons were made. In Class 1, the efferent neurons were activated before, during, and after the standard mechanical overstimulation for a total of 60 s. Class 2, Class 3, and Class 4 present efferent modulation exclusively before, during, and after the mechanical overstimulation, respectively.

### 6.2.4 Mechanical Overstimulation

Refer to Section 5.2.3.

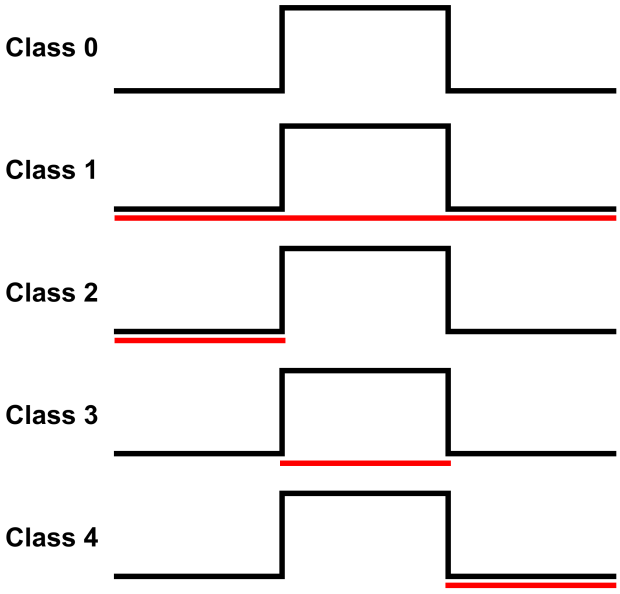


Figure 6.1: To parse the impact of efferent activity on different intervals of hair bundle deflection and recovery, we examined the hair bundle response to mechanical overstimulation under five different efferent stimulus paradigms. In all cases, the duration of mechanical deflection was kept constant at 20 seconds. The five stimulation protocols were designed as follows: Class 0 had no efferent stimulation and solely consisted of a large mechanical deflection. Class 1 included 20 seconds of efference (200 $\mu$A, 3 ms 'on', 10 ms 'off') before, during, and after the mechanical overstimulation. Class 2, Class 3, and Class 4 featured efferent actuation exclusively before, during, or after the mechanical overstimulation, respectively.

### 6.2.5 Data Analysis

#### 6.2.5.1 Baseline Extraction from Overstimulation Recovery

Refer to Section 5.2.4.1.

#### 6.2.5.2 Determination of Instantaneous Oscillation Frequency, Amplitude and Open Probability

Refer to Section 5.2.4.2.

#### 6.2.5.3 Determination of Quiescent Time and Initial Offset

Refer to Section 5.2.4.3.

## 6.3 Results

### 6.3.1 Efferent modulation immediately influences hair cell recovery from mechanical overstimulation

We explored the impact of efferent modulation on a hair cell's recovery from mechanical overstimulation. For these experiments, the overstimulation duration was kept constant at 20 seconds, and we recorded hair bundle recovery both in the presence and absence of efferent stimulation. When efferent activation was concomitantly in effect with a hair bundle's overstimulation recovery, we routinely observed bundles whose oscillatory motion was not abated by the 20 s large-amplitude mechanical deflection (Fig. 6.2A). By contrast, all such recordings obtained without efferent stimulation (Fig. 6.2C) showed the usual suppression of bundle motility. Under both stimulus paradigms, the bundles showed a significant and comparable accumulated offset in their position – an effect discussed in a subsequent section. Efferent actuation seemed to annul the effect of the induced offset and allow for oscillations to return even during the steep initial portion of the recovery from deflection.

For clarity, we also show flattened traces for this set of recordings (Fig. 6.2B), which demon-

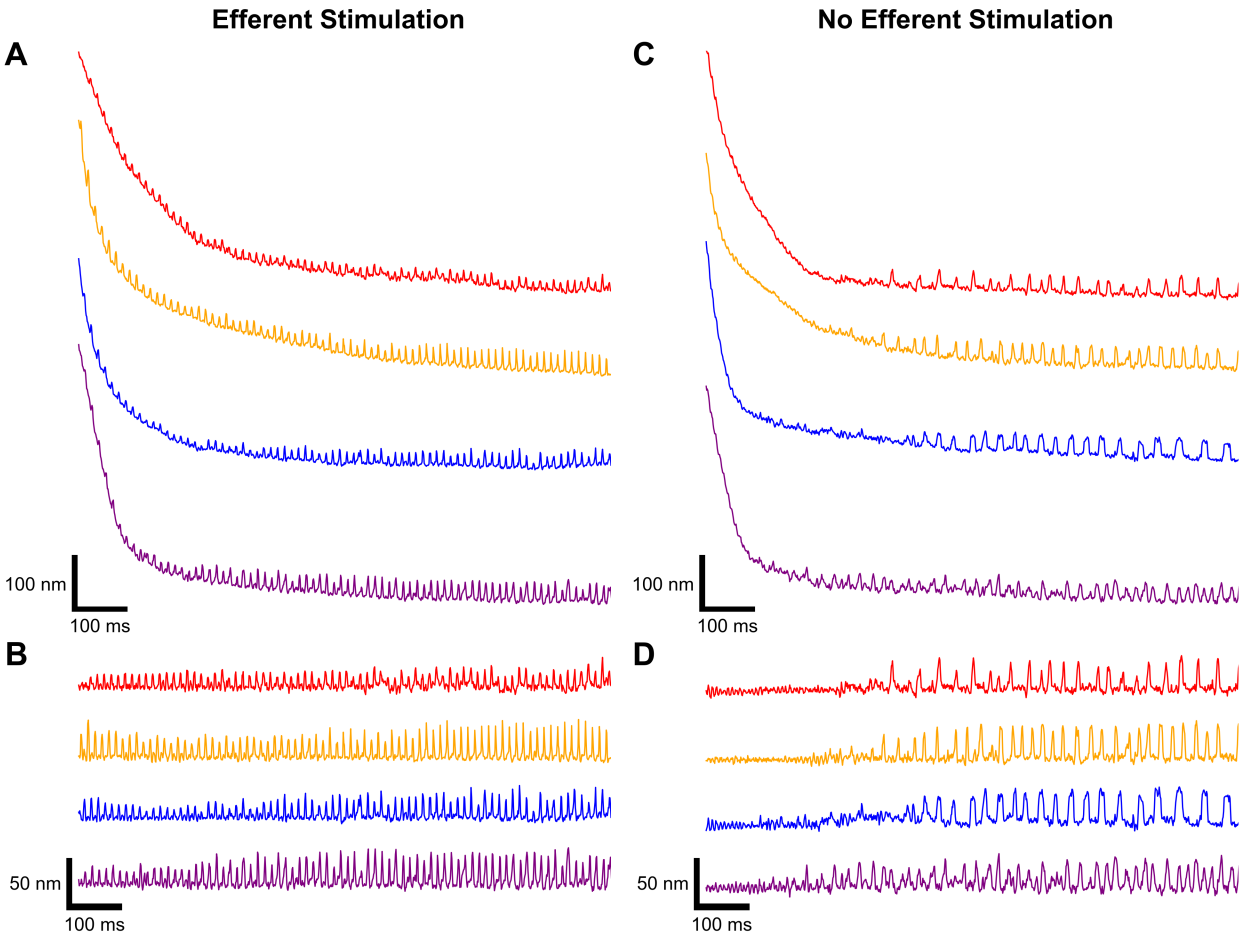


Figure 6.2: Stimulation of efferent neurons provoked an immediate crossover from the quiescent state back to the oscillatory regime. Position traces of four example hair cells recovering from mechanical overstimulation (20 s OD) with concurrent efferent actuation (**A**) illustrate hair bundles in an oscillatory state despite the large positional offsets. Analogous recordings obtained without concurrent efferent actuation (**C**) show an initial quiescent interval. **B**, **D**) Flattening the traces in **A** and **C**, respectively, confirmed that a high-amplitude mechanical deflection did not halt oscillatory motion when the efferents were simultaneously activated. Each of the four bundles originated from a distinct sacculus, are shown in different colors and offset for clarity. All traces corresponding to the same hair cell are displayed in the same color.

strate that stimulating the efferent neurons was able to provoke an immediate crossover from the quiescent state to the oscillatory state prior to recovery from the accrued offset. The corresponding flattened traces obtained in the absence of efferent activity (Fig. 6.2D) display an initial suppression of active motility. We note that this phenomenon varied greatly between bundles, with the occurrence of both hair bundles that do and do not express this feature observed in the same sacculus. This surprising finding indicates that a high-amplitude mechanical deflection does not necessarily halt innate oscillatory motion when the efferents are simultaneously activated. In the subsequent sections, we analyze the temporal dynamics of this influence, the disparate effect on the induced positional offset and oscillatory motion, and variability among bundles.

To parse the impact of efferent activity on different intervals of hair bundle deflection and recovery, we next examined the response to overstimulation under five different efferent stimulus paradigms. In all cases, the duration of mechanical deflection was kept constant at 20 seconds. The five stimulation protocols were designed as follows (Fig. 6.1): Class 0 had no efferent stimulation and solely consisted of a large mechanical deflection. Class 1 included 20 seconds of efference (200 $\mu$A, 3 ms 'on', 10 ms 'off') before, during, and after the mechanical overstimulation. Class 2, Class 3, and Class 4 featured efferent actuation exclusively before, during, or after the mechanical overstimulation, respectively. All recordings began 20 seconds before the onset of the probe deflection and concluded 20 seconds following the probe's retraction for a total recording time of 60 seconds. All reported hair bundles displayed robust spontaneous bundle oscillations prior to mechanical overstimulation.

Fig. 6.3A and Fig. 6.4A illustrate two individual hair bundle's recovery trajectories for each of the five efference paradigms. We performed the full set of experimental protocols on 18 hair cells across five sacculi. In Fig. 6.3B and Fig. 6.4B, we plot the flattened traces, with the first column showing the initial recovery of oscillation, and the remaining two showing the influence of continued efferent actuation (Class 1 and Class 4) on spontaneous oscillation profiles. The trends observed in our recordings indicate that stimulation of efferent neurons either prior to or during the mechanical stimulus (Class 2 and Class 3) had no statistically

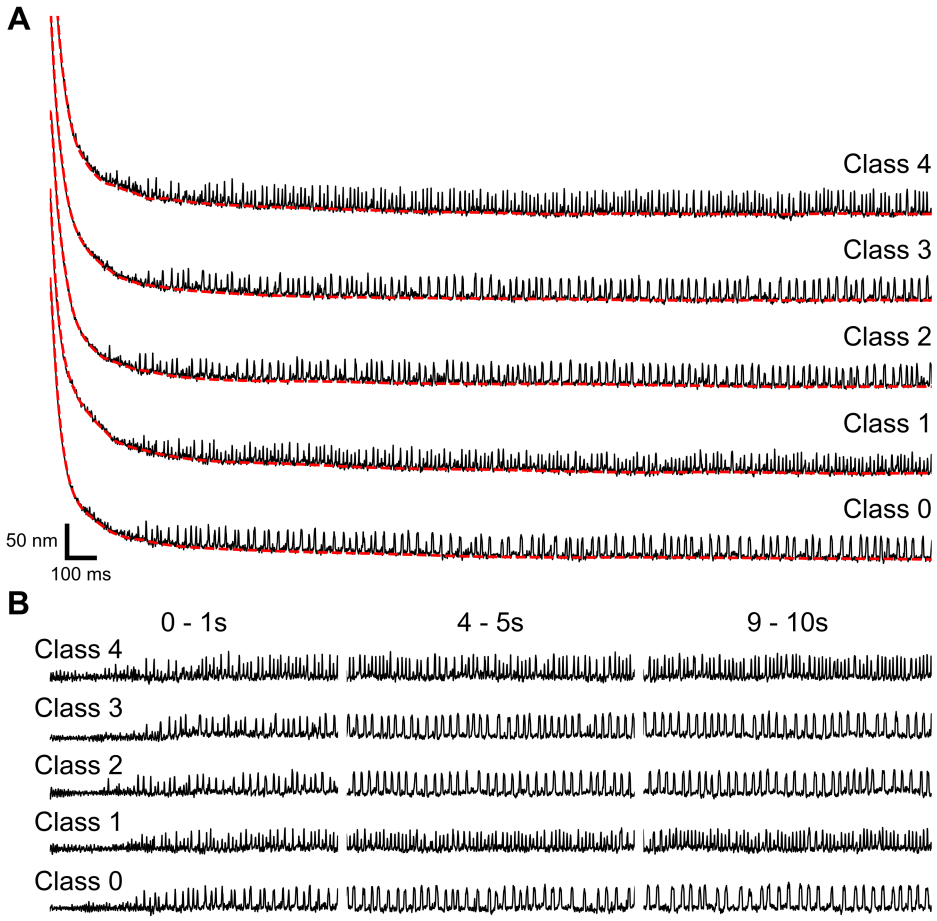


Figure 6.3: Different intervals of efferent stimulation distinctly affected a hair bundle's oscillation profile as it recovered from mechanical overstimulation. **A**) A series of traces are shown of recordings from a hair cell undergoing a combination of mechanical overstimulation and efferent actuation. Each trace depicts hair bundle motion following 20 seconds of large-amplitude mechanical deflection combined with the efference paradigm indicated on the right. The efferents are not actuated in Class 0, and thus Class 0 is treated as the control condition against which comparisons are made. In Class 1, the efferent neurons are activated before, during, and after the mechanical overstimulation for a total of 60 s. Class 2, Class 3, and Class 4 present efferent modulation exclusively before, during, or after the mechanical overstimulation, respectively. The recording order was from bottom to top. Baselines extracted from the traces are displayed in red. A portion of the observed hair bundles exhibited oscillatory motion immediately upon probe release. **B**) A series of flattened recovery traces corresponding to the traces in **A** is shown. Three, chronologically subsequent segments are displayed in the first (0 – 1 s), second (4 – 5 s), and third (9 – 10 s) panels. When efference was present during the hair bundle's recovery (Class 1 and Class 4), the bundle's oscillation profile was significantly altered. Scale bars in **A** are also applicable for **B**.

measurable effect on subsequent recovery profiles. Hence, there was no accumulated persistent change in the bundle dynamics that would affect its response. Finally, the Class 4 paradigm, which was discussed in the previous section, eliminated the initial suppression of oscillation, showing that concurrent efferent activity strongly changes the dynamics of recovery. The Class 1 paradigm, which included all intervals of the efferent stimulus, was statistically indistinguishable from Class 4.

### 6.3.2 Impact of efference on different aspects of the recovery

We next investigated how the full set of efference paradigms affected different components of the recovery.

#### 6.3.2.1 Quiescent times and initial offsets

The quiescent times and initial offsets extracted from the recordings are presented separately in Fig. 6.5A and Fig. 6.6A. Data points originating from the same bundle are linked together. Since we observed that hair bundles whose spontaneous motility exhibited a "spiking" profile (observed as sharp, brief excursions from the channel-closed state, correlating with an average open probability less than 0.2) generally displayed longer quiescent periods, these bundles are distinguished from the others by the use of gray square markers.

Efference paradigms that feature efferent activation during the post-overstimulation period (Class 1 and Class 4) demonstrated a wider range of quiescent times, with five bundles resuming oscillations within 50 ms. To elucidate the differences in the observed response of hair cells to efferent actuation, we plot separately the measured quiescent times for three sets of hair bundles. In the first set (Fig. 6.5B), we group together bundles that displayed an immediate return to oscillation. A hair cell was classified as immediately oscillatory if both the Class 1 and Class 4 quiescent times were less than 50 ms. The second and third sets contain the results obtained from bundles that were not immediately affected by efference; these in turn are grouped based on whether they initially exhibited regular (Fig. 6.5C) or spiking (Fig. 6.5D) oscillations. Each subset was analyzed separately, and the quiescent time

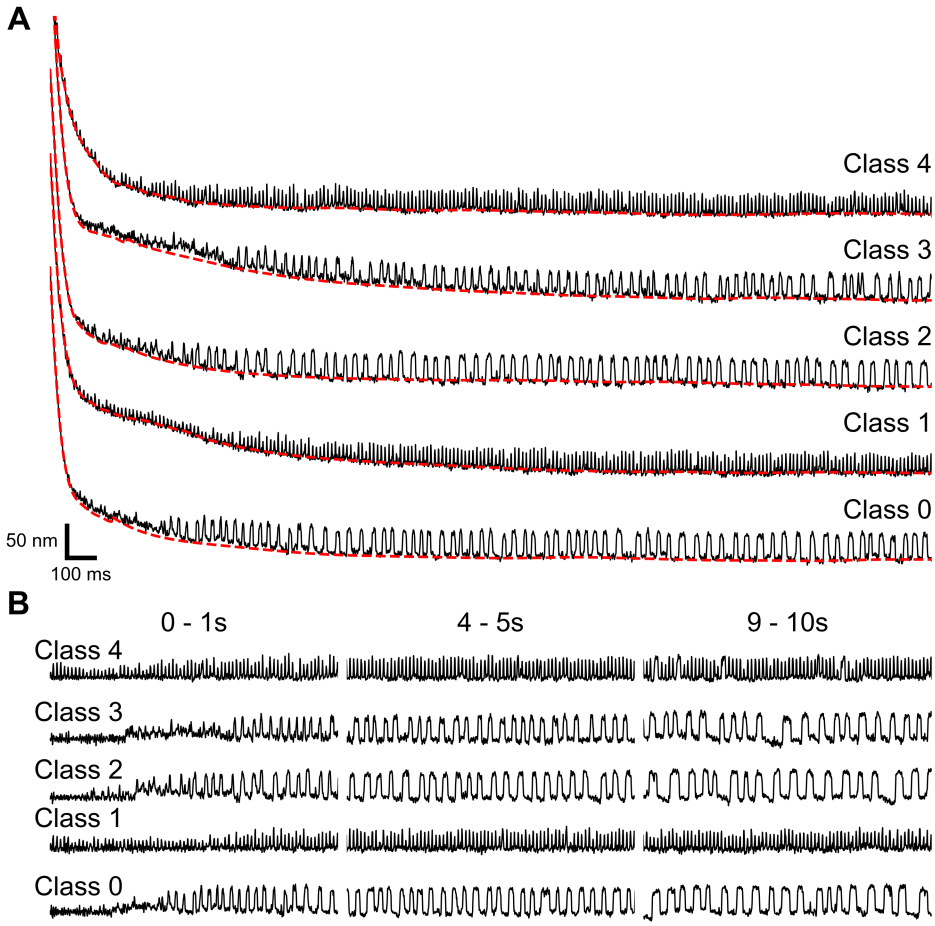


Figure 6.4: Different intervals of efferent stimulation distinctly affected a hair bundle's oscillation profile as it recovered from mechanical overstimulation. **A**) A series of traces are shown of recordings from a hair cell undergoing a combination of mechanical overstimulation and efferent actuation. Each trace depicts hair bundle motion following 20 seconds of large-amplitude mechanical deflection combined with the efference paradigm indicated on the right. The efferents are not actuated in Class 0, and thus Class 0 is treated as the control condition against which comparisons are made. In Class 1, the efferent neurons are activated before, during, and after the mechanical overstimulation for a total of 60 s. Class 2, Class 3, and Class 4 present efferent modulation exclusively before, during, or after the mechanical overstimulation, respectively. The recording order was from bottom to top. Baselines extracted from the traces are displayed in red. A portion of the observed hair bundles exhibited oscillatory motion immediately upon probe release. **B**) A series of flattened recovery traces corresponding to the traces in **A** is shown. Three, chronologically subsequent segments are displayed in the first (0 – 1 s), second (4 – 5 s), and third (9 – 10 s) panels. When efference was present during the hair bundle's recovery (Class 1 and Class 4), the bundle's oscillation profile was significantly altered. Scale bars in **A** are also applicable for **B**.

($T_q$) averages of each efference class for the immediate oscillators (Fig. 6.5B) are as follows: 0.49 ± 0.32 s, 0.02 ± 0.01 s, 0.72 ± 0.59 s, 1.03 ± 0.88 s, and 0.01 ± 0.01 s for Class 0, 1, 2, 3, 4, respectively. With respect to Class 0, the differences in quiescent times are -0.47 ± 0.32 s (one-tailed paired t-test, $t(4)$ = -3.31, $p$ = 0.02), 0.23 ± 0.34 s (one-tailed paired t-test, $t(4)$ = 1.53, $p$ = 0.10), 0.54 ± 0.57 s (one-tailed paired t-test, $t(4)$ = 2.09, $p$ = 0.05), and -0.48 ± 0.32 s (one-tailed paired t-test, $t(4)$ = -3.35, $p$ = 0.01) for Class 0, 1, 2, 3, 4, respectively. Thus, Class 1 and Class 4 both had statistically significant differences in their mean quiescent times for those hair bundles that exhibited oscillatory motion immediately post-overstimulation.

On the other hand, neither the unaffected regular hair cells nor the spiking bundles displayed statistically significant differences in their mean quiescent times with respect to Class 0 for any of the efference paradigms. For the unaffected regular bundles (Fig. 6.5C), the $T_q$ averages are 0.38 ± 0.14 s, 0.47 ± 0.21 s, 0.47 ± 0.38 s, 0.54 ± 0.22 s, and 0.39 ± 0.25 s for Class 0, 1, 2, 3, 4, respectively. With respect to Class 0, the differences in quiescent times are 0.10 ± 0.15 s (one-tailed paired t-test, $t(8)$ = 1.81, $p$ = 0.06), 0.09 ± 0.44 s (one-tailed paired t-test, $t(8)$ = 0.62, $p$ = 0.28), 0.17 ± 0.27 s (one-tailed paired t-test, $t(8)$ = 1.77, $p$ = 0.06), and 0.01 ± 0.20 s (one-tailed paired t-test, $t(8)$ = 0.16, $p$ = 0.44) for Class 0, 1, 2, 3, 4, respectively. Moreover, the average quiescent times for the spiking subset (Fig. 6.5D) are 1.82 ± 0.96 s, 1.86 ± 1.16 s, 3.87 ± 2.18 s, 3.87 ± 3.10 s, and 2.35 ± 1.74 s for Class 0, 1, 2, 3, 4, respectively. With respect to Class 0, the differences in quiescent times are 0.04 ± 0.22 s (one-tailed paired t-test, $t(3)$ = 0.41, $p$ = 0.35), 2.05 ± 1.65 s (one-tailed paired t-test, $t(3)$ = 2.48, $p$ = 0.05), 2.05 ± 2.16 s (one-tailed paired t-test, $t(3)$ = 1.91, $p$ = 0.08), and 0.53 ± 0.87 s (one-tailed paired t-test, $t(3)$ = 1.23, $p$ = 0.15) for Class 0, 1, 2, 3, 4, respectively.

We further examined the effects of different classes of efferent stimulation on the accumulated mechanical offset, which was measured immediately upon retraction of the probe. The $X_o$ averages (Fig. 6.6A) are as follows: 478.42 ± 74.58 nm, 465.13 ± 86.39 nm, 476.07 ± 97.99 nm, 496.7 ± 113.73 nm, and 461.82 ± 100.03 nm for Class 0, 1, 2, 3, 4, respectively. Hence,

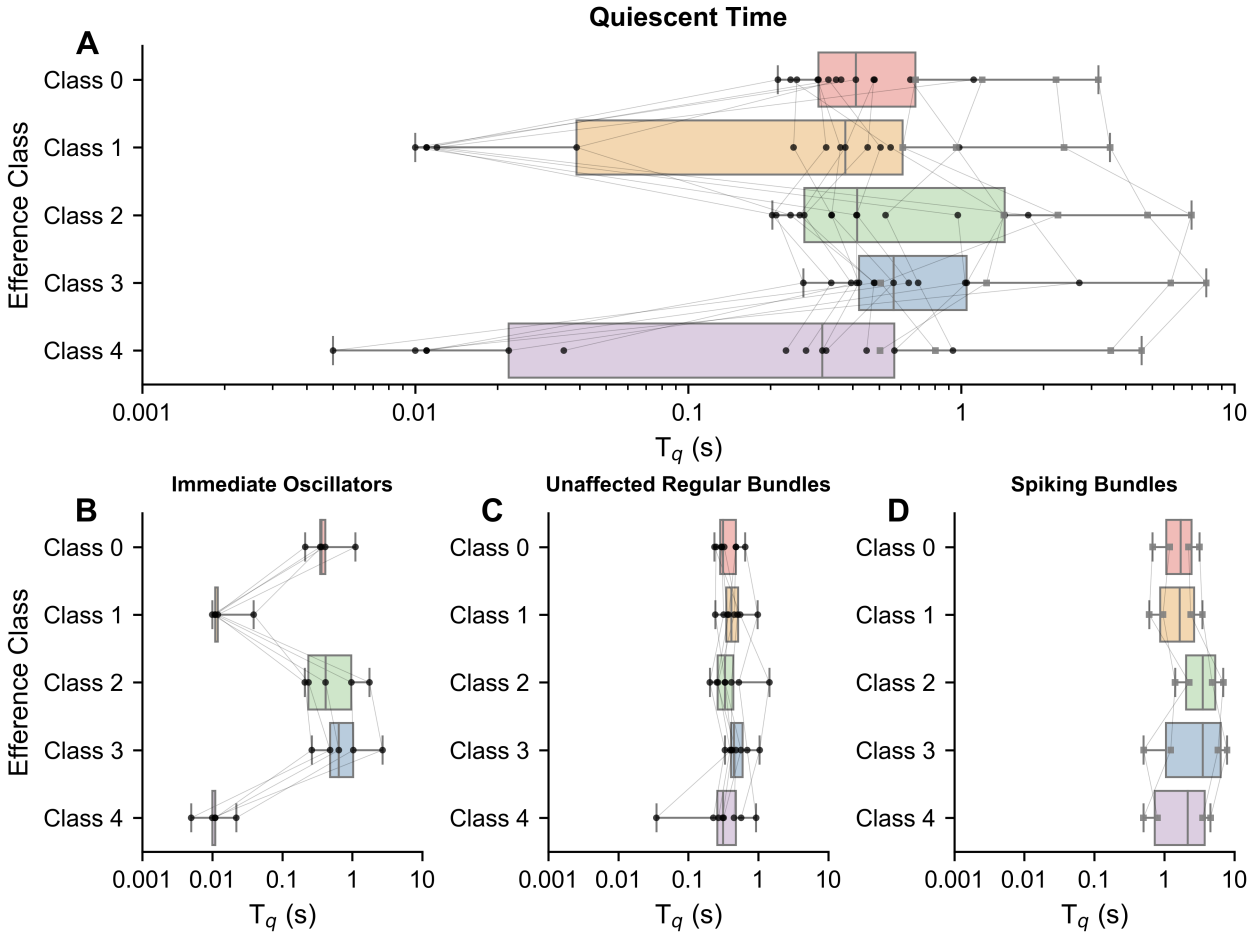


Figure 6.5: Efferent modulation did have an effect on the quiescent period of immediately oscillating bundles. **A**) Box plots illustrate the distribution of quiescent times ($T_q$) across the five efference paradigms. Bundles whose spontaneous oscillations exhibited "spiking" behavior generally had longer quiescent times and are specifically marked with gray squares in both plots. Data points from the same hair bundle are connected together. Efference paradigms that feature efferent activation during the post-overstimulation period (Class 1 and Class 4) displayed wider ranges of quiescent times, with seven bundles having their first oscillation occurring within 50 ms. Data points were obtained from recordings of 18 bundles across 5 sacculi. In the lower panels (**B**, **C**, **D**), we separated the recordings into three groups: hair bundles that displayed an immediate return to oscillation (**C**), those that displayed regular oscillations and were not immediately affected by efference (**D**), and bundles that exhibited spike-like motion (**E**).

the average initial offsets post mechanical overstimulation were comparable for all of the efference stimulus paradigms. With respect to Class 0, the differences in initial offsets are -13.29 ± 57.26 nm (one-tailed paired t-test, $t(17)$ = -0.96, $p$ = 0.18), -2.35 ± 73.19 nm (one-tailed paired t-test, $t(17)$ = -0.13, $p$ = 0.45), 18.27 ± 92.74 nm (one-tailed paired t-test, $t(17)$ = 0.81, $p$ = 0.21), and -16.61 ± 57.90 nm (one-tailed paired t-test, $t(17)$ = -1.18, $p$ = 0.13) for Class 0, 1, 2, 3, 4, respectively.

The hair bundles were sub-divided and further analyzed in the same manner as above. For the immediate oscillators (Fig. 6.6B), the mean initial offsets are 495.16 ± 39.30 nm, 493.41 ± 59.89 nm, 476.20 ± 62.06 nm, 496.99 ± 111.24 nm, and 486.40 ± 93.85 nm for Class 0, 1, 2, 3, 4, respectively. With respect to Class 0, the differences in initial offsets are -1.75 ± 46.53 nm (one-tailed paired t-test, $t(4)$ = -0.08, $p$ = 0.47), -18.96 ± 27.12 nm (one-tailed paired t-test, $t(4)$ = -1.56, $p$ = 0.10), 1.83 ± 83.30 nm (one-tailed paired t-test, $t(4)$ = 0.05, $p$ = 0.48), and -8.76 ± 80.25 nm (one-tailed paired t-test, $t(4)$ = -0.24, $p$ = 0.41) for Class 0, 1, 2, 3, 4, respectively. In the case of the unaffected regular bundles (Fig. 6.6C), the $X_o$ averages are 461.59 ± 65.51 nm, 432.71 ± 69.80 nm, 448.08 ± 61.84 nm, 470.51 ± 87.07 nm, and 446.46 ± 71.17 nm for Class 0, 1, 2, 3, 4, respectively. With respect to Class 0, the differences in initial offsets are -28.88 ± 68.36 nm (one-tailed paired t-test, $t(8)$ = -1.19, $p$ = 0.14), -13.51 ± 61.35 nm (one-tailed paired t-test, $t(8)$ = -0.62, $p$ = 0.28), 8.92 ± 89.07 nm (one-tailed paired t-test, $t(8)$ = 0.28, $p$ = 0.39), and -15.13 ± 42.97 nm (one-tailed paired t-test, $t(8)$ = -1.00, $p$ = 0.18) for Class 0, 1, 2, 3, 4, respectively. Lastly, the mean initial offsets of the spiking subset (Fig. 6.6D) are 491.16 ± 109.77 nm, 494.64 ± 116.28 nm, 531.89 ± 153.83 nm, 548.7 ± 142.36 nm, and 461.80 ± 141.97 nm for Class 0, 1, 2, 3, 4, respectively. With respect to Class 0, the differences in initial offsets are 3.47 ± 30.75 nm (one-tailed paired t-test, $t(3)$ = 0.23, $p$ = 0.42), 40.73 ± 108.94 nm (one-tailed paired t-test, $t(3)$ = 0.75, $p$ = 0.25), 57.54 ± 99.79 nm (one-tailed paired t-test, $t(3)$ = 1.15, $p$ = 0.17), and -29.36 ± 47.56 nm (one-tailed paired t-test, $t(3)$ = -1.23, $p$ = 0.15) for Class 0, 1, 2, 3, 4, respectively. Hence, there were no statistically significant differences in the initial offsets for any of the subgroups of hair cells and under any of the efference paradigms.

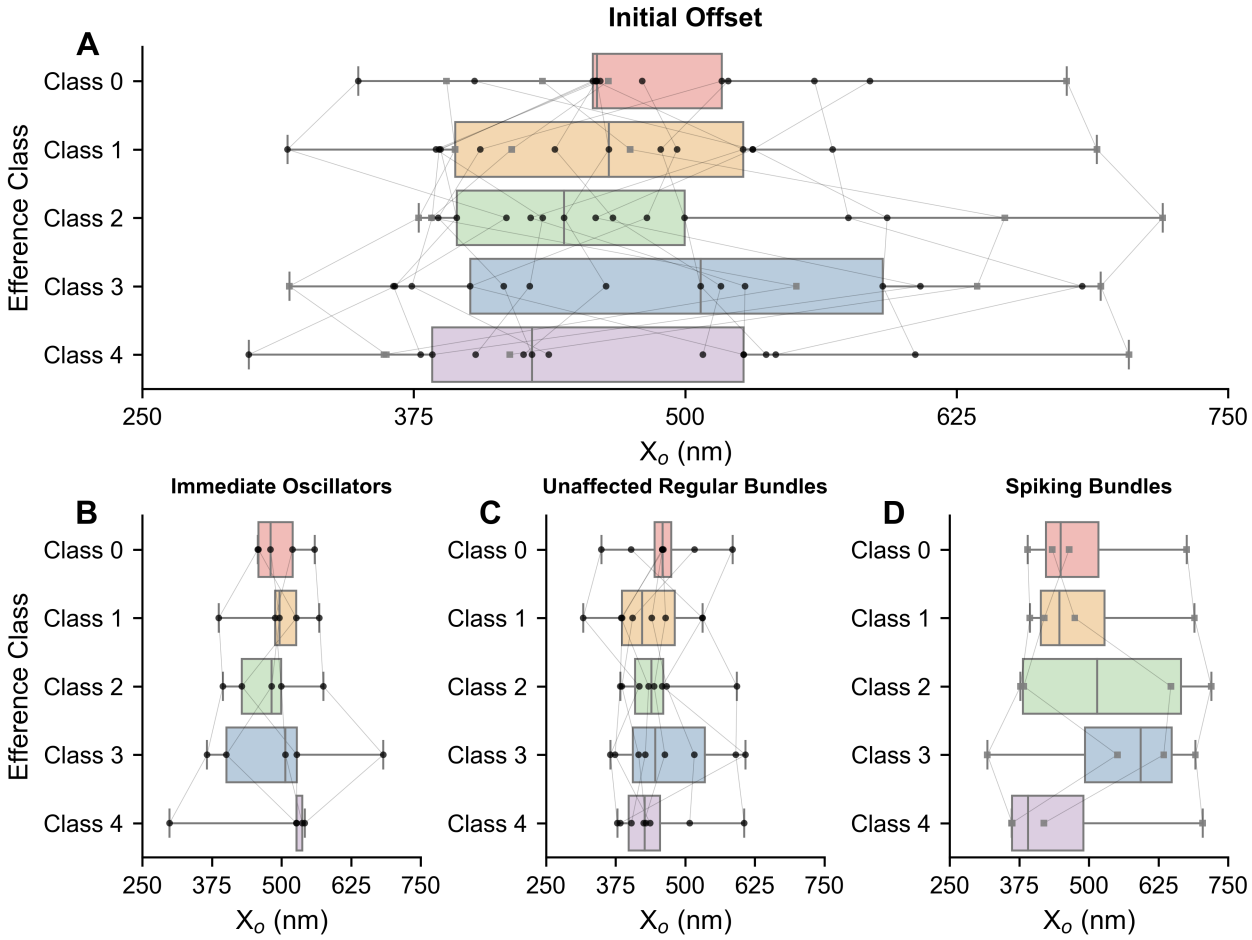


Figure 6.6: Efferent modulation did not influence a hair bundle's induced initial offset. **A**) Box plots illustrate the distribution of initial offsets ($X_o$) across the five efference paradigms. Bundles whose spontaneous oscillations exhibited "spiking" behavior generally had longer quiescent times and are specifically marked with gray squares in both plots. Data points from the same hair bundle are connected together. There were no statistically significant differences in the mean initial offsets of the four classes compared to the Class 0 control. Data points were obtained from recordings of 18 bundles across 5 sacculi. In the lower panels (**B**, **C**, and **D**), we separated the recordings into three groups: hair bundles that displayed an immediate return to oscillation (**C**), those that displayed regular oscillations and were not immediately affected by efference (**D**), and bundles that exhibited spike-like motion (**E**).

#### 6.3.2.2 Extracted baselines (Slow component of recovery)

In order to facilitate comparison of the slow timescale of recovery, the computed baselines shown in red in Fig. 6.3A and Fig. 6.4A are chromatically visualized in Fig. 6.7A and Fig. 6.7C. Fig. 6.8A illustrates the averaged baselines of the same collection of hair cells represented in Fig. 6.5 and Fig. 6.6. The baseline displacement values were normalized by their respective initial offsets. Thus, the range of the colorbars in Fig. 6.7 and Fig. 6.8 extends from 1.0 to 0.0 – with 1.0 corresponding to the bundle at its peak displacement and 0.0 corresponding to the bundle having fully returned to its steady state level. In all paradigms, we found that the bundles had descended a quarter of the way down their trajectories after approximately 25 ms (Fig. 6.8A). These plots indicate that efference did not substantially alter a hair bundle's overall resumption of its steady state position, with a slightly slower rate of recovery observed on average under Class 2 efference paradigm. This result is accordant with our finding that efferent modulation did not manifest statistically significant differences in the hair bundle's induced positional offset.

#### 6.3.2.3 Frequency, amplitude, and open probability trendlines (Fast component of recovery)

As in a previous subsection, we investigated the time-series trendlines of the instantaneous frequencies, amplitudes, and open probabilities of flattened recovery traces for the five efference paradigms. The normalized trendlines displayed in Fig. 6.9A–C and Fig. 6.9D–F were calculated from the flattened traces in Fig. 6.3B and Fig. 6.4B, respectively. Normalization was obtained by taking the ratio of the instantaneous frequency, amplitude, and open probability by their respective characteristic values obtained from a hair bundle's Class 0 steady state spontaneous oscillations. The normalized frequency, amplitude, and open probability trendlines from the previous 18 hair bundles were averaged together, and the mean normalized trendlines for each of the five classes are shown in Fig. 6.10A (frequency), Fig. 6.10B (amplitude), and Fig. 6.10C (open probability). In Fig. 6.9 and Fig. 6.10, trendlines corresponding to Class 0, Class 1, Class 2, Class 3, and Class 4 are plotted in red, gold, green, blue,

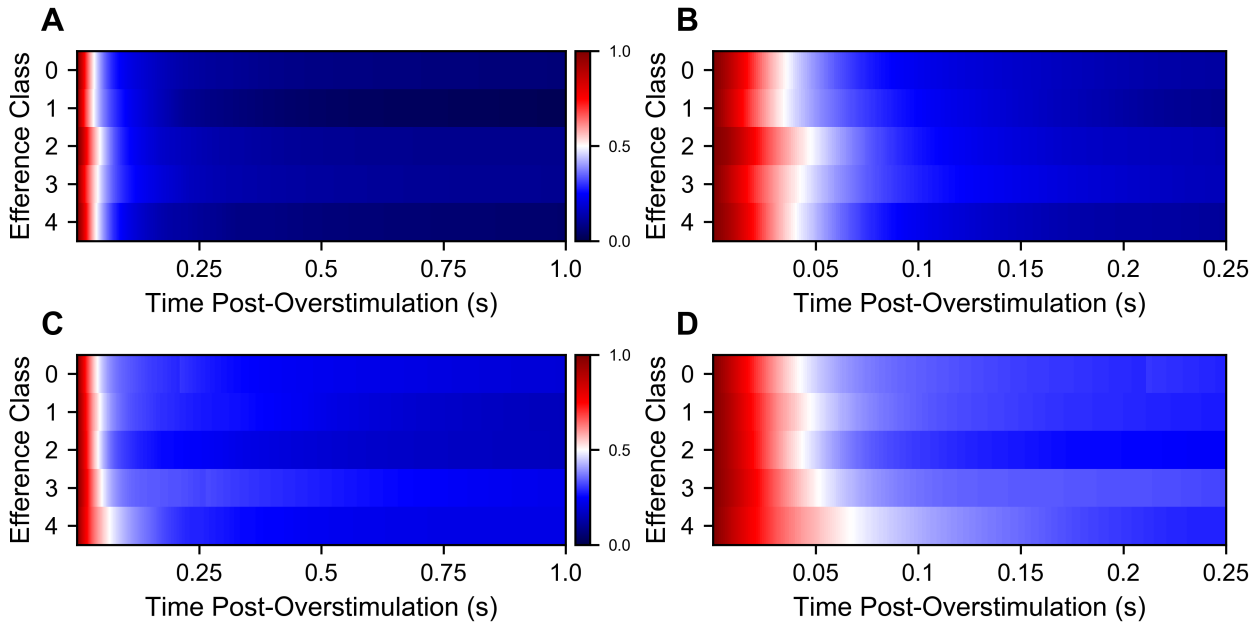


Figure 6.7: Actuation of the efferent neurons did not significantly affect the slow-component of a hair bundle's recovery from mechanical overstimulation. The normalized chromatic representations of the relaxation baselines in **A** and **C** are reflective of those plotted in Fig. 6.3A and Fig. 6.4A, respectively. Baselines were normalized by their respective initial offsets, with 1.0 on the colorbar corresponding to the bundle being at its highest offset and 0.0 corresponding to the bundle having fully returned to its steady state level. **B** and **D** provide a zoom-in of the first 250 ms of **A** and **C**, respectively.

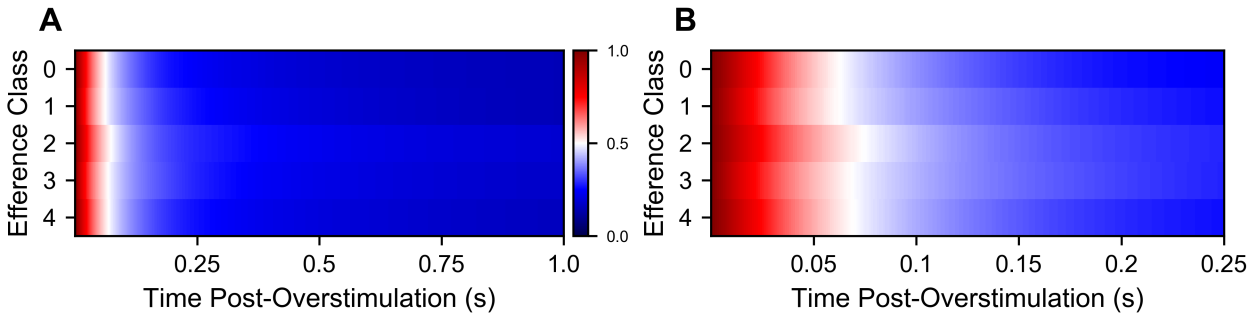


Figure 6.8: Actuation of the efferent neurons did not significantly affect the slow-component of a hair bundle's recovery from mechanical overstimulation. **A**) Baselines recorded from 18 bundles (5 sacculi) were averaged together and the resulting mean baselines are shown. Before averaging, baselines were normalized by their respective initial offsets, with 1.0 on the colorbar corresponding to the bundle being at its highest offset and 0.0 corresponding to the bundle having fully returned to its steady state level. **B** provides a zoom-in of the first 250 ms of **A**. On average, the presence of efferent stimulation did not substantially alter the hair bundle's resumption of its steady state position.

and violet, respectively. The overall shape and trajectory of the trendlines in Fig. 6.10 are similar to those seen in Fig. 5.7. However, there was an explicit dichotomy between the efference protocols that do and do not have efferent stimulation during the post-overstimulation recovery, with the respective trendlines of the two factions generally overlapping. As expected, Class 1 and Class 4 frequency trendlines were shifted upwards with respect to the Class 0 frequency trendline and generally maintained their nascent frequencies for the entire 20 seconds (Fig. 6.10A). In conjunction, the amplitude trendlines of Class 1 and Class 4 were shifted downwards with respect to the Class 0 amplitude trendline and did not experience the same amplitude rise as those of the three other classes (Fig. 6.10B), due to the efferent stimulus's continued effect on the spontaneous oscillations. However, the open probability trendlines of Class 1 and Class 4, initially below that of Class 0, proceeded to gradually increase over time in parallel with the Class 0 trendline (Fig. 6.10C). In total, Fig. 6.10 reveals that the concurrent presence of efferent modulation during the post-overstimulation recovery played a significant role influencing the attributable characteristics of a hair bundle's oscillation profile during its recovery from mechanical overstimulation.

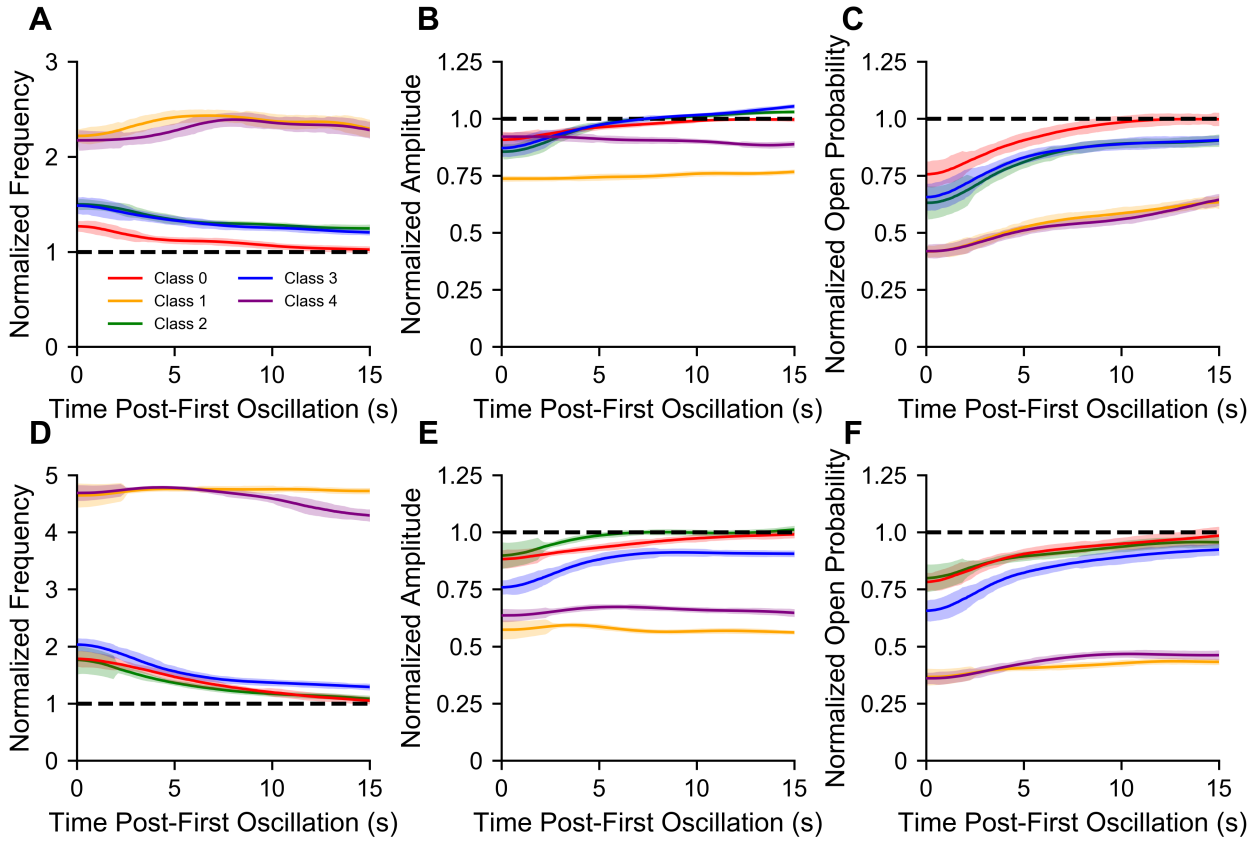


Figure 6.9: Among the five efference paradigms, a clear dichotomy occurred between those classes with and without efferent activation during the hair bundle's recovery. Time-series trendlines of instantaneous frequencies, amplitudes, and open probabilities are plotted for the hair cell in Fig. 6.3 (**A**–**C**) and another cell from a different sacculus (**D**–**F**). All trendlines were normalized by the specific bundle's steady state value. The five efference paradigms (Classes 0, 1, 2, 3, 4) are plotted in red, gold, green, blue, and violet, respectively. Under Class 1 and Class 4, hair bundles returned to the oscillatory regime with a higher frequency, lower amplitude, and smaller open probability than those in the three other classes. Error bands represent the standard deviations of data points in a one second moving window.

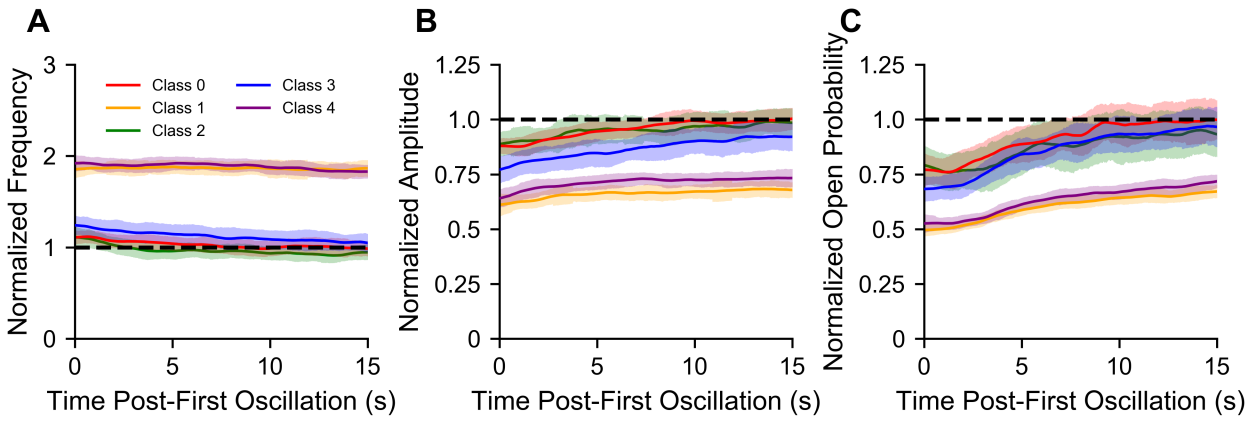


Figure 6.10: Among the five efference paradigms, a clear dichotomy occurred between those classes with and without efferent activation during the hair bundle's recovery. Frequency, amplitude, and open probability trendlines with the same efference classification were averaged together to obtain the mean normalized trendlines in **A**, **B**, **C**, respectively. Before averaging, all trendlines were normalized by the specific bundle's steady state value. The five efference paradigms (Classes 0, 1, 2, 3, 4) are plotted in red, gold, green, blue, and violet, respectively. The Class 1 and Class 4 mean open probability trendlines were initially shifted downwards with respect to the Class 0 trendline (**C**), but proceeded to gradually increase over time, in contrast to the relatively flat frequency (**A**) and amplitude (**B**) trendlines. The averaged trendlines reflect data from 18 bundles (5 sacculi). Error bands represent the standard deviations of data points in a one second moving window.

Lastly, we explored the possibility that the amplitude of the efferent stimulus contributes to modulating the dynamic state of a hair cell as it is recovering from a high-amplitude mechanical deflection. We found the nascent oscillation characteristics were more influenced by the amplitude of an efferent pulse train stimulus than the temporal evolution of the characteristic parameters of a hair bundle's oscillation profile. Time-series trendlines of the instantaneous frequencies (Fig. 6.11A, Fig. 6.11D), amplitudes (Fig. 6.11B, Fig. 6.11E), and open probabilities (Fig. 6.11C, Fig. 6.11F) are shown in Fig. 6.11 for two distinct hair cells originating from the same sacculus. Trendlines corresponding to a stimulus amplitude of 0 $\mu$A, 50 $\mu$A, 100 $\mu$A, 150 $\mu$A, or 200 $\mu$A are plotted in red, gold, green, blue, and violet, respectively. The pulse duration and inter-pulse interval of the applied efferent pulse train were kept constant (3 ms 'on', 10 ms 'off'), and the stimulus amplitude was varied. The main impact of the stimulus amplitude appeared to be in designating a hair bundle's burgeoning oscillation profile immediately upon efferent modulation, and thus its evolution over time. Elevated stimulus amplitudes appeared to shift the hair cell's nascent oscillatory state further away from its original dynamic state.

#### 6.3.2.4 Power spectral densities

Fig. 6.12A and Fig. 6.12B show the time-evolved power spectral densities of the flattened recovery position traces in Fig. 6.3B and Fig. 6.4B, respectively. The first through fifth consecutive panel of each sub-figure corresponds successively to Class 0 through Class 4, respectively. PSDs of four successive five-second sections of a bundle's flattened position trace are plotted in red, gold, green, and blue, respectively. The power spectral density of each hair cell's fundamental spontaneous oscillations is plotted in gray. Akin to our previous observations in Fig. 5.9, the power spectral densities of Class 2 and Class 3 were initially shifted rightward before gradually regaining its prior shape. Hair bundles exhibited almost no recovery in the frequency domain under the Class 1 and Class 4 efference paradigms. It is of interest to note that there appears to be no distinguishable feature other than a peak at the efference pulse train frequency of 77 Hz for at least the first 15 seconds of a hair bundle's recovery under the Class 1 or Class 4 paradigms. These findings were consistent amongst

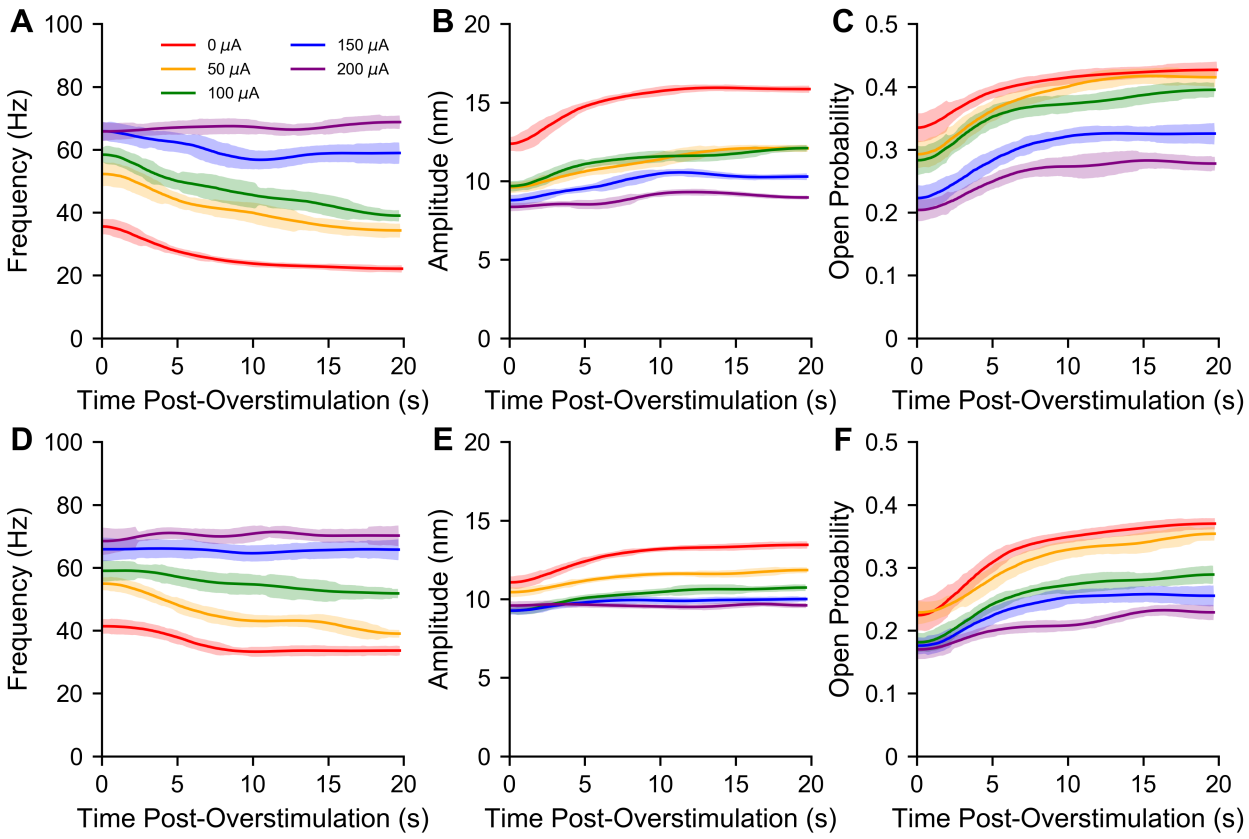


Figure 6.11: The temporal evolution of the characteristic parameters of a hair bundle's post-overstimulation recovery oscillation profile were influenced by the amplitude of the efferent pulse train stimulus. The mode of efferent stimulation was maintained at Class 1 while the amplitude of the efferent stimulus was varied. Time-series trendlines of the instantaneous frequencies (**A**,**D**), amplitudes (**B**,**E**), and open probabilities (**C**,**F**) are displayed for two distinct hair cells originating from the same sacculus. Trendlines corresponding to a stimulus amplitude of 0 $\mu$A, 50 $\mu$A, 100 $\mu$A, 150 $\mu$A, or 200 $\mu$A are plotted in red, gold, green, blue, and violet, respectively. The pulse duration and inter-pulse interval of the applied efferent pulse train were kept constant (3 ms 'on', 10 ms 'off'). The main impact of the stimulus amplitude appeared to be in shifting the characteristic parameters of a hair bundle's oscillation profile when the bundle re-entered the oscillatory regime. Elevated stimulus amplitudes appeared to shift a hair cell further away from its original dynamic state. Error bands represent the standard deviations of data points in a one second moving window.

the 18 recorded hair cells.

## 6.4 Discussion

Prior studies have extensively delved into the physiology of efferent neurons, with a particular focus on the medial olivocochlear (MOC) subset. These efferents synapse onto hair cells and stimulate the $\alpha 9\alpha 10$ nicotinic acetylcholine receptors (nAChR) by releasing acetylcholine (ACh) [31, 9, 33, 108]. Binding of ACh to the receptors then prompts a cascade of ion channel openings in the cell soma from which a complex spectrum of behaviors has been identified [109]. Predominantly, however, efferent activation leads to hyperpolarization of the membrane potential [4, 32]. Prior studies in this field have specifically indicated that the influx of $Ca^{2+}$ through the cholinergic receptors is followed by a consequent outflow of $K^{+}$ through SK2 channels [11, 80, 91], which lead to an overall hyperpolarization of the soma [26, 25, 50, 15].

Electrophysiological measurements of hair cells from the American bullfrog sacculus demonstrated the hyperpolarization of the hair cell soma as a result of efferent modulation [15]. Intensifying the strength of the efferent stimulation extended the hyperpolarization up to a saturation limit. Furthermore, the results of Chapter 3 and Chapter 4, which linked efferent activity and active hair bundle motility, were in agreement with the hyperpolarization of the membrane potential [55]. Specifically, characteristic aspects of a hair bundle's spontaneous oscillation profile (i.e. frequency, amplitude, open probability) transformed in a manner that concurred with electrophysiologically hyperpolarizing the hair cell. Moreover, the changes in oscillation shape were found to depend on the level of efferent modulation in a way that corresponds with increasing hyperpolarization of the cell soma.

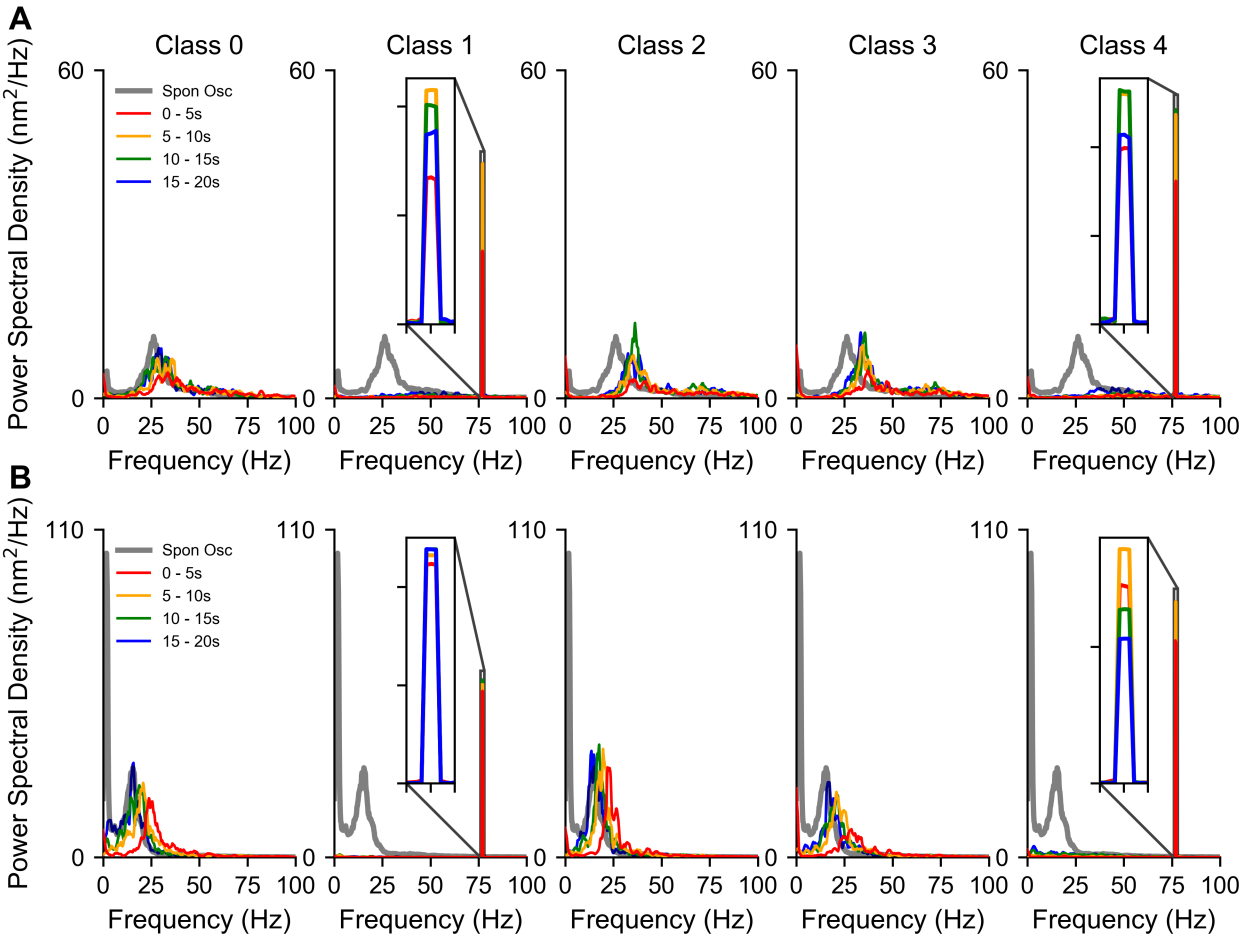


Figure 6.12: Hair bundles exhibited almost no recovery in the frequency domain under the Class 1 and Class 4 efference paradigms. **A**, **B**) Sets of time-lapsed power spectral densities of two hair bundles from two distinct sacculi are displayed. **A** and **B** reflect the hair bundle position traces in Fig. 6.3B and Fig. 6.4B, respectively. The PSDs were computed from the flattened recovery traces of each respective hair cell. Time-lapsed PSDs corresponding to an efference classification of Class 0, 1, 2, 3, and 4 are displayed in the first, second, third, fourth, and fifth panels, respectively. Power spectral densities of a bundle's flattened return are plotted in red, gold, green, and blue for each five second segment up to 20s, respectively, following the cessation of mechanical overstimulation. The power spectral density of a hair bundle's spontaneous oscillations is plotted in gray.

### 6.4.1 The efferent system provides a biological mechanism for controlling a hair bundle's dynamic state

Two characteristic features resulting from a high-amplitude mechanical deflection of the hair bundle are a transient induced offset and a temporary crossover from the oscillatory regime to the quiescent state. It was previously proposed that both an offset in bundle position and $Ca^{2+}$ concentration exert an effect on the dynamic state of the hair cell. However, under conditions in which the efferents were active during the bundle's relaxation from overstimulation, we regularly observed hair bundles in an oscillatory state while still at a significant mechanical offset. Thus, actuating the efferent neurons is capable of producing an immediate transition from the quiescent state back to the oscillatory regime even at a large positional offset. This suggests that the efferent system behaves like a direct control mechanism for the hair bundle's dynamic state. Moreover, compared to the no efference condition, we found no statistical differences in the mean induced offsets of any of the four efference paradigms, despite apparent distinctions in their recovery behavior. Taken together, these findings indicate that a hair bundle's position alone does not determine its dynamic regime, and efference does not impact a bundle's dynamic state by influencing its positional offset.

A likely pathway by which the efferent system exerts its effect on hair cells is through modulation of the somatic potential, which in turn affects $Ca^{2+}$ feedback processes within the sterovilli. Specifically, $Ca^{2+}$ influx has been seen to affect a hair bundle's dynamics at multiple timescales [21, 44, 23], from $Ca^{2+}$-mediated channel reclosure and control of adaptation motors [40, 41, 6, 106, 29, 89], to modulation of an internal gating spring stiffness [66, 69, 88, 10]. Furthermore, while activation of nAChRs seems to be a requisite component for the efferent effect on hair bundle dynamics, we cannot eliminate the possible role of other neuromodulators reported to constitute a portion of the efferent mechanism [49]. Parsing the confluence of the different cellular processes comprising the efferent feedback system represents a future direction for both theoretical and experimental studies.

In this work, we found that the concurrent actuation of the efferent neurons with a hair cell's post-overstimulation recovery significantly affected the hair bundle's dynamic state. Hair bundles were observed in an oscillatory state even at large positional offsets. Furthermore, prominent differences in the innate motility of the bundle demonstrated that its internal active processes were substantially impacted by efferent stimulation. Thus, efferent modulation presents a mechanism by which hair bundles can quickly resume the oscillatory regime after being detuned by a high-amplitude mechanical deflection. The efferent architecture's ability to directly control both the dynamic state and the mechanical sensitivity of the hair bundle may contribute to enhancing the robustness of the hair cell and thus protect it from damage.

# Bibliography


[1] Guillaume Andéol, Anne Guillaume, Christophe Micheyl, Sophie Savel, Lionel Pellieux, and Annie Moulin. Auditory efferents facilitate sound localization in noise in humans. *Journal of Neuroscience*, 31(18):6759–6763, 2011.

[2] JJ Art, Andrew Charles Crawford, Robert Fettiplace, and Paul Albert Fuchs. Efferent regulation of hair cells in the turtle cochlea. *Proceedings of the Royal Society of London. Series B. Biological Sciences*, 216(1204):377–384, 1982.

[3] JJ Art and R Fettiplace. Efferent desensitization of auditory nerve fibre responses in the cochlea of the turtle pseudemys scripta elegans. *The Journal of Physiology*, 356(1):507–523, 1984.

[4] JJ Art, R Fettiplace, and Paul Albert Fuchs. Synaptic hyperpolarization and inhibition of turtle cochlear hair cells. *The Journal of Physiology*, 356(1):525–550, 1984.

[5] JF Ashmore and IJ Russell. Effect of efferent nerve-stimulation on hair-cells of the frog sacculus. In *Journal of Physiology - London*, volume 329, pages P25–P26. Cambridge Univ Press 40 West 20th Street, New York, NY 10011-4211, 1982.

[6] JA Assad and David P Corey. An active motor model for adaptation by vertebrate hair cells. *Journal of Neuroscience*, 12(9):3291–3309, 1992.

[7] John A Assad, Nir Hacohen, and David P Corey. Voltage dependence of adaptation and active bundle movement in bullfrog saccular hair cells. *Proceedings of the National Academy of Sciences*, 86(8):2918–2922, 1989.

[8] John A Assad, Gordon MG Shepherd, and David P Corey. Tip-link integrity and mechanical transduction in vertebrate hair cells. *Neuron*, 7(6):985–994, 1991.

[9] Jimena Ballestero, Javier Zorrilla de San Martín, Juan Goutman, Ana Belén Elgoyhen, Paul A Fuchs, and Eleonora Katz. Short-term synaptic plasticity regulates the level of olivocochlear inhibition to auditory hair cells. *Journal of Neuroscience*, 31(41):14763–14774, 2011.

[10] Maryline Beurg, Jong-Hoon Nam, Andrew Crawford, and Robert Fettiplace. The actions of calcium on hair bundle mechanics in mammalian cochlear hair cells. *Biophysical Journal*, 94(7):2639–2653, 2008.

[11] Christophe Blanchet, Carlos Erostegui, Masashi Sugasawa, and Didier Dulon. Acetylcholine-induced potassium current of guinea pig outer hair cells: its dependence on a calcium influx through nicotinic-like receptors. *Journal of Neuroscience*, 16(8):2574–2584, 1996.

[12] Luis E Boero, Valeria C Castagna, Mariano N Di Guilmi, Juan D Goutman, Ana Belén Elgoyhen, and María Eugenia Gómez-Casati. Enhancement of the medial olivocochlear system prevents hidden hearing loss. *Journal of Neuroscience*, 38(34):7440–7451, 2018.

[13] D Bozovic and AJ Hudspeth. Hair-bundle movements elicited by transepithelial electrical stimulation of hair cells in the sacculus of the bullfrog. *Proceedings of the National Academy of Sciences*, 100(3):958–963, 2003.

[14] Sébastien Camalet, Thomas Duke, Frank Jülicher, and Jacques Prost. Auditory sensitivity provided by self-tuned critical oscillations of hair cells. *Proceedings of the National Academy of Sciences*, 97(7):3183–3188, 2000.

[15] Manuel Castellano-Muñoz, Samuel H Israel, and AJ Hudspeth. Efferent control of the electrical and mechanical properties of hair cells in the bullfrog's sacculus. *PLoS One*, 5(10):e13777, 2010.

[16] Yong Choe, Marcelo O Magnasco, and AJ Hudspeth. A model for amplification of hair-bundle motion by cyclical binding of ca2+ to mechanoelectrical-transduction channels. *Proceedings of the National Academy of Sciences*, 95(26):15321–15326, 1998.

[17] William W Clark. Recent studies of temporary threshold shift (tts) and permanent threshold shift (pts) in animals. *The Journal of the Acoustical Society of America*, 90(1):155–163, 1991.

[18] NP Cooper and JJ Guinan Jr. Efferent-mediated control of basilar membrane motion. *The Journal of Physiology*, 576(1):49–54, 2006.

[19] Keith N Darrow, Stéphane F Maison, and M Charles Liberman. Cochlear efferent feedback balances interaural sensitivity. *Nature Neuroscience*, 9(12):1474, 2006.

[20] Iván Díaz, Ana Cecilia Colmenárez-Raga, David Pérez-González, Venezia G Carmona, Ignacio Plaza Lopez, and Miguel A Merchán. Effects of multisession anodal electrical stimulation of the auditory cortex on temporary noise-induced hearing loss in the rat. *Frontiers in Neuroscience*, page 622, 2021.

[21] Ruth Anne Eatock. Adaptation in hair cells. *Annual Review of Neuroscience*, 23(1):285–314, 2000.

[22] Víctor M Eguíluz, Mark Ospeck, Y Choe, AJ Hudspeth, and Marcelo O Magnasco. Essential nonlinearities in hearing. *Physical Review Letters*, 84(22):5232, 2000.

[23] Robert Fettiplace. Hair cell transduction, tuning, and synaptic transmission in the mammalian cochlea. *Comprehensive Physiology*, 7(4):1197–1227, 2017.

[24] Lea Fredrickson-Hemsing, Seung Ji, Robijn Bruinsma, and Dolores Bozovic. Mode-locking dynamics of hair cells of the inner ear. *Physical Review E*, 86(2):021915, 2012.

[25] Paul Fuchs. The synaptic physiology of cochlear hair cells. *Audiology and Neurotology*, 7(1):40–44, 2002.

[26] Paul Albert Fuchs and BW Murrow. A novel cholinergic receptor mediates inhibition of chick cochlear hair cells. *Proceedings of the Royal Society of London. Series B: Biological Sciences*, 248(1321):35–40, 1992.

[27] T Furukawa. Effects of efferent stimulation on the saccule of goldfish. *The Journal of Physiology*, 315(1):203–215, 1981.

[28] C Daniel Geisler. *From Sound to Synapse: Physiology of the Mammalian Ear*. Oxford University Press, USA, 1998.

[29] Peter G Gillespie and David P Corey. Myosin and adaptation by hair cells. *Neuron*, 19(5):955–958, 1997.

[30] Anne Lise Giraud, Stéphane Garnier, Christophe Micheyl, Geneviève Lina, André Chays, and Sylviane Chéry-Croze. Auditory efferents involved in speech-in-noise intelligibility. *Neuroreport*, 8(7):1779–1783, 1997.

[31] María Eugenia Gómez-Casati, Paul A Fuchs, Ana Belén Elgoyhen, and Eleonora Katz. Biophysical and pharmacological characterization of nicotinic cholinergic receptors in rat cochlear inner hair cells. *The Journal of Physiology*, 566(1):103–118, 2005.

[32] Juan Diego Goutman, Paul Albert Fuchs, and Elisabeth Glowatzki. Facilitating efferent inhibition of inner hair cells in the cochlea of the neonatal rat. *The Journal of Physiology*, 566(1):49–59, 2005.

[33] John J Guinan. Physiology of the medial and lateral olivocochlear systems. In *Auditory and Vestibular Efferents*, pages 39–81. Springer, 2011.

[34] John J Guinan Jr. Olivocochlear efferents: their action, effects, measurement and uses, and the impact of the new conception of cochlear mechanical responses. *Hearing Research*, 362:38–47, 2018.

[35] PS Guth, A Dunn, K Kronomer, and CH Norris. The cholinergic pharmacology of the frog saccule. *Hearing Research*, 75(1-2):225–232, 1994.

[36] Michael Handrock and Joachim Zeisberg. The influence of the efferent system on adaptation, temporary and permanent threshold shift. *Archives of oto-rhino-laryngology*, 234(2):191–195, 1982.

[37] John A Hartigan, Pamela M Hartigan, et al. The dip test of unimodality. *The Annals of Statistics*, 13(1):70–84, 1985.

[38] Stephen M Highstein. The central nervous system efferent control of the organs of balance and equilibrium. *Neuroscience Research*, 12(1):13–30, 1991.

[39] Stephen M Highstein and Robert Baker. Action of the efferent vestibular system on primary afferents in the toadfish, opsanus tau. *Journal of Neurophysiology*, 54(2):370–384, 1985.

[40] J Howard and AJ Hudspeth. Mechanical relaxation of the hair bundle mediates adaptation in mechanoelectrical transduction by the bullfrog's saccular hair cell. *Proceedings of the National Academy of Sciences*, 84(9):3064–3068, 1987.

[41] J Howard and AJ Hudspeth. Compliance of the hair bundle associated with gating of mechanoelectrical transduction channels in the bullfrog's saccular hair cell. *Neuron*, 1(3):189–199, 1988.

[42] A James Hudspeth. The hair cells of the inner ear. *Scientific American*, 248(1):54–65, 1983.

[43] AJ Hudspeth. Integrating the active process of hair cells with cochlear function. *Nature Reviews Neuroscience*, 15(9):600, 2014.

[44] AJ Hudspeth, Y Choe, AD Mehta, and P Martin. Putting ion channels to work: mechanoelectrical transduction, adaptation, and amplification by hair cells. *Proceedings of the National Academy of Sciences*, 97(22):11765–11772, 2000.

[45] Mohsen Jamali, Soroush G Sadeghi, and Kathleen E Cullen. Response of vestibular nerve afferents innervating utricle and saccule during passive and active translations. *Journal of Neurophysiology*, 101(1):141–149, 2009.

[46] Albert Kao, Sebastiaan WF Meenderink, and Dolores Bozovic. Mechanical overstimulation of hair bundles: suppression and recovery of active motility. *PLoS One*, 8(3):e58143, 2013.

[47] Mahvand Khamesian and Alexander B Neiman. Effect of receptor potential on mechanical oscillations in a model of sensory hair cell. *The European Physical Journal Special Topics*, 226(9):1953–1962, 2017.

[48] SungHee Kim, Robert D Frisina, and D Robert Frisina. Effects of age on speech understanding in normal hearing listeners: Relationship between the auditory efferent system and speech intelligibility in noise. *Speech Communication*, 48(7):855–862, 2006.

[49] Siân R Kitcher, Alia M Pederson, and Catherine JC Weisz. Diverse identities and sites of action of cochlear neurotransmitters. *Hearing Research*, page 108278, 2021.

[50] Jee-Hyun Kong, John P Adelman, and Paul A Fuchs. Expression of the sk2 calcium-activated potassium channel is required for cholinergic function in mouse cochlear hair cells. *The Journal of Physiology*, 586(22):5471–5485, 2008.

[51] Sharon G Kujawa and M Charles Liberman. Adding insult to injury: cochlear nerve degeneration after "temporary" noise-induced hearing loss. *Journal of Neuroscience*,

29(45):14077–14085, 2009.

[52] U Ajith Kumar and CS Vanaja. Functioning of olivocochlear bundle and speech perception in noise. *Ear and Hearing*, 25(2):142–146, 2004.

[53] Loïc Le Goff, Dolores Bozovic, and AJ Hudspeth. Adaptive shift in the domain of negative stiffness during spontaneous oscillation by hair bundles from the internal ear. *Proceedings of the National Academy of Sciences*, 102(47):16996–17001, 2005.

[54] Jeffery T Lichtenhan and Mark E Chertoff. Temporary hearing loss influences post-stimulus time histogram and single neuron action potential estimates from human compound action potentials. *The Journal of the Acoustical Society of America*, 123(4):2200–2212, 2008.

[55] Chia-Hsi Jessica Lin and Dolores Bozovic. Effects of efferent activity on hair bundle mechanics. *Journal of Neuroscience*, 40(12):2390–2402, 2020.

[56] R Llinás and Wolfgang Precht. The inhibitory vestibular efferent system and its relation to the cerebellum in the frog. *Experimental Brain Research*, 9(1):16–29, 1969.

[57] Enrique A Lopez-Poveda. Olivocochlear efferents in animals and humans: From anatomy to clinical relevance. *Frontiers in Neurology*, 9:197, 2018.

[58] Enrique A Lopez-Poveda, Almudena Eustaquio-Martín, Joshua S Stohl, Robert D Wolford, Reinhold Schatzer, and Blake S Wilson. Roles of the contralateral efferent reflex in hearing demonstrated with cochlear implants. In *Physiology, Psychoacoustics and Cognition in Normal and Impaired Hearing*, pages 105–114. Springer, Cham, 2016.

[59] Ellen A Lumpkin and AJ Hudspeth. Detection of ca2+ entry through mechanosensitive channels localizes the site of mechanoelectrical transduction in hair cells. *Proceedings of the National Academy of Sciences*, 92(22):10297–10301, 1995.

[60] Ellen A Lumpkin and AJ Hudspeth. Regulation of free ca2+ concentration in hair-cell stereocilia. *Journal of Neuroscience*, 18(16):6300–6318, 1998.

[61] Ellen A Lumpkin, Robert E Marquis, and AJ Hudspeth. The selectivity of the hair cell's mechanoelectrical-transduction channel promotes ca2+ flux at low ca2+ concentrations. *Proceedings of the National Academy of Sciences*, 94(20):10997–11002, 1997.

[62] Stephane F Maison and M Charles Liberman. Predicting vulnerability to acoustic injury with a noninvasive assay of olivocochlear reflex strength. *Journal of Neuroscience*, 20(12):4701–4707, 2000.

[63] Stéphane F Maison, Anne E Luebke, M Charles Liberman, and Jian Zuo. Efferent protection from acoustic injury is mediated via $\alpha 9$ nicotinic acetylcholine receptors on outer hair cells. *Journal of Neuroscience*, 22(24):10838–10846, 2002.

[64] Stéphane F Maison, Hajime Usubuchi, and M Charles Liberman. Efferent feedback minimizes cochlear neuropathy from moderate noise exposure. *Journal of Neuroscience*, 33(13):5542–5552, 2013.

[65] Dáibhid Ó Maoiléidigh and Anthony J Ricci. A bundle of mechanisms: Inner-ear hair-cell mechanotransduction. *Trends in Neurosciences*, 2019.

[66] Robert E Marquis and AJ Hudspeth. Effects of extracellular ca2+ concentration on hair-bundle stiffness and gating-spring integrity in hair cells. *Proceedings of the National Academy of Sciences*, 94(22):11923–11928, 1997.

[67] P Martin and AJ Hudspeth. Compressive nonlinearity in the hair bundle's active response to mechanical stimulation. *Proceedings of the National Academy of Sciences*, 98(25):14386–14391, 2001.

[68] P Martin, AJ Hudspeth, and F Jülicher. Comparison of a hair bundle's spontaneous oscillations with its response to mechanical stimulation reveals the underlying active process. *Proceedings of the National Academy of Sciences*, 98(25):14380–14385, 2001.

[69] P Martin, AD Mehta, and AJ Hudspeth. Negative hair-bundle stiffness betrays a mechanism for mechanical amplification by the hair cell. *Proceedings of the National Academy of Sciences*, 97(22):12026–12031, 2000.

[70] Pascal Martin, D Bozovic, Y Choe, and AJ Hudspeth. Spontaneous oscillation by hair bundles of the bullfrog's sacculus. *Journal of Neuroscience*, 23(11):4533–4548, 2003.

[71] Pascal Martin and AJ Hudspeth. Active hair-bundle movements can amplify a hair cell's response to oscillatory mechanical stimuli. *Proceedings of the National Academy of Sciences*, 96(25):14306–14311, 1999.

[72] Sebastiaan WF Meenderink, Patricia M Quiñones, and Dolores Bozovic. Voltage-mediated control of spontaneous bundle oscillations in saccular hair cells. *Journal of Neuroscience*, 35(43):14457–14466, 2015.

[73] William Melnick. Human temporary threshold shift (tts) and damage risk. *The Journal of the Acoustical Society of America*, 90(1):147–154, 1991.

[74] Christophe Micheyl and Lionel Collet. Involvement of the olivocochlear bundle in the detection of tones in noise. *The Journal of the Acoustical Society of America*, 99(3):1604–1610, 1996.

[75] Christophe Micheyl, Xavier Perrot, and Lionel Collet. Relationship between auditory intensity discrimination in noise and olivocochlear efferent system activity in humans. *Behavioral Neuroscience*, 111(4):801, 1997.

[76] Marcelo J Moglie, Diego L Wengier, A Belén Elgoyhen, and Juan D Goutman. Synaptic contributions to cochlear outer hair cell ca2+ dynamics. *Journal of Neuroscience*,

41(32):6812–6821, 2021.

[77] Euan Murugasu and Ian J Russell. The effect of efferent stimulation on basilar membrane displacement in the basal turn of the guinea pig cochlea. *Journal of Neuroscience*, 16(1):325–332, 1996.

[78] Björn Nadrowski, Pascal Martin, and Frank Jülicher. Active hair-bundle motility harnesses noise to operate near an optimum of mechanosensitivity. *Proceedings of the National Academy of Sciences*, 101(33):12195–12200, 2004.

[79] Kazuya Ohata, Makoto Kondo, Yoshiyuki Ozono, Yukiko Hanada, Takashi Sato, Hidenori Inohara, and Shoichi Shimada. Cochlear protection against noise exposure requires serotonin type 3a receptor via the medial olivocochlear system. *The FASEB Journal*, 35(5):e21486, 2021.

[80] Dominik Oliver, Nikolaj Klöcker, Jochen Schuck, Thomas Baukrowitz, J Peter Ruppersberg, and Bernd Fakler. Gating of ca2+-activated k+ channels controls fast inhibitory synaptic transmission at auditory outer hair cells. *Neuron*, 26(3):595–601, 2000.

[81] Robert Patuzzi. Non-linear aspects of outer hair cell transduction and the temporary threshold shifts after acoustic trauma. *Audiology and Neurotology*, 7(1):17–20, 2002.

[82] AS Pikovsky, MG Rosenblum, and J Kurths. *Synchronization—A unified approach to nonlinear science*. Cambridge University Press, Cambridge, 2001.

[83] Ivo Prigioni, Paolo Valli, and Cesare Casella. Peripheral organization of the vestibular efferent system in the frog: an electrophysiological study. *Brain Research*, 269(1):83–90, 1983.

[84] Richard D Rabbitt and William E Brownell. Efferent modulation of hair cell function. *Current opinion in otolaryngology & head and neck surgery*, 19(5):376, 2011.

[85] D Ramunno-Johnson, CE Strimbu, A Kao, L Fredrickson Hemsing, and D Bozovic. Effects of the somatic ion channels upon spontaneous mechanical oscillations in hair bundles of the inner ear. *Hearing Research*, 268(1-2):163–171, 2010.

[86] Damien Ramunno-Johnson, C Elliott Strimbu, Lea Fredrickson, Katsushi Arisaka, and Dolores Bozovic. Distribution of frequencies of spontaneous oscillations in hair cells of the bullfrog sacculus. *Biophysical Journal*, 96(3):1159–1168, 2009.

[87] Evan R Reiter and M Charles Liberman. Efferent-mediated protection from acoustic overexposure: relation to slow effects of olivocochlear stimulation. *Journal of Neurophysiology*, 73(2):506–514, 1995.

[88] AJ Ricci, AC Crawford, and R Fettiplace. Mechanisms of active hair bundle motion in auditory hair cells. *Journal of Neuroscience*, 22(1):44–52, 2002.

[89] AJ Ricci, YC Wu, and R Fettiplace. The endogenous calcium buffer and the time course of transducer adaptation in auditory hair cells. *Journal of Neuroscience*, 18(20):8261–8277, 1998.

[90] Benjamin Louis Robinson and David McAlpine. Gain control mechanisms in the auditory pathway. *Current Opinion in Neurobiology*, 19(4):402–407, 2009.

[91] Kevin N Rohmann, Eric Wersinger, Jeremy P Braude, Sonja J Pyott, and Paul Albert Fuchs. Activation of bk and sk channels by efferent synapses on outer hair cells in high-frequency regions of the rodent cochlea. *Journal of Neuroscience*, 35(5):1821–1830, 2015.

[92] Yuttana Roongthumskul, Lea Fredrickson-Hemsing, Albert Kao, and Dolores Bozovic. Multiple-timescale dynamics underlying spontaneous oscillations of saccular hair bundles. *Biophysical Journal*, 101(3):603–610, 2011.

[93] Maria Lisa Rossi, Ivo Prigioni, Paolo Valli, and Cesare Casella. Activation of the efferent system in the isolated frog labyrinth: effects on the afferent epsps and spike discharge recorded from single fibers of the posterior nerve. *Brain Research*, 185(1):125–137, 1980.

[94] Ian J Russell and Euan Murugasu. Medial efferent inhibition suppresses basilar membrane responses to near characteristic frequency tones of moderate to high intensities. *The Journal of the Acoustical Society of America*, 102(3):1734–1738, 1997.

[95] Joshua D Salvi, Dáibhid Ó Maoiléidigh, Brian A Fabella, Mélanie Tobin, and AJ Hudspeth. Control of a hair bundle's mechanosensory function by its mechanical load. *Proceedings of the National Academy of Sciences*, 112(9):E1000–E1009, 2015.

[96] Joshua D Salvi, Dáibhid Ó Maoiléidigh, and AJ Hudspeth. Identification of bifurcations from observations of noisy biological oscillators. *Biophysical Journal*, 111(4):798–812, 2016.

[97] J Seebacher, A Franke-Trieger, V Weichbold, P Zorowka, and K Stephan. Improved interaural timing of acoustic nerve stimulation affects sound localization in single-sided deaf cochlear implant users. *Hearing Research*, 371:19–27, 2019.

[98] Roie Shlomovitz, Lea Fredrickson-Hemsing, Albert Kao, Sebastiaan WF Meenderink, Robijn Bruinsma, and Dolores Bozovic. Low frequency entrainment of oscillatory bursts in hair cells. *Biophysical Journal*, 104(8):1661–1669, 2013.

[99] David W Smith and Andreas Keil. The biological role of the medial olivocochlear efferents in hearing: separating evolved function from exaptation. *Frontiers in Systems Neuroscience*, 9:12, 2015.

[100] Tokio Sugai, Michio Sugitani, and Hiroshi Ooyama. Effects of activation of the diver-

gent efferent fibers on the spontaneous activity of vestibular afferent fibers in the toad. *The Japanese Journal of Physiology*, 41(2):217–232, 1991.

[101] Tokio Sugai, Jiro Yano, Michio Sugitani, and Hiroshi Ooyama. Actions of cholinergic agonists and antagonists on the efferent synapse in the frog sacculus. *Hearing Research*, 61(1-2):56–64, 1992.

[102] Julian Taranda, Stéphane F Maison, Jimena A Ballestero, Eleonora Katz, Jessica Savino, Douglas E Vetter, Jim Boulter, M Charles Liberman, Paul A Fuchs, and A Belén Elgoyhen. A point mutation in the hair cell nicotinic cholinergic receptor prolongs cochlear inhibition and enhances noise protection. *PLoS Biology*, 7(1):e1000018, 2009.

[103] Palmer Taylor and Joan Heller Brown. Synthesis, storage and release of acetylcholine. In *Basic Neurochemistry: Molecular, Cellular and Medical Aspects. 6th edition.* Lippincott-Raven, 1999.

[104] Jean-Yves Tinevez, Frank Jülicher, and Pascal Martin. Unifying the various incarnations of active hair-bundle motility by the vertebrate hair cell. *Biophysical Journal*, 93(11):4053–4067, 2007.

[105] Paolo Valli, Laura Botta, Gianpiero Zucca, and Cesare Casella. Functional organization of the peripheral efferent vestibular system in the frog. *Brain Research*, 362(1):92–97, 1986.

[106] Richard G Walker and AJ Hudspeth. Calmodulin controls adaptation of mechanoelectrical transduction by hair cells of the bullfrog's sacculus. *Proceedings of the National Academy of Sciences*, 93(5):2203–2207, 1996.

[107] Yixiang Wang, Maya Sanghvi, Alexandra Gribizis, Yueyi Zhang, Lei Song, Barbara Morley, Daniel G Barson, Joseph Santos-Sacchi, Dhasakumar Navaratnam, and Michael Crair. Efferent feedback controls bilateral auditory spontaneous activity. *Nature Communications*, 12(1):1–16, 2021.

[108] Carolina Wedemeyer, Lucas G Vattino, Marcelo J Moglie, Jimena Ballestero, Stéphane F Maison, Mariano N Di Guilmi, Julian Taranda, M Charles Liberman, Paul A Fuchs, Eleonora Katz, et al. A gain-of-function mutation in the $\alpha 9$ nicotinic acetylcholine receptor alters medial olivocochlear efferent short-term synaptic plasticity. *Journal of Neuroscience*, 38(16):3939–3954, 2018.

[109] Eric Wersinger and Paul Albert Fuchs. Modulation of hair cell efferents. *Hearing Research*, 279(1-2):1–12, 2011.

[110] T.C. Westfall. *Cholinergic Neurotransmission in the Autonomic and Somatic Motor Nervous System*, pages 827–834. 12 2009.

[111] Naohiro Yoshida, M Charles Liberman, M Christian Brown, and William F Sewell. Fast, but not slow, effects of olivocochlear activation are resistant to apamin. *Journal of Neurophysiology*, 85(1):84–88, 2001.

[112] Xiang-Yang Zheng, Sandra L McFadden, Da-Lian Ding, and Donald Henderson. Cochlear de-efferentation and impulse noise-induced acoustic trauma in the chinchilla. *Hearing Research*, 144(1-2):187–195, 2000.

[113] Stefan Zirn, Julian Angermeier, Susan Arndt, Antje Aschendorff, and Thomas Wesarg. Reducing the device delay mismatch can improve sound localization in bimodal cochlear implant or hearing-aid users. *Trends in Hearing*, 23:2331216519843876, 2019.